JOURNAL OF PETROLOGY | VOLUME 48 | NUMBER 8 | PAGES 1605–1639 | 2007 | doi:10.1093/petrology/egm032

Archaean to Proterozoic Crustal Evolution in the Central Zone of the Limpopo Belt (South Africa–Botswana): Constraints from Combined U–Pb and Lu–Hf Isotope Analyses of Zircon

ARMIN ZEH[1]*, AXEL GERDES[2], REINER KLEMD[1] AND JACKSON M. BARTON, JR[3]

[1]MINERALOGISCHES INSTITUT DER UNIVERSITÄT WÜRZBURG, AM HUBLAND, D-97074 WÜRZBURG, GERMANY

[2]INSTITUT FÜR GEOWISSENSCHAFTEN, SENCKENBERGANLAGE 28, D-60054 FRANKFURT AM MAIN, GERMANY

[3]DEPARTMENT OF GEOLOGY, UNIVERSITY OF FORT HARE, PRIVATE BAG X1314, ALICE, 5700, SOUTH AFRICA

RECEIVED JANUARY 9, 2007; ACCEPTED MAY 24, 2007

A combined set of U–Pb and Lu–Hf in situ *laser ablation ICP-(MC)-MS zircon analyses were obtained from orthogneisses and granitoids in the Central Zone of the Limpopo Belt, which comprises the Beit Bridge and Mahalapye complexes. The results indicate that by combining the two isotope systems primary magmatic zircon domains can be distinguished from those formed during later metamorphic events, even if the distinct zircon domains underwent multiple Pb loss and the texture–age relationships, as obtained by cathodoluminescence images and U–Pb analyses, are ambiguous. Furthermore, the applied technique allows distinction of zircon grains formed in juvenile magmas from those generated by melting of older continental crust or affected by substantial crustal contamination. The combined U–Pb and Lu–Hf data reveal that the Sand River gneiss suite of the Beit Bridge Complex was emplaced at 3283 ± 8 Ma and formed from melting of an older Archaean crust, which was derived from a depleted mantle source at around 3·65 Ga. The hafnium model age (T_{DM}^{Hf}) is significantly older than those obtained from zircons from numerous Neoarchaean granitoids of the Beit Bridge Complex, comprising the Singelele gneiss (2647 ± 12 Ma), the Bulai granite (2612 ± 7 Ma), the Regina gneiss (2649 ± 9 Ma) and two samples of the Zanzibar gneiss (2613 ± 6 Ma). These granitoids show initial $\varepsilon Hf(t)$ values between +0·5 and −7·1, which correspond to initial T_{DM}^{Hf} between 3·46 and 3·01 Ga. These variable $T_{DM}^{Hf}{}_{initial}$ and $\varepsilon Hf(t)_{initial}$ values are interpreted to be the result of different mixtures of reworked 3·65 Ga Palaeoarchaean crust with juvenile magmas extracted from the depleted mantle during the Neoarchaean at ~2·65 Ga. This conclusion is supported by results obtained from the Mahalapye Complex, which was affected by migmatization and granite intrusions during the Palaeoproterozoic at 2·02–2·06 Ga. The Mokgware granite (2019 ± 9 Ma) contains zircon xenocrysts with Pb–Pb ages of 2·52–2·65 Ga and 2·93 Ga and hafnium model ages of 3·0–3·4 Ga, indicating that this granite is derived from remelting of Archaean crust. In contrast, uniform $T_{DM}^{Hf}{}_{initial}$ ages of 2·61–2·67 Ga obtained from a diorite gneiss (2061 ± 6 Ma) of the Mahalapye Complex indicate that its protolith may have been formed from remelting of a Neoarchaean juvenile crust. Variable $\varepsilon Hf(t)_{initial}$ values from −3·7 to +6·3 of zircon cores (2711 ± 11 Ma) in an adjacent leucosome also support a model of mixing of juvenile mantle derived matter with older crust in the Neoarchaean.*

KEY WORDS: *Archaean; Palaeoproterozoic; Limpopo Belt; zircon, U–Pb dating; Lu–Hf isotopes; LA-ICP-MS*

INTRODUCTION

Isotope methods applied to Archaean magmatic rocks provide important information about the formation and

*Corresponding author. Telphone: +49-931-888-5415.
E-mail: armin.zeh@mail.uni-wuerzburg.de

evolution of the continental crust during the early Earth's history. Such methods can provide answers to some of the most controversial questions; for instance, about the timing of Archaean to Proterozoic crust-forming events and the recycling of this crust during subsequent orogenic processes (e.g. Armstrong, 1968, 1991; O'Nions *et al.*, 1979; O'Nions & Hamilton, 1981; Patchett *et al.*, 1981; Allègre, 1987; Albarède & Brouxel, 1987; Allègre & Lewin, 1989; Stevenson & Patchett, 1990; Amelin *et al.*, 1999; Rino *et al.*, 2004; Condie *et al.*, 2005; Harrison *et al.*, 2005; Iizuka *et al.*, 2005). In detail, such investigations provide valuable information on the timing of magma generation and its source, such as a juvenile depleted mantle, a reworked older crust or a combination of both (e.g. Vervoort & Blichert-Toft, 1999; Davis *et al.*, 2005; Gerdes & Zeh, 2006; Hawkesworth & Kemp, 2006).

For such studies, the mineral zircon has been shown to be an ideal candidate, for the following reasons. (1) Zircon crystallization ages can be obtained very precisely using the U–Pb isotope system even for very old rocks (e.g. Krogh, 1973; Compston *et al.*, 1984; Gerdes & Zeh, 2006; Iizuka *et al.*, 2006). (2) Zircon can incorporate high concentrations of Hf (>1 wt %) but only minor Lu (~1 ppm) in its lattice and, thus, the initial Hf isotope compositions of the magma at the time of zircon crystallization can be obtained with high precision, in particular by means of inductively coupled plasma mass spectrometry (ICP-MS) techniques (e.g. Patchett *et al.*, 1981; Vervoort & Blichert-Toft, 1999; Griffin *et al.*, 2004; Gerdes & Zeh, 2006). (3) *In situ* analytical methods such as ion probes (e.g. sensitive high-resolution ion microprobe; SHRIMP) and laser ablation (LA)-ICP-MS allow the analyses of different parts of individual zircon grains. Consequently, it is possible to recognize inherited zircon domains as well as younger overgrowth and/or alteration zones (e.g. Gerdes & Zeh, 2006, and therein). Furthermore, the combined consideration of the U–Pb and Lu–Hf system for zircon grains in orthogneisses may help to constrain whether distinct zircon grains or domains were affected by single or multiple Pb loss, and/or if distinct zircon zones were formed at different times (e.g. Amelin *et al.*, 2000, and therein).

In this study we investigate zircon from orthogneisses and granitoids in the Central Zone of the Limpopo Belt, which represents a mobile belt squeezed between the Zimbabwe Craton to the north and the Kaapvaal Craton to the south (Fig. 1). As shown by previous studies, the (meta)magmatic rocks of the Limpopo Belt were formed during at least three distinct magmatic periods, during the Palaeoarchaean at 3·25 Ga, the Neoarchaean at 2·5–2·7 Ga and the Palaeoproterozoic at *c.* 2·0 Ga (e.g. Barton *et al.*, 1994; Barton & Sergeev, 1997; Jaeckel *et al.*, 1997; Kröner *et al.*, 1998, 1999; Chavagnac *et al.*, 2001). In addition, a few detrital zircon grains and xenocrysts point to magmatic events as old as 3·8 Ga (Armstrong *et al.*, 1988; Kröner *et al.*, 1998). The available geochronological data show that the Limpopo Central Zone represents a unique orogenic belt where Archaean to Proterozoic magmatism, which took place over a period of more than 1300 Myr, can be studied in a very restricted area. Furthermore, the position of the Limpopo Belt between the Kaapvaal and Zimbabwe Cratons makes it important for obtaining information about the crust–mantle processes that took place during the amalgamation of these two cratons.

In contrast to the abundant geochronological data mentioned above, little is known about the source(s) of the magmatic rocks that were emplaced during the three distinct events. A few Sm–Nd isotope whole-rock analyses indicate that the orthogneisses with ages of 3·25–3·3 Ga and 2·6 Ga were derived from a source with an average crustal residence age (T_{DM}^{Nd}) between 2·8 and 3·4 Ga (Harris *et al.*, 1987; Barton, 1996; Kröner *et al.*, 1998; 1999), whereas some 2·0 Ga migmatitic–magmatic rocks yielded younger crustal residence ages between 2·4 and 2·9 Ga (Chavagnac *et al.*, 2001). To clarify the crustal evolution of the Limpopo Belt's Central Zone in more detail, we present new *in situ* U–Pb LA-ICP-MS age data from magmatic zircons and combine this information with multicollector (MC-)ICP-MS Lu–Hf isotope analyses from the same zircon domains.

GEOLOGICAL SETTING, CURRENT INTERPRETATIONS AND SAMPLES

The Limpopo Belt is a high-grade metamorphic province bounded by the Zimbabwe and Kaapvaal Cratons, comprising Archaean to Palaeoproterozoic rocks (Fig. 1) (e.g. Roering *et al.*, 1992; Berger *et al.*, 1995; Kamber *et al.*, 1995a, 1995b; Rollinson & Blenkinsop, 1995; Berger & Rollinson, 1997; Holzer *et al.*, 1998, 1999). Lithologically and structurally, it can be subdivided into three distinct domains, which are separated by major shear zones (McCourt & Vearncombe, 1987, 1992; Holzer *et al.*, 1999; Schaller *et al.*, 1999). The Central Zone is structurally bounded by the >10 km wide Palala–Zoetfontain and Triangle shear zones against the Southern and Northern Marginal zones, respectively. These steeply dipping shear zones were formed and/or activated under high-grade metamorphic conditions at about 2·0 Ga (Holzer *et al.*, 1998, 1999; Chavagnac *et al.*, 2001; Kreissig *et al.*, 2001). The Southern Marginal Zone consists of high-grade, intensely deformed and metamorphosed, tonalitic, trondjemitic and granodioritic rocks (TTGs) with minor greenstones, interpreted as reworked counterparts of the Kaapvaal Craton (e.g. Coward *et al.*, 1976; van Reenen *et al.*, 1987, 1992), whereas the Northern Marginal Zone

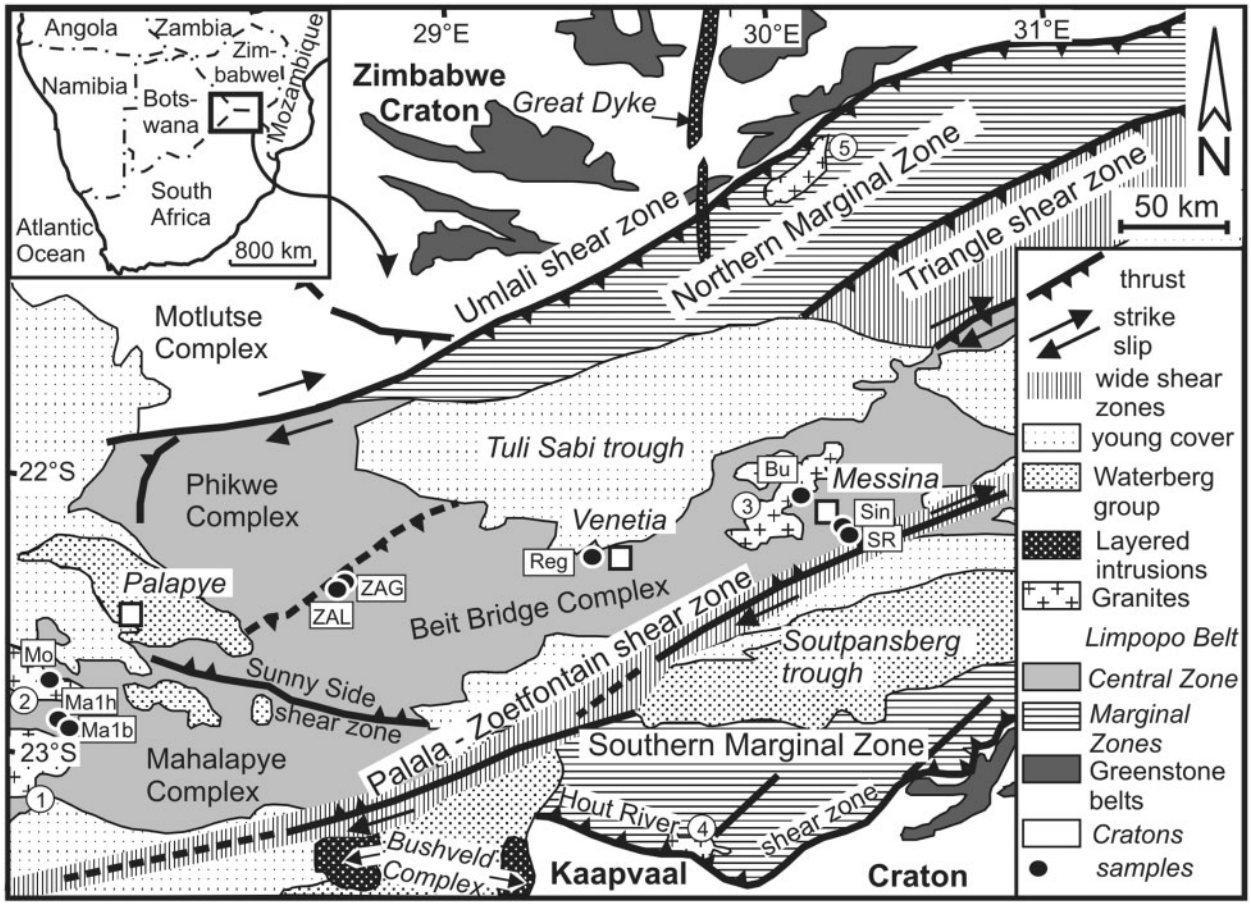

Fig. 1. Geological map of the Limpopo Belt with sample locations. 1, Mahalapye granite; 2, Mokgware granite; 3, Bulai granite; 4, Matok granite; 5, Razi granite.

is dominated by enderbite and charnoenderbitic orthogneisses with some greenstones and granitoid rocks (e.g. Mason, 1973; Berger *et al.*, 1995; Kamber & Biino, 1995; Berger & Rollinson, 1997; Jelsma & Dirks, 2002). The rocks of both marginal zones were thrust onto their adjacent cratons along >10 km wide, steeply dipping shear zones, the Hout River and Umlali shear zones, respectively (Fig. 1). According to Kreissig *et al.* (2001), magmatic intrusions and metamorphism of the Southern Marginal Zone occurred between 2·69 and 2·62 Ga, coeval with or slightly younger than the magmatic–metamorphic evolution in the Northern Marginal zone between 2·72 and 2·58–2·62 Ga (Berger *et al.*, 1995; Kamber & Biino, 1995; Mkweli *et al.*, 1995).

What was traditionally called the Central Zone proper was subdivided by Aldiss (1991) into three complexes, which were interpreted by Barton *et al.* (2006) as terranes: (1) the Mahalapye Complex, which is dominated by *c.* 2·02–2·0 Ga granites with minor high-grade sedimentary rocks (Hisada & Miyano, 1996; McCourt & Armstrong, 1998; Holzer *et al.*, 1999; Chavagnac *et al.*, 2001); (2) the Phikwe Complex, which is dominated by Archaean, hornblende-bearing, tonalitic and trondjemitic gneisses and igneous rocks (Brandl, 1992); (3) the Beit Bridge Complex. The Beit Bridge Complex hosts the *c.* 3·2–3·3 Ga Sand River TTG suite and Messina layered intrusion (Barton, 1983; Barton & Sergeev, 1997; Kröner *et al.*, 1999) and numerous Neoarchaean granitic to granodioritic orthogneisses with ages between 2·73 and 2·60 Ga, such as the Alldays, Singelele, Bulai, Zanzibar and Zoetfontain gneisses (e.g. Jaeckel *et al.*, 1997; Kröner *et al.*, 1999). Based on detrital zircon ages and lithological–structural differences, the supracrustal paragneisses of the Beit Bridge Complex can be divided into three unconformity-bounded successions, with ages >3·1 Ga, 3·1–2·6 Ga and < 2·6 Ga (e.g. Erikson *et al.*, 1988; Brandl, 1992; Kröner *et al.*, 1998, 1999; Barton *et al.*, 2003; Buick *et al.*, 2003). Quartzites and metapelites from within the oldest unconformity-bounded succession contain zircons with U–Pb ages of 3·2–3·8 Ga, suggesting that a yet unrecognized, very old protolith must exist within the Beit Bridge Complex (Armstrong *et al.*, 1988; Barton & Sergeev, 1997; Kröner *et al.*, 1998).

Table 1: Co-ordinates of sample localities

Sample	Local name	Locality	Longitude	Latitude
Beit Bridge Complex				
SR1	Sand River gneiss	Sand River bed	30°06′00″E	22°24′13″S
Sin	Singelele gneiss	Messina area (Singelelekop)	30°01′63″E	22°23′27″S
Bu1	Bulai granite	W Messina	29°56′80″E	22°18′38″S
Reg1	Regina gneiss	farm Regina (N Alldays)	29°13′21″E	22°21′79″S
ZAG	Zanzibar granodiorite gneiss	valley of the Seoka river (Botswana)	28°22′10″E	22°33′25″S
ZAL	Zanzibar granite gneiss	valley of the Seoka river (Botswana)	28°22′10″E	22°33′25″S
Mahalapye Complex				
Mo1	Mokgware granite	street Palapye–Mahalapye	26°53′26″E	22°46′83″S
Ma1h	garnet–biotite gneiss	Lose quarry	26°53′84″E	22°56′93″S
Ma1b	leucosome	Lose quarry	26°53′84″E	22°56′93″S

Further subdivision of the Limpopo Belt comes from Pb isotopic data, indicating that the Zimbabwe Craton, Northern Marginal Zone, and Beit Bridge and Phikwe terranes were all derived from a source with a long-lived, high μ value (>11–12), whereas the rocks in the Southern Marginal Zone and the Kaapvaal Craton were derived from a source with lower μ values close to Bulk Earth (Barton *et al.*, 1983; Taylor *et al.*, 1991; Barton, 1996; Berger & Rollinson, 1997; Kreissig *et al.*, 2000). Hence, the rocks of the Zimbabwe Craton, Northern Marginal Zone, and Beit Bridge and Phikwe terranes may stem from the same mantle source, but they cannot be genetically related in a straightforward way to those of the Kaapvaal Craton and Southern Marginal Zone (Barton *et al.*, 2006). Based on geochemical and Sm–Nd–Pb isotope data and petrogenetic modelling, Berger & Rollinson (1997) suggested that the 2·6–2·7 Ga enderbitic to charnoenderbitic rocks of the Northern Marginal Zone represent a mixture of a pre-existing Archaean TTG–crust, which was partially remelted and mixed with a more juvenile magma derived from the depleted mantle at 2·6–2·7 Ga.

In the present study zircon grains from nine granitoid samples were investigated, six from the Beit Bridge Complex (Sand River gneiss, Singelele gneiss, Bulai granite, Regina gneiss, grey and leucocratic Zanzibar gneiss) and three from the Mahalapye Complex (Mogkware granite, a garnet–biotite gneiss and a leucosome from the Lose quarry). The sample localities and co-ordinates are shown in Fig. 1 and Table 1, respectively.

ANALYTICAL TECHNIQUES

U–Pb and Lu–Hf LA-ICP(MC)-MS analyses

Zircon concentrates were prepared at Würzburg, Giessen and Frankfurt Universities using standard crushing and heavy mineral separation techniques. Selected grains were separated under alcohol and set in epoxy resin to form discs. Subsequently, the zircons were polished to expose their centres. Prior to analysis all mounts were photographed and zircon grains were imaged by SEM cathodoluminescence (CL) to identify homogeneous growth domains, using the JEOL JSM-6400 electron microprobe at the Institute of Geosciences, Frankfurt University. Selected zircon domains were analysed, following the procedure as outlined in detail by Gerdes & Zeh (2006). First, U–Pb analyses were carried out by LA-ICP-MS at Frankfurt University using a Thermo-Finnigan Element II sector field ICP-MS system coupled to a New Wave UP213 ultraviolet laser system. A teardrop-shaped, low-volume laser cell was used to allow the precise detection of heterogeneous material (e.g. inclusion or different growth zones) during time-resolved data acquisition (see Janousek *et al.*, 2006). Each analysis consisted of *c.* 20 s background acquisition followed by 35 s data acquisition, using a laser spot-size of 30 μm. A common-Pb correction based on the interference- and background-corrected ^{204}Pb signal and a model Pb composition (Stacey & Kramers, 1975) was carried out if necessary. The necessity of the correction is judged on whether the corrected ^{207}Pb/^{206}Pb lies outside the internal errors of the measured ratios. Discordant analyses were generally interpreted with care. Reported uncertainties were propagated by quadratic addition of the external reproducibility (standard deviation) obtained from the standard zircon GJ-1 ($n = 12$; ~0·5% and 0·5–0·9% for ^{207}Pb/^{206}Pb and ^{206}Pb/^{238}U, respectively) during individual analytical sessions (33 analyses of unknowns and 12 standards) and the within-run precision of each analysis (standard error). Concordia diagrams (2σ error ellipses), concordia ages and upper intercept ages (95% confidence level) were calculated using

Isoplot/Ex 2.49 (Ludwig, 2001). Subsequently, the same zircon domains were studied using the same laser system with a 40 μm spot-size, and the Lu, Hf and Yb isotopes were measured with a Thermo-Finnigan Neptune multi-collector ICP-MS system. The isotopes ^{172}Yb, ^{173}Yb and ^{175}Lu were simultaneously monitored during each analysis step to allow the correction of isobaric interferences between Lu and Yb isotopes on mass 176. ^{176}Yb and ^{176}Lu were calculated using $^{176}Yb/^{173}Yb = 0{\cdot}796218$ (Chu *et al.*, 2002) and $^{176}Lu/^{175}Lu = 0{\cdot}02658$ (see Gerdes & Zeh, 2006), and by taking the instrumental mass fractionation of each individual analysis into account. For instrumental mass bias correction Yb isotope ratios were normalized to $^{172}Yb/^{173}Yb = 1{\cdot}35274$ (Chu *et al.*, 2002) and Hf isotope ratios to $^{179}Hf/^{177}Hf = 0{\cdot}7325$ using an exponential law. The protocol was tested by replicate analysis of a 50 ppb JMC 475 solution that was doped with variable amounts of pure Yb and Lu (see Gerdes & Zeh, 2006). The accuracy of the interference correction could be verified even for a $^{176}Yb/^{177}Hf$ ratio of 0·241 and a $^{176}Lu/^{177}Hf$ ratio of 0·021, which clearly exceed the highest observed Yb and Lu amounts in the studied zircon grains. Analyses of a pure 50 ppb JMC 475 solution yielded $^{176}Hf/^{177}Hf = 0{\cdot}282146 \pm 8$ (2σ, $n = 22$). For better comparison all analyses are reported relative to the JMC 475 $^{176}Hf/^{177}Hf$ value of 0·282160. Ten and 16 LA-MC-ICP-MS analyses of the GJ-1 zircon (*c.* 9600 ppm Hf) during the two analytical session gave a $^{176}Hf/^{177}Hf$ ratio of $0{\cdot}282007 \pm 15$ (2σ) and $0{\cdot}282006 \pm 15$ (2σ), respectively (Table 3). This is identical, within error, to results obtained by solution MC-ICP-MS analyses of the Lu- and Yb-free Hf fraction ($0{\cdot}281999 \pm 8$, 2σ, $n = 10$). Multiple LA-MC-ICP-MS analyses of the 91500 zircon standard over a period of 9 months yielded $^{176}Hf/^{177}Hf = 0{\cdot}282297 \pm 22$ (2σ, $n = 112$). Our results are shown in Tables 2 and 3, and in Figs 2–8. All uncertainties in this paper are quoted at the $\pm 2\sigma$ level.

Constants and calculation parameters

Depleted mantle Hf model ages (T_{DM}^{Hf}) were calculated using a decay constant of $1{\cdot}867 \times 10^{-11}$ (Scherer *et al.*, 2001; Söderlund *et al.*, 2004), $^{176}Lu/^{177}Hf = 0{\cdot}0384$ and $^{176}Hf/^{177}Hf = 0{\cdot}28325$ for the depleted mantle (Chauvel & Blichert-Toft, 2001), a mean $^{176}Lu/^{177}Hf$ value of 0·0113 for the Palaeoproterozoic–Archaean crust [mean of average continental crust as suggested by Taylor & McLennan (1985) and Wedepohl (1995)], and the measured $^{176}Lu/^{177}Hf$ value of each spot for the time since zircon crystallization. The applied decay constant is, according to various workers (e.g. Davis *et al.*, 2005; Albarède *et al.*, 2006; Scherer *et al.*, 2007), more appropriate to derive information about Archaean crustal growth processes than that estimated by the analyses of meteorites [$(1{\cdot}958 \pm 0{\cdot}044) \times 10^{-11}$; Albarède *et al.*, 2006, and references herein). The use of the 'meteoritic' constant would increase the calculated εHf(t) for our samples on average by about 2·5 epsilon units, and would give slightly younger (0·10–0·003 Ga) hafnium model ages. A more significant impact on the calculated hafnium model ages results from the assumed $^{176}Lu/^{177}Hf$ value for the Palaeoproterozoic–Archaean crust. A lower $^{176}Lu/^{177}Hf$ value of 0·007, which is typical for present-day upper crust (Taylor & McLennan, 1985; Wedepohl, 1995), would decrease the T_{DM}^{Hf} of our zircon analyses by about 0·01–0·25 Ga (mean for all analyses = 0·10 Ga). A higher $^{176}Lu/^{177}Hf$ value of 0·015, as proposed by Rudnick & Gao (2003) for the bulk continental crust, would increase our calculated T_{DM}^{Hf} by about 0·12 Ga (average). Additional uncertainties with similar influence on the calculated T_{DM}^{Hf} result from the $^{176}Lu/^{177}Hf$ heterogeneity of depleted mantle melts (e.g. Chauvel & Blichert-Toft, 2001).

For calculation of εHf(t) we used the chondritic uniform reservoir (CHUR) recommended by Blichert-Toft & Albarède (1997; $^{176}Lu/^{177}Hf$ and $^{176}Hf/^{177}Hf$ values of 0·0332 and 0·282772, respectively), and the apparent Pb–Pb ages obtained for the respective zircon domains. By means of this procedure many zircon analyses from individual granitoid samples plot on linear arrays in the εHf(t) vs apparent Pb–Pb age diagram, in the initial $^{176}Hf/^{177}Hf$ vs apparent Pb–Pb age diagram, and in the T_{DM}^{Hf} vs apparent Pb–Pb age diagram (Figs 4 and 8). Given the case that the initial $^{176}Hf/^{177}Hf$ values of all of these zircon analyses are identical, within error, such an array suggests that all zircon domains were formed at the same time, but that some of them underwent multiple Pb loss afterwards, while maintaining their initial $^{176}Hf/^{177}Hf$ (see Amelin *et al.*, 2000). Thus, for all zircon analyses that plot on such an array initial εHf(t) values [$=\varepsilon Hf(t)_{initial}$] were recalculated using the respective magma crystallization ages (e.g. Fig. 9a and b). The same criterion was used to calculate initial T_{DM}^{Hf} values ($=T_{DM}^{Hf}{}_{initial}$), which are younger than the T_{DM}^{Hf} obtained by using the respective apparent Pb–Pb age (Table 3). The depleted mantle curve, as shown in Fig. 9, is extrapolated from average modern-day values of mid-ocean ridge basalts (MORB) ($^{176}Lu/^{177}Hf = 0{\cdot}0384$, $^{176}Hf/^{177}Hf = 0{\cdot}28325$; Chauvel & Blichert-Toft, 2001) assuming a linear behaviour.

RESULTS AND INTERPRETATION OF U–PB AND LU–HF ZIRCON ISOTOPE ANALYSES

Beit Bridge Complex

Sand River gneiss (sample SR)

This tonalitic gneiss sample, which mainly consists of plagioclase, quartz, biotite, minor hornblende, and orthopyroxene, was taken from the bed of the Sand River near the Causeway locality south of Messina (Fig. 1, Table 1). It represents a grey banded gneiss that is truncated and cut by numerous later melt batches. CL images

Table 2: Results of in situ *U–Pb zircon dating*

Spot/zrc[1]	^{207}Pb[2] (c.p.s.)	U[3] (ppm)	Pb[3] (ppm)	Th/U	$^{206}Pb/^{204}Pb$	$(^{206}Pb/^{238}U)$[4]	±2σ (%)	$(^{207}Pb/^{235}U)$[4]	±2σ (%)	Rho[5]	$(^{207}Pb/^{206}Pb)$[4]	±2σ (%)	Age $(^{207}Pb/^{236}U)$	±2σ	$^{206}Pb/^{238}U$	±2σ	$^{207}Pb/^{206}Pb$	±2σ	Con[6] (%)
Sample SR																			
2c/zrc1	447598	586	468	0·35	33102	0·6660	2·2	24·42	2·3	0·94	0·2659	0·8	3285	23	3291	57	3282	12	100
3c/zrc2	240058	351	281	0·54	14095	0·6589	2·4	24·22	2·5	0·95	0·2666	0·8	3277	25	3263	61	3286	13	99
4r/zrc2	266297	682	383	0·21	35245	0·5220	1·2	12·66	1·4	0·85	0·1758	0·7	2654	13	2708	26	2614	12	104
5c/zrc3	164681	272	146	0·70	4266	0·4105	2·3	14·55	2·5	0·93	0·2571	0·9	2786	24	2217	44	3229	14	69
6c/zrc4	408762	593	438	0·56	49731	0·5855	2·0	21·12	2·2	0·92	0·2616	0·8	3144	22	2971	49	3256	13	91
7c/zrc5	185216	491	101	0·56	5197	0·1530	19	5·087	19	1·00	0·2411	1·1	1834	173	918	162	3127	17	29
12c/zrc6	383729	995	437	1·17	1334	0·3282	2·8	11·50	2·9	0·96	0·2541	0·8	2565	28	1830	45	3211	13	57
10r/zrc7	132551	787	284	0·12	25246	0·3584	1·3	6·085	1·6	0·84	0·1231	0·9	1988	14	1975	23	2002	15	99
11c/zrc8	478753	878	574	0·58	12635	0·5365	3·6	18·72	3·7	0·97	0·2530	0·9	3027	37	2769	82	3204	14	86
13c/zrc8	192070	684	280	0·41	4969	0·3888	6·9	9·409	7·0	0·99	0·1755	1·1	2379	66	2117	125	2611	19	81
14r/zrc9	82256	387	163	0·39	3418	0·3835	1·2	6·600	1·6	0·75	0·1248	1·0	2059	14	2092	21	2026	19	103
16/zrc10	205225	2338	334	0·04	1251	0·1409	2·0	2·220	2·5	0·81	0·1143	1·4	1187	18	850	16	1869	26	45
17/zrc11	260983	453	384	0·83	37967	0·6523	2·3	23·77	3·0	0·77	0·2642	1·9	3259	29	3237	58	3272	30	99
18/zrc11	105390	545	222	0·42	9376	0·3708	1·7	6·364	2·0	0·86	0·1245	1·0	2027	17	2033	30	2022	18	101
20/zrc12	71799	1208	152	0·26	32752	0·1199	1·3	1·844	1·7	0·80	0·1116	1·0	1061	11	730	9	1825	18	40
21/zrc12	55097	1486	144	0·26	20205	0·0940	1·4	1·233	1·9	0·73	0·0952	1·3	816	10	579	8	1532	24	38
22/zrc12	172533	284	183	0·24	12081	0·5526	1·8	19·35	2·1	0·89	0·2540	1·0	3059	20	2836	43	3210	15	88
23c/zrc13	107645	167	137	0·57	15472	0·6554	1·6	24·03	2·1	0·78	0·2660	1·3	3270	21	3249	42	3282	21	99
24c/zrc14	225271	296	253	0·73	35529	0·6575	1·6	24·17	1·8	0·89	0·2666	0·8	3275	18	3258	42	3286	13	99
25c/zrc15	228464	288	229	0·25	70718	0·6805	1·5	25·00	1·7	0·84	0·2665	0·9	3308	17	3346	38	3286	15	102
26c/zrc15	116998	1126	236	0·17	695	0·1931	3·2	3·413	3·4	0·94	0·1282	1·1	1507	27	1138	34	2074	20	55
27c/zrc16	258970	877	375	0·36	1709	0·3718	2·4	10·67	2·5	0·93	0·2081	0·9	2495	24	2038	41	2891	15	70
30c/zrc17	293148	1408	880	0·31	35118	0·5387	2·7	17·87	2·8	0·95	0·2405	0·8	2983	27	2778	61	3124	13	89
31c/zrc18	206917	276	239	0·79	50252	0·6628	1·4	24·35	1·6	0·83	0·2665	0·9	3283	16	3278	35	3285	14	100
32c/zrc19	141820	225	172	0·57	9374	0·6300	2·0	21·15	2·1	0·92	0·2435	0·8	3145	21	3149	49	3143	13	100
34c/zrc20	268770	629	302	0·34	8824	0·4312	3·2	14·01	3·5	0·92	0·2356	1·4	2750	34	2311	63	3091	22	75
35c/zrc21	419847	825	429	0·49	27966	0·4236	3·4	14·12	3·7	0·91	0·2418	1·6	2758	36	2277	65	3132	25	73
Sample Bu																			
3r/zrc1	123276	555	312	0·40	7597	0·4986	2·2	12·09	2·4	0·92	0·1759	0·9	2612	23	2608	47	2614	15	100
4r/zrc1	226188	707	380	0·48	4975	0·4691	2·5	11·21	2·7	0·95	0·1734	0·9	2541	25	2480	53	2590	14	96
5c/zrc2	145368	465	223	0·31	48781	0·4446	2·3	9·518	2·6	0·88	0·1553	1·2	2389	24	2371	45	2405	21	99

6c/zrc3	147338	489	309	1·21	6722	0·5008	2·2	12·16	2·5	0·89	0·1761	1·2	2617	24	2617	48	2617	19	100
7c/zrc4	187064	678	383	0·68	5453	0·4801	4·4	11·34	4·8	0·92	0·1714	1·8	2552	45	2528	93	2571	30	98
8c/zrc5	85326	264	147	0·68	10261	0·4641	1·9	10·68	2·5	0·74	0·1669	1·7	2496	24	2457	38	2527	28	97
10c/zrc6	145890	748	246	0·70	6546	0·2721	2·8	5·491	3·0	0·94	0·1464	1·1	1899	26	1551	39	2304	18	67
11c/zrc7	134753	505	264	0·83	12389	0·4507	3·1	9·979	3·4	0·91	0·1606	1·4	2433	32	2398	63	2462	24	97
12c/zrc8	164767	668	305	0·88	6624	0·3824	2·0	8·489	2·3	0·85	0·1610	1·2	2285	22	2088	36	2466	21	85
14c/zrc9	132673	321	179	0·35	4139	0·4994	1·8	12·16	2·0	0·91	0·1767	0·8	2617	19	2611	39	2622	14	100
15r/zrc9	159951	422	235	0·42	4507	0·5022	2·1	12·14	2·2	0·93	0·1753	0·8	2615	21	2623	45	2609	13	101
16r/zrc10	149453	395	222	0·44	29597	0·5015	1·9	12·20	2·0	0·90	0·1764	0·9	2620	19	2620	40	2619	15	100
17c/zrc11	217076	643	577	0·57	6697	0·4563	2·1	10·25	2·3	0·91	0·1629	0·9	2458	21	2423	42	2486	15	97
18c/zrc12	177506	474	281	0·64	5651	0·5004	3·4	12·12	3·5	0·97	0·1756	0·8	2614	34	2616	74	2612	14	100
19r/zrc13	285239	1335	463	0·18	93986	0·3268	1·9	6·904	2·1	0·90	0·1532	0·9	2099	19	1823	31	2382	16	77
20r/zrc14	143826	393	235	0·56	8387	0·4977	2·1	12·01	2·3	0·88	0·1750	1·1	2605	22	2604	44	2606	19	100
21c/zrc15	153151	390	229	0·57	49542	0·5029	1·8	12·20	2·0	0·89	0·1759	0·9	2620	19	2626	39	2614	15	100
22c/zrc16	77583	195	132	1·20	20465	0·4991	2·8	12·12	3·0	0·93	0·1761	1·1	2613	28	2610	60	2616	18	100
23r/zrc16	250475	671	437	0·89	5271	0·4999	2·3	12·03	2·4	0·94	0·1745	0·8	2607	23	2613	50	2601	13	100
24c/zrc17	216233	625	320	0·33	83305	0·4649	2·6	10·98	2·8	0·94	0·1713	0·9	2521	26	2461	53	2570	16	96
25c/zrc18	174828	565	280	0·36	10254	0·4552	3·1	10·11	3·2	0·95	0·1610	1·0	2445	30	2418	62	2467	17	98
27c/zrc19	184604	717	412	0·87	49926	0·4769	5·2	11·15	5·3	0·97	0·1696	1·3	2536	51	2514	109	2554	22	98
28c/zrc20	106632	295	182	0·83	4898	0·5008	2·4	12·09	2·7	0·90	0·1751	1·2	2611	26	2617	53	2607	19	100
29c/zrc21	212153	534	407	1·12	14746	0·5004	2·3	12·13	2·5	0·94	0·1758	0·8	2615	23	2616	50	2614	14	100
30/zrc22	156626	475	245	0·53	30301	0·4517	2·2	10·46	2·4	0·91	0·1680	1·0	2477	22	2403	44	2538	17	95
31r/zrc23	270115	802	432	0·25	41092	0·4981	3·1	11·99	3·2	0·96	0·1746	0·9	2603	31	2605	67	2602	15	100
33c/zrc24	233801	607	346	0·40	15393	0·5040	2·1	12·10	2·4	0·90	0·1740	1·0	2612	22	2631	46	2597	17	101
Sample Sin																			
23c/zrc1	553246	1564	594	0·45	6160	0·3387	4·9	7·390	5·1	0·96	0·1583	1·4	2160	47	1880	81	2437	23	77
25c/zrc2	211464	437	233	0·43	7750	0·4733	3·8	10·955	3·9	0·97	0·1679	1·0	2519	37	2498	79	2537	17	98
26r/zrc3	535963	1346	518	0·63	8851	0·3058	4·3	7·443	4·4	0·99	0·1765	0·8	2166	40	1720	66	2621	13	66
27r/zrc3	124852	428	159	0·04	10017	0·3716	3·8	6·452	3·9	0·96	0·1259	1·1	2039	35	2037	66	2042	19	100
28c/zrc4	402248	1407	367	0·14	6057	0·2420	4·1	4·824	4·2	0·97	0·1446	1·0	1789	36	1397	51	2283	17	61
29c/zrc5	160950	1261	236	0·49	20249	0·1715	3·9	2·880	4·1	0·97	0·1218	1·0	1377	31	1020	37	1983	18	51
30r/zrc6	210456	683	223	0·37	13832	0·2924	4·3	6·162	4·4	0·97	0·1528	1·2	1999	39	1654	62	2378	20	70
31/zrc7	29387	58	31	0·42	2909	0·4570	3·7	11·05	3·9	0·94	0·1754	1·4	2527	37	2427	75	2609	23	93
32c/zrc8	335040	986	391	0·62	87140	0·3444	3·7	7·522	3·8	0·97	0·1584	0·9	2176	34	1908	61	2439	15	78
1c/zrc9	217520	283	145	0·33	4635	0·4560	2·3	11·00	2·4	0·93	0·1750	0·9	2523	23	2422	46	2606	14	93
2c/zrc10	86878	96	55	0·38	16314	0·5109	2·7	12·62	2·8	0·95	0·1791	0·9	2652	27	2660	59	2645	14	101
3c/zrc11	216497	248	145	0·45	40231	0·5118	2·8	12·72	3·0	0·96	0·1802	0·9	2659	28	2664	62	2655	15	100

(Continued)

Table 2: Continued

Spot/zrc[1]	^{207}Pb[2] (c.p.s.)	U[3] (ppm)	Pb[3] (ppm)	Th/U	$^{206}Pb/^{204}Pb$	$(^{206}Pb/^{238}U)$[4]	±2σ (%)	$(^{207}Pb/^{235}U)$[4]	±2σ (%)	Rho[5]	$(^{207}Pb/^{206}Pb)$[4]	±2σ (%)	Age $(^{207}Pb/^{236}U)$	±2σ	Age $^{206}Pb/^{238}U$	±2σ	Age $^{207}Pb/^{206}Pb$	±2σ	Con[6] (%)
4r/zrc11	56248	74	36	0·20	5839	0·4547	2·6	10·88	2·8	0·95	0·1735	0·9	2513	26	2416	53	2592	14	93
5c/zrc12	327150	431	235	0·63	101709	0·4742	2·5	10·515	2·6	0·96	0·1608	0·8	2481	25	2502	53	2464	13	102
6c/zrc13	303198	584	205	0·09	1835	0·2965	4·2	6·230	4·3	0·97	0·1524	1·1	2009	39	1674	62	2373	19	71
7c/zrc14	469442	883	225	0·43	182273	0·2095	3·9	5·066	4·0	0·96	0·1754	1·1	1830	35	1226	43	2610	19	47
8r/zrc14	272634	386	198	0·45	10988	0·4460	2·5	10·20	2·6	0·97	0·1658	0·6	2453	25	2377	51	2516	10	94
9c/zrc15	144528	742	164	0·52	17628	0·2006	3·0	2·846	3·2	0·93	0·1029	1·2	1368	25	1178	33	1677	21	70
10r/zrc16	97406	107	61	0·39	6184	0·5045	2·4	12·39	2·5	0·95	0·1781	0·8	2634	24	2633	52	2635	13	100
11c/zrc17	364326	1040	275	0·19	11069	0·2487	2·7	4·768	2·8	0·97	0·1391	0·6	1779	24	1432	35	2215	11	65
14r/zrc18	176792	368	119	0·35	12840	0·2909	2·7	6·099	2·9	0·95	0·1521	0·9	1990	25	1646	40	2369	15	69
15r/zrc19	116405	279	91	0·14	3746	0·3146	2·7	5·575	2·9	0·92	0·1285	1·2	1912	25	1763	41	2078	20	85
16c/zrc20	152110	947	187	0·53	16540	0·1761	2·5	2·648	2·6	0·96	0·1091	0·8	1314	20	1046	24	1784	14	59
18c/zrc21	72960	104	55	0·34	9816	0·4765	4·7	11·10	4·9	0·95	0·1689	1·5	2531	47	2512	98	2547	25	99
19c/zrc22	417737	988	251	0·18	9944	0·2186	3·7	3·432	3·9	0·94	0·1138	1·3	1512	31	1275	43	1861	23	68
20r/zrc23	321394	748	267	0·06	98951	0·3588	2·8	6·393	2·9	0·97	0·1292	0·7	2031	26	1977	48	2087	13	95
21r/zrc24	269267	923	237	0·47	2959	0·2266	2·7	3·907	3·1	0·87	0·1251	1·5	1615	25	1316	32	2030	27	65
22c/zrc24	282736	495	223	0·38	4190	0·4102	2·5	8·799	2·6	0·96	0·1556	0·8	2317	24	2216	47	2408	13	92
36c/zrc25	36320	261	59	0·51	4235	0·1938	2·8	3·800	3·3	0·86	0·1422	1·7	1593	27	1142	30	2254	30	51
38c/zrc26	28469	74	42	0·35	10483	0·5004	2·4	12·38	2·8	0·86	0·1794	1·5	2634	27	2616	52	2648	24	99
39c/zrc27	41091	97	59	0·57	3187	0·5090	2·5	12·60	2·7	0·93	0·1796	1·0	2650	25	2652	54	2649	16	100
40c/zrc28	18326	51	31	0·59	4532	0·5130	2·6	12·64	3·0	0·88	0·1788	1·4	2653	29	2669	58	2641	24	101
41r/zrc29	30843	98	82	0·35	11206	0·4994	2·4	12·52	2·6	0·90	0·1819	1·1	2645	25	2611	51	2670	19	98
42/zrc30	73235	78	321	0·60	25854	0·3539	2·3	8·038	2·6	0·88	0·1647	1·2	2235	24	1953	38	2505	21	78
43c/zrc31	45604	72	147	0·43	4079	0·3380	4·7	8·125	4·9	0·97	0·1743	1·2	2245	45	1877	78	2600	20	72
44r/zrc32	57582	101	129	0·33	14544	0·5057	2·4	12·29	2·6	0·93	0·1763	1·0	2627	25	2638	53	2618	16	101
45c/zrc33	70159	89	175	0·12	3295	0·4300	3·6	10·36	3·8	0·96	0·1747	1·0	2467	35	2306	71	2603	17	89
46c/zrc34	54362	86	151	0·45	9901	0·4151	2·6	9·915	2·9	0·89	0·1732	1·3	2427	27	2238	49	2589	22	86
47r/zrc35	54279	83	171	0·40	5467	0·3698	2·5	8·090	2·7	0·94	0·1587	0·9	2241	24	2028	43	2442	16	83
48r/zrc35	34520	99	70	0·40	10912	0·4905	2·9	11·75	3·1	0·91	0·1737	1·3	2585	30	2573	61	2594	22	99
49c/zrc36	19483	44	273	0·73	16252	0·1164	2·5	1·601	3·1	0·81	0·0998	1·8	971	20	710	17	1619	34	44
50r/zrc36	32845	70	91	0·38	4593	0·3096	3·2	6·896	3·9	0·82	0·1615	2·2	2098	35	1739	48	2472	38	70
51c/zrc37	57019	77	134	0·50	25683	0·3567	4·8	8·281	4·9	0·98	0·1684	0·9	2262	45	1966	82	2542	16	77
52r/zrc37	53821	102	74	0·37	29147	0·5235	2·4	12·98	2·7	0·90	0·1798	1·2	2678	25	2714	53	2651	19	102

53c/zrc38	19298	85	34	0·25	4639	0·4093	3·4	9·829	3·6	0·94	0·1742	1·3	2419	34	2212	63	2598	21	85
54r/zrc38	31936	90	81	0·05	15555	0·3604	2·9	6·839	3·2	0·90	0·1376	1·4	2091	29	1984	50	2198	24	90
55r/zrc39	39889	68	102	0·71	4149	0·3056	3·1	7·089	3·7	0·86	0·1682	1·9	2123	33	1719	47	2540	32	68
56r/zrc40	39798	84	71	0·64	5328	0·3855	2·8	8·755	3·0	0·93	0·1647	1·1	2313	28	2102	50	2504	19	84
57c/zrc40	20655	48	195	0·59	16663	0·1204	3·4	1·588	3·7	0·90	0·0957	1·6	965	23	733	23	1541	30	48
58c/zrc41	56873	86	85	0·55	22149	0·4043	2·4	9·489	2·5	0·93	0·1702	0·9	2386	24	2189	44	2560	15	86
59r/zrc42	8188	99	12	0·33	3402	0·4590	2·6	10·15	3·5	0·75	0·1603	2·3	2448	33	2435	53	2459	39	99
61c/zrc43	33261	53	87	0·51	9505	0·2108	4·2	4·342	4·5	0·93	0·1494	1·6	1701	38	1233	47	2339	28	53
62r/zrc43	22151	59	119	0·01	15742	0·1670	2·8	2·381	3·3	0·86	0·1034	1·7	1237	24	996	26	1686	31	59
Sample Reg																			
1r/zrc1	130851	324	184	0·53	9793	0·4995	2·2	11·93	2·6	0·83	0·1732	1·5	2599	69	2612	57	2589	24	101
1c/zrc1	167352	406	205	0·31	6914	0·4557	2·7	11·09	3·0	0·91	0·1765	1·3	2531	75	2420	65	2620	21	92
3c/zrc2	133627	250	127	0·54	47081	0·4352	2·3	10·75	2·7	0·88	0·1792	1·3	2502	66	2329	54	2646	21	88
3r/zrc2	160352	329	174	0·41	12025	0·4752	2·2	10·98	2·5	0·91	0·1675	1·0	2521	62	2506	56	2533	18	99
4c1/zrc3	194209	1387	378	0·44	2750	0·1670	3·6	2·789	4·1	0·87	0·1211	2·0	1353	55	996	35	1973	36	50
5c2/zrc3	202627	492	274	0·45	11621	0·4980	2·4	11·92	2·5	0·95	0·1736	0·8	2598	66	2605	63	2593	13	100
7c/zrc4	312437	1197	641	0·61	35975	0·4434	3·6	10·90	3·8	0·94	0·1783	1·3	2515	96	2366	85	2637	21	90
8r/zrc4	119919	269	136	0·41	6190	0·4537	2·8	10·87	3·1	0·91	0·1738	1·3	2512	78	2412	68	2594	22	93
9c/zrc5	175626	2710	197	0·32	2926	0·0614	4·0	0·996	4·1	0·96	0·1177	1·2	702	29	384	15	1922	21	20
12r/zrc6	116991	249	141	0·39	14174	0·5092	2·7	12·59	2·9	0·93	0·1793	1·0	2649	76	2653	71	2646	17	100
14c/zrc7	138515	262	149	0·57	11011	0·4876	2·7	12·06	2·9	0·95	0·1795	0·9	2609	75	2560	70	2648	15	97
15c/zrc8	221940	481	285	0·65	41967	0·5109	2·2	12·68	2·4	0·94	0·1800	0·8	2656	63	2660	59	2653	13	100
16c/zrc9	218902	537	301	0·48	8319	0·4989	2·6	12·33	2·8	0·95	0·1792	0·8	2630	73	2609	69	2646	14	99
17c/zrc10	127478	301	170	0·54	20558	0·5030	2·5	12·16	2·6	0·94	0·1753	0·9	2617	69	2627	65	2609	15	101
21c/zrc11	166355	571	263	1·01	43033	0·3541	3·1	7·956	3·2	0·96	0·1630	0·9	2226	72	1954	60	2487	16	79
Sample ZAG																			
1r/zrc1	388850	1685	489	0·31	13618	0·2717	2·5	5·283	2·6	0·95	0·1410	0·8	1866	23	1550	35	2240	15	69
2c/zrc1	342683	1428	450	0·37	26911	0·2835	5·0	5·468	5·1	0·98	0·1399	0·9	1896	45	1609	72	2226	15	72
3r/zrc1	210885	422	248	0·55	17220	0·4982	1·7	12·16	1·9	0·91	0·1770	0·8	2616	18	2606	36	2625	13	99
4c/zrc2	283264	589	328	0·36	41893	0·4955	1·8	12·01	1·9	0·92	0·1758	0·8	2605	18	2595	38	2614	13	99
5r/zrc2	260245	743	330	0·92	32685	0·3678	4·1	8·248	4·3	0·96	0·1626	1·2	2259	40	2019	72	2483	20	81
6c/zrc3	153268	306	168	0·25	9208	0·5005	1·7	12·02	1·9	0·90	0·1742	0·8	2606	18	2616	37	2598	14	101
7c/zrc4	331696	678	342	0·09	72756	0·4842	1·8	11·63	2·0	0·91	0·1741	0·8	2575	19	2546	38	2598	13	98
8r/zrc4	115996	275	140	0·61	11909	0·4180	3·4	9·98	3·6	0·93	0·1731	1·3	2433	34	2252	64	2588	22	87
9c/zrc5	251904	620	415	0·82	22025	0·4687	2·6	10·90	2·8	0·95	0·1686	0·9	2514	26	2478	54	2544	14	97
10r/zrc5	314076	674	356	0·29	7583	0·4794	1·7	11·28	1·9	0·90	0·1706	0·8	2547	18	2525	36	2564	14	98
11c/zrc6	96833	179	105	0·41	7914	0·5129	2·6	12·56	2·9	0·92	0·1776	1·1	2647	27	2669	58	2631	19	101

(Continued)

Table 2: Continued

Spot/zrc[1]	^{207}Pb[2] (c.p.s.)	U[3] (ppm)	Pb[3] (ppm)	Th/U	$^{206}Pb/^{204}Pb$	$(^{206}Pb/^{238}U)$[4]	±2σ (%)	$(^{207}Pb/^{235}U)$[4]	±2σ (%)	Rho[5]	$(^{207}Pb/^{206}Pb)$[4]	±2σ (%)	Age $(^{207}Pb/^{236}U)$	±2σ	Age $^{206}Pb/^{238}U$	±2σ	Age $^{207}Pb/^{206}Pb$	±2σ	Con[6] (%)
18c/zrc11	80794	179	109	1·07	3664	0·4517	3·0	10·48	3·2	0·95	0·1682	1·0	2478	30	2403	60	2540	17	95
21c/zrc14	178870	413	253	1·14	5096	0·4617	2·1	10·76	2·3	0·91	0·1690	0·9	2502	22	2447	43	2548	16	96
22r/zrc15	113401	391	163	0·29	3146	0·3801	2·5	7·275	2·8	0·89	0·1388	1·3	2146	26	2077	45	2213	22	94
23c/zrc16	77025	148	85	0·45	25054	0·5019	1·8	12·22	2·0	0·88	0·1766	1·0	2622	19	2622	38	2621	16	100
24c/zrc17	254934	643	352	1·05	3493	0·3787	4·0	8·274	4·2	0·96	0·1584	1·2	2261	38	2070	71	2439	20	85
25r/zrc17	220272	445	250	0·40	16968	0·4987	1·9	11·97	2·1	0·93	0·1741	0·8	2602	20	2608	42	2597	13	100
26c/zrc18	76581	152	103	1·20	3089	0·5004	3·0	12·18	3·2	0·94	0·1765	1·1	2618	31	2615	66	2620	19	100
28c/zrc19	168714	338	224	1·21	40744	0·4857	2·5	11·64	2·6	0·96	0·1738	0·8	2576	25	2552	53	2595	13	98
30r/zrc20	207187	559	278	0·53	3333	0·4111	2·9	8·701	3·0	0·95	0·1535	1·0	2307	28	2220	55	2385	16	93
31c/zrc21	74250	182	124	1·32	40594	0·4994	1·7	12·08	1·9	0·88	0·1754	0·9	2611	18	2611	37	2610	15	100
32c/zrc22	171692	407	163	0·43	64368	0·3586	2·7	8·507	3·0	0·93	0·1721	1·1	2287	27	1975	47	2578	19	77
33c/zrc23	66585	143	76	0·46	20857	0·4652	2·1	10·88	2·3	0·90	0·1696	1·0	2513	22	2462	43	2554	17	96
Sample ZAL																			
1c/zrc1	276954	1396	718	0·56	1084	0·2528	5·2	4·222	5·4	0·97	0·1211	1·3	1678	45	1453	68	1973	24	74
2r/zrc1	219493	791	269	0·23	23163	0·3192	1·7	6·432	1·9	0·89	0·1461	0·9	2037	17	1786	27	2301	15	78
3c/zrc2	64179	133	80	1·09	25021	0·4540	1·8	10·71	2·0	0·87	0·1711	1·0	2498	19	2413	35	2568	17	94
4r/zrc2	241632	857	283	0·35	57513	0·3009	2·3	6·426	2·6	0·89	0·1549	1·2	2036	23	1696	35	2401	20	71
5c/zrc3	92375	210	104	0·57	2210	0·4059	2·4	9·378	2·6	0·93	0·1676	0·9	2376	24	2196	45	2533	15	87
6r/zrc3	146745	1375	244	0·27	4857	0·1645	1·9	2·522	2·1	0·88	0·1112	1·0	1278	15	982	17	1819	18	54
7c/zrc4	216471	981	320	0·37	3065	0·2917	5·0	5·460	5·3	0·95	0·1358	1·6	1894	46	1650	73	2174	29	76
8r/zrc4	131581	1108	223	0·21	5861	0·1958	2·2	2·947	2·6	0·85	0·1091	1·4	1394	20	1153	23	1785	25	65
9c/zrc5	243286	630	288	0·15	48543	0·4329	4·3	9·678	4·4	0·98	0·1621	0·9	2405	41	2319	85	2478	15	94
10c/zrc6	261736	1559	355	0·43	1265	0·1824	2·5	3·531	2·8	0·91	0·1404	1·1	1534	22	1080	25	2232	20	48
11c/zrc7	160731	346	186	0·45	19756	0·4788	2·0	11·43	2·2	0·93	0·1731	0·8	2559	21	2522	43	2588	14	97
12r/zrc8	246240	722	251	0·15	12830	0·3160	1·9	6·763	2·2	0·89	0·1552	1·0	2081	19	1770	30	2404	16	74
16c/zrc9	206615	494	317	1·30	3580	0·4708	1·9	11·29	2·0	0·94	0·1740	0·7	2548	19	2487	40	2596	12	96
19r/zrc10	174913	1120	273	0·18	26686	0·2388	3·3	4·028	3·7	0·87	0·1223	1·8	1640	31	1381	41	1990	32	69
20r/zrc11	374179	736	385	0·25	117034	0·4856	1·7	11·81	1·9	0·91	0·1764	0·8	2589	18	2552	36	2619	13	97
24r/zrc12	175592	883	281	0·31	5773	0·2797	3·5	4·637	3·7	0·97	0·1203	0·9	1756	31	1590	50	1960	16	81
27c/zrc13	94114	217	144	1·30	11599	0·4613	2·4	10·98	2·6	0·93	0·1726	1·0	2522	24	2445	49	2583	16	95
30r/zrc14	212175	609	251	0·20	8245	0·3871	2·8	8·527	3·1	0·91	0·1598	1·3	2289	29	2110	51	2453	23	86
31c/zrc15	124566	445	218	1·31	6480	0·3171	5·5	6·702	5·8	0·96	0·1533	1·6	2073	52	1776	87	2383	26	75
32r/zrc16	169551	1239	269	0·15	96359	0·2150	4·0	3·527	4·3	0·92	0·1190	1·7	1533	35	1255	45	1941	31	65

Sample Mo																			
1c/zrc1	70269	443	146	0·41	3909	0·2939	2·8	5·011	3·0	0·94	0·1236	1·0	1821	25	1661	41	2009	17	83
2r/zrc1	53226	253	104	0·52	7670	0·3720	2·8	6·418	3·0	0·93	0·1251	1·1	2035	27	2039	49	2030	20	100
3c/zrc2	136275	703	277	0·70	35049	0·3411	2·2	5·840	2·3	0·93	0·1242	0·9	1952	21	1892	36	2017	16	94
4c/zrc3	239513	852	403	0·75	3250	0·4078	2·4	9·345	2·7	0·91	0·1662	1·1	2372	25	2205	45	2520	18	88
5c/zrc4	133956	692	349	0·91	14604	0·3255	2·8	5·551	3·0	0·95	0·1237	0·9	1909	26	1817	45	2010	16	90
6c/zrc5	92551	439	192	0·81	19064	0·3674	2·4	6·325	2·6	0·94	0·1249	0·9	2022	23	2017	42	2027	16	100
8c/zrc6	120123	230	180	1·15	5393	0·5800	2·7	17·04	2·8	0·95	0·2131	0·9	2937	28	2949	65	2929	14	101
9r/zrc6	118571	2832	290	0·05	4441	0·1019	2·3	1·289	2·5	0·93	0·0918	0·9	841	14	625	14	1463	17	43
10c/zrc7	232251	559	277	0·30	7504	0·3879	4·5	9·583	4·6	0·96	0·1792	1·2	2396	44	2113	81	2645	20	80
11c/zrc8	54632	280	109	0·66	4097	0·3250	2·0	5·629	2·3	0·86	0·1256	1·2	1921	20	1814	32	2038	21	89
12c/zrc9	281644	775	235	0·39	654	0·2640	2·1	4·480	2·2	0·96	0·1231	0·6	1727	38	1510	32	2001	11	75
13c/zrc10	105895	252	98	0·41	6882	0·3562	2·4	6·068	2·5	0·97	0·1236	0·6	1986	49	1964	47	2008	10	98
14c/zrc11	187813	333	142	0·40	4449	0·3762	2·3	8·784	2·5	0·93	0·1693	0·9	2316	58	2059	48	2551	15	81
17c/zrc12	237608	1432	236	0·36	5368	0·1325	9·7	1·925	9·8	0·99	0·1054	1·0	1090	106	802	78	1721	19	47
18c/zrc13	80999	191	72	0·50	23215	0·3376	2·4	5·789	2·5	0·96	0·1244	0·6	1945	48	1875	45	2020	11	93
20r/zrc13	77400	178	72	0·47	12583	0·3690	2·1	6·341	2·2	0·95	0·1246	0·7	2024	45	2025	43	2023	13	100
21/zrc14	176203	577	82	0·13	617	0·1086	9·2	1·848	9·2	1·00	0·1235	0·7	1063	98	664	61	2007	12	33
Sample Ma1b		U	Pb	6/4															
36cp/zrc1	527061	950	618	0·17	979	0·4578	3·9	10·70	4·1	0·95	0·1695	1·3	2497	39	2430	80	2553	21	95
37co/zrc2	157879	341	211	0·53	2901	0·5176	2·0	13·38	2·1	0·92	0·1874	0·8	2707	20	2689	44	2720	14	99
38cp/zrc3	397408	555	388	0·25	5932	0·4489	2·2	9·98	2·9	0·76	0·1612	1·9	2433	27	2390	44	2468	31	97
39co/zrc3	315451	783	437	0·32	6282	0·4773	2·7	11·30	2·9	0·95	0·1718	0·9	2549	27	2516	58	2575	16	98
44co/zrc4	49043	143	65	0·22	1338	0·4046	3·5	9·591	4·3	0·81	0·1719	2·6	2396	41	2190	65	2576	43	85
42co/zrc4	80745	165	100	0·50	28564	0·5227	3·0	13·49	3·2	0·92	0·1871	1·2	2714	31	2711	66	2717	20	100
43co/zrc5	163206	404	229	0·47	3552	0·4778	3·1	12·24	3·3	0·95	0·1858	1·0	2623	31	2518	65	2706	16	93
45co/zrc6	169156	423	231	0·47	7769	0·4675	2·4	11·76	2·7	0·88	0·1824	1·3	2586	26	2473	49	2675	21	92
46rd/zrc6	76401	2612	127	0·09	491	0·0409	18	0·4258	18	0·98	0·0755	3·4	360	57	258	45	1082	67	24
47co/zrc7	112419	239	139	0·53	11400	0·4898	3·1	12·39	3·4	0·89	0·1834	1·6	2634	33	2570	66	2684	26	96
48co/zrc8	123553	203	126	0·35	1503	0·4670	3·0	10·86	3·6	0·84	0·1686	1·9	2511	34	2470	62	2544	32	97
49co/zrc9	74156	150	94	0·58	26164	0·5321	2·5	13·81	2·7	0·93	0·1882	1·0	2737	26	2750	57	2726	17	101
50cp/zrc10	59518	2458	143	0·11	17582	0·0602	6·9	0·6338	7·2	0·96	0·0763	2·0	498	29	377	25	1104	40	34
51co/zrc11	351669	808	495	0·55	4178	0·5251	2·2	13·45	2·4	0·88	0·1858	1·2	2712	23	2721	48	2705	19	101
52co/zrc12	194052	400	257	0·42	4226	0·5321	1·9	13·48	2·2	0·86	0·1838	1·1	2714	21	2750	44	2687	19	102
54co/zrc13	169996	325	207	0·42	4467	0·5169	2·1	13·26	2·5	0·86	0·1860	1·3	2698	23	2686	46	2707	21	99
55co/zrc14	61798	121	78	0·54	3392	0·5401	2·5	13·88	2·8	0·89	0·1864	1·2	2741	26	2784	56	2710	21	103
23co/zrc15	263540	668	382	0·37	1306	0·5007	2·2	12·06	2·5	0·91	0·1747	1·0	2609	23	2617	48	2604	17	101

(Continued)

Table 2: Continued

Spot/zrc[1]	^{207}Pb[2] (c.p.s.)	U[3] (ppm)	Pb[3] (ppm)	Th/U	$^{206}Pb/^{204}Pb$	$(^{206}Pb/^{238}U)$[4]	±2σ (%)	$(^{207}Pb/^{235}U)$[4]	±2σ (%)	Rho[5]	$(^{207}Pb/^{206}Pb)$[4]	±2σ (%)	Age $(^{207}Pb/^{236}U)$	±2σ	$^{206}Pb/^{238}U$	±2σ	$^{207}Pb/^{206}Pb$	±2σ	Con[6] (%)
25co/zrc15	307489	859	466	0·49	1321	0·4431	2·4	9·83	2·5	0·93	0·1609	0·9	2419	24	2364	47	2465	15	96
26cp/zrc16	425541	1815	683	0·32	1493	0·3313	3·5	6·860	3·6	0·97	0·1502	0·8	2094	32	1844	56	2348	14	79
27co/zrc17	250818	574	360	0·22	2011	0·5116	2·7	13·12	3·0	0·90	0·1860	1·3	2688	29	2663	59	2707	22	98
30cp/zrc18	360055	8477	586	0·03	2865	0·0610	5·9	0·706	6·0	0·98	0·0839	1·3	542	26	382	22	1291	25	30
31cp/zrc19	134542	2103	236	0·48	1975	0·0915	3·3	1·316	3·8	0·86	0·1043	1·9	853	22	564	18	1703	36	33
32co/zrc20	162853	346	220	0·45	2808	0·5269	2·9	13·42	3·1	0·95	0·1847	1·0	2710	30	2728	65	2696	16	101
33co/zrc20	232875	577	342	0·31	1493	0·4851	2·3	11·80	2·6	0·89	0·1765	1·2	2589	25	2550	49	2620	19	97
Sample Ma1h																			
1/zrc1	60686	288	117	0·45	31845	0·3752	1·9	6·597	2·2	0·86	0·1275	1·1	2059	20	2054	33	2064	20	99
2/zrc2	52786	246	104	0·59	27620	0·3801	1·8	6·664	2·2	0·81	0·1272	1·3	2068	20	2077	32	2059	23	101
3/zrc3	70092	4131	115	0·03	2871	0·0252	4·5	0·4599	4·6	0·98	0·1322	0·9	384	15	161	7	2127	16	8
4/zrc4	39736	183	76	0·53	20681	0·3784	1·3	6·625	1·8	0·76	0·1270	1·2	2063	16	2069	24	2056	20	101
5/zrc5	33343	145	62	0·44	6250	0·3824	1·7	6·657	2·1	0·83	0·1262	1·2	2067	18	2088	31	2046	20	102
6/zrc6	41422	197	84	0·68	13354	0·3767	1·5	6·563	1·9	0·82	0·1264	1·1	2054	17	2061	27	2048	19	101
7/zrc7	42778	207	85	0·55	22622	0·3744	1·4	6·517	1·7	0·79	0·1262	1·1	2048	15	2050	24	2046	19	100
8/zrc8	31242	137	59	0·49	16280	0·3837	1·6	6·730	2·1	0·79	0·1272	1·3	2077	18	2093	29	2060	22	102
10/zrc9	42349	203	86	0·62	22364	0·3750	1·4	6·545	1·8	0·75	0·1266	1·2	2052	16	2053	24	2051	21	100
11/zrc10	49988	299	109	0·52	9713	0·3230	3·2	5·667	3·3	0·95	0·1272	1·1	1926	29	1805	50	2060	19	88
12/zrc11	33823	416	43	0·22	7825	0·0835	19	1·465	19	1·00	0·1272	1·2	916	122	517	95	2060	21	25
13/zrc12	57978	279	118	0·64	30174	0·3734	1·4	6·559	1·7	0·80	0·1274	1·0	2054	15	2045	24	2062	18	99
14/zrc13	41769	198	85	0·68	21765	0·3774	1·5	6·643	1·8	0·80	0·1277	1·1	2065	16	2064	26	2066	19	100
15/zrc14	51119	238	101	0·57	22101	0·3811	1·5	6·743	1·8	0·85	0·1283	0·9	2078	16	2081	27	2075	16	100
16/zrc15	50402	233	100	0·59	16059	0·3817	1·5	6·672	1·8	0·81	0·1268	1·1	2069	16	2084	26	2053	19	102
17/zrc16	43258	202	85	0·56	22456	0·3780	1·4	6·646	1·8	0·80	0·1275	1·1	2065	16	2067	25	2064	19	100
18/zrc17	52270	250	104	0·59	13129	0·3686	1·2	6·453	1·6	0·75	0·1270	1·1	2040	14	2023	21	2057	19	98
19/zrc18	41966	193	82	0·56	21816	0·3839	1·6	6·738	1·9	0·82	0·1273	1·1	2078	17	2095	28	2061	20	102
20/zrc19	23864	111	46	0·46	12423	0·3778	1·9	6·652	2·3	0·82	0·1277	1·3	2066	21	2066	33	2067	24	100
21/zrc20	36962	174	76	0·66	19526	0·3839	1·7	6·685	2·0	0·83	0·1263	1·1	2071	18	2095	30	2047	20	102

[1]Spot, spot number; zrc, zircon number; c, core, r rim.
[2]Within-run background-corrected mean ^{207}Pb signal.
[3]U and Pb content and Th/U ratio were calculated relative to GJ-1 reference.
[4]Corrected for background, within-run Pb/U fractionation and common Pb using Stacy & Kramers (1975) model Pb composition and subsequently normalized to GJ-1 (ID-TIMS value/measured value); $^{207}Pb/^{235}U$ calculated using $^{207}Pb/^{206}Pb/(^{238}U/^{206}Pb \times 1/137{\cdot}88)$.
[5]Rho is the error correlation, defined as $err^{206}Pb/^{238}U/err^{207}Pb/^{235}U$.
[6]Degree of concordance $[=(^{238}U/^{206}Pb \text{ age} \times 100)/^{207}Pb/^{206}Pb \text{ age}]$.

Table 3: Results of in situ Lu–Hf zircon analyses

	$^{176}Yb/^{177}Hf$[1]	±2σ	$^{176}Lu/^{177}Hf$[1]	±2σ	$^{178}Hf/^{177}Hf$	$^{180}Hf/^{177}Hf$	VHf[2]	$^{176}Hf/^{177}Hf$	±2σ	$^{176}Hf/^{177}Hf(t)$[3]	εHf(t)[3]	±2σ	T_{DM}[4]	Age (Ma)	±2σ
Sample Sr1															
2c/zrc1	0·0270	12	0·00110	3	1·46718	1·88661	9	0·280721	17	0·280651	−0·8	0·6	3·62	3282	12
3c/zrc2	0·0241	22	0·00098	6	1·46712	1·88660	12	0·280718	17	0·280657	−1·4	0·6	3·63	3250	12
5c/zrc3	0·0238	21	0·00100	9	1·46717	1·88675	9	0·280740	17	0·280678	−1·1	0·6	3·60	3229	13
17c/zrc4	0·0154	12	0·00065	4	1·46715	1·88650	11	0·280676	17	0·280636	−2·0	0·6	3·67	3254	19
23c/zrc13	0·0400	14	0·00145	5	1·46716	1·88675	12	0·280720	16	0·280628	−2·1	0·6	3·68	3261	18
24c/zrc14	0·0291	24	0·00120	8	1·46713	1·88668	10	0·280726	18	0·280650	−0·7	0·6	3·62	3290	13
25c/zrc15	0·0313	25	0·00099	7	1·46713	1·88647	12	0·280695	16	0·280632	−1·3	0·6	3·65	3290	13
31c/zrc18	0·0308	21	0·00120	5	1·46716	1·88654	9	0·280732	18	0·280657	−1·0	0·6	3·62	3267	13
32c/zrc19	0·0249	15	0·00105	8	1·46712	1·88655	10	0·280770	17	0·280706	−2·0	0·6	3·59	3147	13
Sample Bu															
4r/zrc1	0·0157	7	0·00055	2	1·46719	1·88658	11	0·281023	16	0·280996	−4·7	0·6	3·28	2590	14
5c/zrc2	0·0135	13	0·00053	1	1·46729	1·88671	12	0·281072	20	0·281048	−7·1	0·7	3·26	2405	21
6c/zrc3	0·0221	11	0·00075	3	1·46724	1·88675	10	0·281057	15	0·281020	−3·2	0·5	3·22	2617	19
7c/zrc4	0·0167	6	0·00067	2	1·46714	1·88651	10	0·281060	14	0·281027	−4·0	0·5	3·23	2571	30
8c/zrc5	0·0164	12	0·00058	1	1·46731	1·88685	7	0·281070	17	0·281042	−4·5	0·6	3·22	2527	28
14czrc9	0·0077	9	0·00029	1	1·46728	1·88682	12	0·281030	16	0·281016	−3·2	0·6	3·23	2622	14
16r/zrc10	0·0160	10	0·00055	1	1·46720	1·88662	9	0·281032	18	0·281005	−3·9	0·6	3·25	2609	13
17c/zrc11	0·0242	10	0·00088	1	1·46724	1·88663	9	0·281080	16	0·281038	−5·6	0·6	3·25	2486	15
18c/zrc12	0·0245	17	0·00085	1	1·46725	1·88685	9	0·281057	18	0·281015	−3·5	0·7	3·23	2612	14
20r/zrc14	0·0149	5	0·00056	1	1·46718	1·88669	10	0·281037	17	0·281009	−3·8	0·6	3·25	2606	19
21c/zrc15	0·0116	2	0·00043	0	1·46718	1·88659	11	0·281012	13	0·280991	−4·3	0·5	3·28	2614	15
22c/zrc16	0·0223	7	0·00078	2	1·46714	1·88654	7	0·281058	19	0·281019	−3·2	0·7	3·22	2616	18
24c/zrc17	0·0136	6	0·00050	2	1·46722	1·88667	9	0·281050	18	0·281025	−4·1	0·7	3·23	2570	16
25c/zrc18	0·0180	14	0·00065	2	1·46722	1·88671	8	0·281073	20	0·281042	−5·9	0·7	3·25	2467	17
27c/zrc20	0·0181	13	0·00065	1	1·46726	1·88673	8	0·281068	17	0·281036	−4·1	0·6	3·22	2554	22
28c/zrc20	0·0174	7	0·00063	1	1·46725	1·88673	9	0·281063	17	0·281032	−3·0	0·6	3·20	2607	19
29c/zrc21	0·0158	9	0·00055	3	1·46710	1·88681	10	0·281060	16	0·281033	−2·8	0·6	3·20	2614	14
31r/zrc23	0·0132	11	0·00048	3	1·46713	1·88682	9	0·281040	19	0·281016	−3·7	0·7	3·23	2602	15
33c/zrc24	0·0423	28	0·00143	4	1·46713	1·88682	9	0·281105	17	0·281034	−3·2	0·6	3·20	2597	17
Sample Sin															
1c/zrc9	0·0356	7	0·00121	4	1·46716	1·88655	18	0·281023	16	0·280963	−5·4	0·6	3·32	2607	13
2c/zrc10	0·0271	5	0·00089	1	1·46713	1·88649	16	0·281049	17	0·281004	−3·0	0·6	3·22	2648	14
3c/zrc11	0·0327	14	0·00015	3	1·46720	1·88668	14	0·280948	12	0·280941	−5·1	0·4	3·44	2658	15
10r/zrc16	0·0197	11	0·00075	3	1·46725	1·88670	7	0·280994	20	0·280956	−5·2	0·7	3·31	2639	13
15r/zrc16	0·0230	3	0·00077	1	1·46724	1·88674	17	0·281196	13	0·281165	−10·4	0·5	3·16	2081	20
16c/zrc20	0·0756	29	0·00262	5	1·46715	1·88687	20	0·281023	18	0·280934	−25·3	0·6	3·73	1787	14
18c/zrc21	0·0420	24	0·00150	10	1·46716	1·88670	18	0·281021	12	0·280948	−7·3	0·4	3·37	2550	25
19c/zrc22	0·0462	38	0·00182	11	1·46724	1·88675	20	0·281055	9	0·280990	−21·5	0·3	3·59	1865	23
20r/zrc23	0·0087	3	0·00037	0	1·46727	1·88678	8	0·281165	20	0·281150	−10·7	0·7	3·19	2091	13
21r/zrc24	0·0358	13	0·00124	2	1·46715	1·88670	9	0·281005	15	0·280957	−18·8	0·5	3·59	2034	27
22c/zrc24	0·0607	29	0·00232	11	1·46727	1·88670	8	0·281092	18	0·280986	−9·1	0·6	3·36	2412	13
23c/zrc1	0·0594	13	0·00208	5	1·46724	1·88675	20	0·281079	14	0·280982	−8·7	0·5	3·36	2437	23
25c/zrc2	0·0322	23	0·00111	5	1·46722	1·88669	11	0·281035	28	0·280981	−6·4	1·0	3·31	2537	17
26r/zrc3	0·1055	106	0·00321	23	1·46709	1·88671	20	0·281116	22	0·280955	−5·4	0·8	3·33	2621	13
27r/zrc3	0·0058	6	0·00020	2	1·46723	1·88683	8	0·281677	25	0·281669	6·6	0·9	2·20	2042	19

Table 3: Continued

	$^{176}Yb/^{177}Hf$[1]	±2σ	$^{176}Lu/^{177}Hf$[1]	±2σ	$^{178}Hf/^{177}Hf$	$^{180}Hf/^{177}Hf$	VHf[2]	$^{176}Hf/^{177}Hf$	±2σ	$^{176}Hf/^{177}Hf(t)$[3]	εHf(t)[3]	±2σ	T_{DM}[4]	Age (Ma)	±2σ
28c/zrc4	0·0491	10	0·00194	4	1·46708	1·88643	19	0·281068	13	0·280983	−12·2	0·5	3·43	2283	17
29c/zrc5	0·0741	15	0·00258	4	1·46727	1·88683	19	0·281052	18	0·280954	−20·1	0·7	3·61	1983	18
31/zrc7	0·0298	7	0·00113	2	1·46722	1·88668	13	0·281056	13	0·280999	−4·1	0·5	3·24	2609	23
32c/zrc8	0·0647	41	0·00225	11	1·46711	1·88653	19	0·281120	14	0·281016	−7·5	0·5	3·29	2439	15
36c/zrc25	0·0800	44	0·00198	10	1·46718	1·88685	16	0·281067	16	0·280982	−13·0	0·6	3·46	2254	29
36c/zrc25	0·0711	35	0·00171	6	1·46720	1·88685	17	0·281057	15	0·280984	−12·9	0·5	3·58	2254	29
38c/zrc26	0·0350	7	0·00086	1	1·46718	1·88687	18	0·281044	16	0·281001	−3·3	0·6	3·36	2648	20
39c/zrc27	0·0459	30	0·00115	7	1·46722	1·88671	15	0·281077	18	0·281019	−2·5	0·6	3·24	2649	16
40c/zrc28	0·0579	31	0·00153	11	1·46711	1·88682	12	0·281064	23	0·280987	−3·9	0·8	3·31	2641	21
41r/zrc29	0·0359	10	0·00094	2	1·46716	1·88675	15	0·281047	13	0·280999	−2·7	0·5	3·27	2670	19
42/zrc30	0·0660	32	0·00163	9	1·46724	1·88681	19	0·281085	16	0·281007	−6·3	0·6	3·33	2505	20
43c/zrc31	0·0556	22	0·00136	6	1·46727	1·88683	16	0·281071	14	0·281003	−4·2	0·5	3·29	2600	19
44r/zrc32	0·0434	4	0·00108	2	1·46725	1·88685	17	0·281025	16	0·280971	−5·2	0·6	3·35	2618	16
45c/zrc33	0·0826	76	0·00204	18	1·46725	1·88672	16	0·281113	24	0·281012	−3·9	0·9	3·28	2603	16
46c/zrc34	0·1163	57	0·00282	11	1·46703	1·88689	17	0·281102	18	0·280963	−5·9	0·6	3·38	2589	22
47r/zrc35	0·0358	19	0·00091	4	1·46710	1·88688	16	0·281329	35	0·281286	2·2	1·2	2·81	2442	16
48r/zrc35	0·0455	12	0·00119	6	1·46716	1·88688	17	0·281046	16	0·280987	−4·9	0·6	3·33	2594	22
49c/zrc36	0·0983	11	0·00244	3	1·46731	1·88688	17	0·281091	18	0·281017	−26·2	0·7	3·69	1619	34
50r/zrc36	0·0270	8	0·00075	2	1·46719	1·88682	21	0·281078	13	0·281043	−5·8	0·5	3·28	2472	38
51c/zrc37	0·0808	58	0·00205	15	1·46745	1·88689	17	0·281077	22	0·280978	−6·5	0·8	3·37	2542	16
52r/zrc37	0·0363	23	0·00101	3	1·46715	1·88674	17	0·281053	21	0·281001	−3·1	0·7	3·27	2651	19
53c/zrc38	0·0423	28	0·00117	8	1·46716	1·88677	14	0·281091	20	0·281033	−3·2	0·7	3·24	2598	21
54r/zrc38	0·0172	14	0·00054	4	1·46714	1·88688	13	0·281298	26	0·281276	−3·8	0·9	2·95	2198	24
55r/zrc39	0·1253	61	0·00310	12	1·46741	1·88698	16	0·281327	28	0·281177	0·6	1·0	3·29	2540	32
56r/zrc40	0·0531	4	0·00130	0	1·46721	1·88678	19	0·281053	15	0·280991	−6·9	0·5	3·36	2504	19
57c/zrc40	0·1403	46	0·00340	11	1·46720	1·88673	18	0·281101	22	0·281002	−28·5	0·8	3·75	1541	30
58c/zrc41	0·1000	22	0·00246	7	1·46727	1·88684	17	0·281056	19	0·280935	−7·5	0·7	3·44	2560	15
59r/zrc42	0·0457	12	0·00124	7	1·46728	1·88691	15	0·281056	19	0·280998	−7·7	0·7	3·37	2459	39
61c/zrc43	0·0739	51	0·00194	15	1·46733	1·88690	17	0·281086	19	0·281000	−10·4	0·7	3·42	2339	28
62r/zrc43	0·0407	26	0·00112	12	1·46727	1·88686	16	0·281071	25	0·281035	−24·0	0·9	3·67	1686	31
Sample Reg															
1c/zrc1	0·0241	8	0·00089	1	1·46712	1·88656	7	0·281027	18	0·280983	−4·4	0·6	3·29	2620	21
3c/zrc2	0·0490	12	0·00177	3	1·46723	1·88671	13	0·281027	15	0·280937	−5·5	0·5	3·37	2646	21
5c2/zrc3	0·0243	2	0·00090	2	1·46718	1·88663	15	0·281012	12	0·280967	−5·6	0·4	3·34	2593	13
7c/zrc4	0·0383	14	0·00138	4	1·46721	1·88677	16	0·281009	12	0·280939	−5·6	0·4	3·37	2637	21
8r/zrc4	0·0184	16	0·00074	5	1·46717	1·88659	15	0·281024	13	0·280987	−4·9	0·5	3·29	2594	22
12r/zrc6	0·0215	14	0·00076	3	1·46707	1·88647	6	0·281016	26	0·280977	−4·1	0·9	3·29	2646	17
14c/zrc7	0·0574	24	0·00197	4	1·46725	1·88676	13	0·281034	14	0·280934	−5·5	0·5	3·37	2648	14
15c/zrc8	0·0494	27	0·00178	5	1·46719	1·88664	14	0·281038	11	0·280948	−4·9	0·4	3·34	2653	13
16c/zrc9	0·0367	19	0·00133	3	1·46708	1·88651	15	0·281041	11	0·280973	−4·2	0·4	3·30	2646	17
17c/zrc10	0·0225	7	0·00086	3	1·46719	1·88654	14	0·281016	16	0·280974	−5·0	0·6	3·31	2609	15
21c/zrc11	0·0541	31	0·00216	7	1·46710	1·88652	15	0·281095	14	0·280993	−7·2	0·5	3·33	2487	16
Sample ZAG															
3r/zrc1	0·0108	5	0·00043	1	1·46714	1·88674	14	0·281094	10	0·281072	−1·1	0·4	3·11	2625	13
4c/zrc2	0·0125	11	0·00052	3	1·46713	1·88652	16	0·281087	13	0·281061	−1·8	0·5	3·14	2614	13
6c/zrc3	0·0270	40	0·00098	15	1·46721	1·88671	14	0·281123	13	0·281074	−1·7	0·5	3·12	2598	14

(Continued)

Table 3: Continued

	$^{176}Yb/^{177}Hf$[1]	±2σ	$^{176}Lu/^{177}Hf$[1]	±2σ	$^{178}Hf/^{177}Hf$	$^{180}Hf/^{177}Hf$	VHf[2]	$^{176}Hf/^{177}Hf$	±2σ	$^{176}Hf/^{177}Hf(t)$[3]	εHf(t)[3]	±2σ	T_{DM}[4]	Age (Ma)	±2σ
7c/zrc4	0·0100	4	0·00042	2	1·46717	1·88681	16	0·281083	13	0·281062	−2·1	0·5	3·15	2598	13
9c/zrc5	0·0287	16	0·00121	8	1·46726	1·88670	15	0·281124	13	0·281065	−3·3	0·5	3·17	2544	14
10r/zrc5	0·0064	2	0·00027	0	1·46714	1·88667	6	0·281098	21	0·281084	−2·1	0·7	3·12	2564	14
11c/zrc6	0·0276	39	0·00098	14	1·46721	1·88677	13	0·281125	13	0·281076	−0·9	0·5	3·11	2631	19
18c/zrc11	0·0084	4	0·00033	1	1·46721	1·88678	5	0·281109	32	0·281093	−2·4	1·1	3·11	2540	17
21c/zrc14	0·0190	13	0·00073	4	1·46710	1·88655	13	0·281101	16	0·281066	−3·2	0·6	3·16	2548	16
23c/zrc16	0·0046	3	0·00022	2	1·46723	1·88692	7	0·281069	18	0·281058	−1·7	0·7	3·14	2621	16
25r/zrc17	0·0068	3	0·00027	1	1·46721	1·88688	6	0·281055	22	0·281041	−2·9	0·8	3·19	2597	13
26c/zrc18	0·0159	14	0·00062	4	1·46722	1·88679	13	0·281110	21	0·281078	−1·0	0·7	3·10	2620	19
28c/zrc19	0·0157	12	0·00062	4	1·46725	1·88673	15	0·281107	20	0·281076	−1·7	0·7	3·12	2595	13
31c/zrc21	0·0269	8	0·00099	3	1·46718	1·88701	11	0·281104	25	0·281054	−2·1	0·9	3·16	2610	15
33c/zrc23	0·0271	15	0·00093	4	1·46713	1·88696	14	0·281096	14	0·281050	−3·6	0·5	3·19	2554	17
1r/zrc1	0·0260	11	0·00077	3	1·46718	1·88658	10	0·281120	14	0·281088	−9·5	0·5	3·26	2240	15
2c/zrc1	0·0266	13	0·00075	3	1·46713	1·88668	9	0·281151	15	0·281119	−8·7	0·5	3·21	2226	15
5r/zrc2	0·0169	17	0·00050	4	1·46720	1·88673	8	0·281121	15	0·281097	−3·5	0·5	3·13	2483	20
8r/zrc4	0·0154	5	0·00045	1	1·46724	1·88683	7	0·281148	18	0·281126	−0·1	0·6	3·03	2588	22
22r/zrc15	0·0190	16	0·00054	4	1·46710	1·88655	5	0·281129	21	0·281106	−9·5	0·8	3·24	2213	22
24c/zrc17	0·0264	13	0·00077	4	1·46722	1·88692	6	0·281150	30	0·281114	−3·9	1·1	3·12	2439	20
30r/zrc20	0·0213	7	0·00065	2	1·46729	1·88682	6	0·281159	19	0·281130	−4·6	0·7	3·11	2385	16
32c/zrc22	0·0124	12	0·00044	3	1·46732	1·88697	6	0·281122	24	0·281101	−1·2	0·9	3·08	2578	19
Sample ZAL															
1c/zrc1	0·0491	25	0·00184	7	1·46725	1·88665	6	0·281164	36	0·281095	−15·3	1·3	3·37	1973	13
2r/zrc1	0·0140	4	0·00056	1	1·46715	1·88683	8	0·281137	23	0·281112	−7·3	0·8	3·19	2295	14
3c/zrc2	0·0202	15	0·00077	7	1·46721	1·88674	6	0·281103	24	0·281065	−2·7	0·9	3·16	2568	17
5c/zrc3	0·0208	10	0·00071	4	1·46720	1·88663	6	0·281083	20	0·281049	−3·7	0·7	3·20	2551	24
6r/zrc4	0·0248	9	0·00089	3	1·46718	1·88682	9	0·281104	15	0·281073	−19·5	0·5	3·47	1823	17
7c/zrc5	0·0368	15	0·00151	4	1·46722	1·88669	18	0·281143	12	0·281080	−11·2	0·4	3·31	2174	29
8r/zrc6	0·0186	6	0·00077	2	1·46716	1·88690	7	0·281105	33	0·281079	−20·2	1·2	3·48	1785	25
10c/zrc6	0·0375	25	0·00126	7	1·46718	1·88668	8	0·281154	17	0·281099	−8·4	0·6	3·23	2270	19
11c/zrc7	0·0284	23	0·00103	8	1·46721	1·88660	7	0·281118	22	0·281067	−2·4	0·8	3·15	2577	13
16c/zrc9	0·0389	20	0·00144	8	1·46713	1·88693	14	0·281113	13	0·281042	−3·8	0·5	3·21	2555	18
19r/zrc10	0·0173	11	0·00069	4	1·46719	1·88689	16	0·281125	16	0·281099	−14·8	0·6	3·35	1990	32
20r/zrc11	0·0122	6	0·00047	1	1·46716	1·88668	18	0·281130	15	0·281106	0·1	0·5	3·05	2625	13
27c/zrc13	0·0261	22	0·00093	7	1·46713	1·88663	16	0·281108	16	0·281062	−2·9	0·6	3·16	2563	19
31c/zrc15	0·0371	21	0·00143	9	1·46718	1·88683	15	0·281147	17	0·281082	−6·6	0·6	3·21	2372	27
32r/zrc16	0·0230	12	0·00089	4	1·46722	1·88685	14	0·281167	18	0·281122	−14·7	0·6	3·33	1941	31
Sample Mo															
1c/zrc1	0·0112	3	0·00040	0	1·46718	1·88662	17	0·281221	12	0·281206	−10·6	0·4	3·14	2009	17
2r/zrc1	0·0075	3	0·00027	1	1·46712	1·88653	8	0·281236	13	0·281226	−9·4	0·5	3·09	2030	20
3c/zrc2	0·0229	9	0·00084	4	1·46721	1·88667	17	0·281262	14	0·281229	−9·5	0·5	3·09	2017	16
4c/zrc3	0·0418	11	0·00163	6	1·46716	1·88667	15	0·281096	12	0·281033	−5·0	0·4	3·24	2520	18
5c/zrc4	0·0230	3	0·00077	1	1·46724	1·88674	17	0·281196	13	0·281166	−12·0	0·5	3·21	2010	16
6c/zrc5	0·0149	5	0·00054	1	1·46719	1·88666	15	0·281238	10	0·281217	−9·7	0·4	3·11	2027	16
8c/zrc6	0·0400	34	0·00128	10	1·46707	1·88648	9	0·280907	22	0·280857	−1·7	0·8	3·39	2929	14
9r/zrc6	0·0447	19	0·00169	4	1·46720	1·88663	10	0·281354	15	0·281289	−20·0	0·5	3·21	1463	17
10c/zrc7	0·0653	47	0·00222	13	1·46707	1·88661	9	0·281193	19	0·281108	0·6	0·7	3·03	2645	20

(Continued)

Table 3: Continued

	$^{176}Yb/^{177}Hf$[1]	±2σ	$^{176}Lu/^{177}Hf$[1]	±2σ	$^{178}Hf/^{177}Hf$	$^{180}Hf/^{177}Hf$	VHf[2]	$^{176}Hf/^{177}Hf$	±2σ	$^{176}Hf/^{177}Hf(t)$[3]	εHf(t)[3]	±2σ	T_{DM}[4]	Age (Ma)	±2σ
11c/zrc8	0·0118	5	0·00043	2	1·46717	1·88671	17	0·281203	15	0·281186	−10·6	0·5	3·16	2038	21
13c/zrc10	0·0131	9	0·00047	2	1·46711	1·88655	16	0·281229	11	0·281211	−10·4	0·4	3·13	2008	10
17c/zrc12	0·0334	21	0·00128	5	1·46719	1·88662	19	0·281186	12	0·281137	−19·6	0·4	3·39	1721	19
18c/zrc13	0·0040	2	0·00013	0	1·46726	1·88685	18	0·281164	9	0·281160	−12·0	0·3	3·22	2020	11
14c/zrc11	0·0161	13	0·00062	5	1·46722	1·88674	20	0·281182	12	0·281159	0·2	0·4	2·98	2551	15
Sample Ma1b															
23co/zrc15	0·0388	13	0·00146	4	1·46701	1·88661	34	0·281263	11	0·281191	2·6	0·4	2·89	2604	17
26cp/zrc16	0·0732	15	0·00249	7	1·46712	1·88653	30	0·281207	14	0·281096	−6·7	0·5	3·20	2348	14
27cp/zrc17	0·0425	15	0·00145	3	1·46709	1·88667	26	0·281186	17	0·281110	2·1	0·6	3·00	2707	22
30cp/zrc18	0·0200	10	0·00075	2	1·46722	1·88683	12	0·281012	16	0·280994	−34·3	0·6	3·83	1291	25
31cp/zrc19	0·0265	5	0·00095	1	1·46698	1·88662	24	0·281091	13	0·281060	−22·7	0·5	3·55	1703	36
31r/zrc19	0·1412	22	0·00528	8	1·46724	1·88680	47	0·281476	13	0·281275	−8·3	0·4	3·01	2000[5]	1
32cp/zrc19	0·0446	24	0·00135	6	1·46714	1·88682	13	0·281105	16	0·281054	−16·2	0·6	3·43	2000[5]	1
33co/zrc20	0·1373	80	0·00493	26	1·46720	1·88681	21	0·281418	30	0·281171	2·2	1·1	2·92	2620	19
34r/zrc20	0·1741	33	0·00628	10	1·46703	1·88662	26	0·281632	33	0·281393	−4·1	1·2	2·78	2000[5]	1
35r/zrc20	0·1390	108	0·00515	33	1·46714	1·88686	27	0·281466	26	0·281270	−8·5	0·9	3·01	2000[5]	1
36cp/zrc1	0·0440	42	0·00147	12	1·46732	1·88687	6	0·281090	25	0·281018	−4·7	0·9	3·25	2553	21
38cp/zrc3	0·1731	167	0·00580	56	1·46718	1·88686	9	0·281333	38	0·281059	−5·2	1·3	3·21	2468	31
39co/zrc3	0·0484	8	0·00172	2	1·46714	1·88674	29	0·281157	13	0·281072	−2·3	0·5	3·14	2575	16
42co/zrc4	0·0336	10	0·00114	2	1·46717	1·88694	27	0·281025	11	0·280966	−2·8	0·4	3·28	2717	20
43co/zrc5	0·0559	32	0·00174	5	1·46713	1·88653	14	0·281041	12	0·280951	−3·6	0·4	3·31	2706	16
44co/zrc4	0·1145	32	0·00424	10	1·46717	1·88684	43	0·281452	11	0·281243	3·8	0·4	2·80	2576	43
51co/zrc11	0·0402	10	0·00142	3	1·46704	1·88657	28	0·281232	21	0·281158	3·8	0·7	2·91	2705	19
52co/zrc12	0·0309	7	0·00116	2	1·46708	1·88662	9	0·281066	17	0·281006	−2·0	0·6	3·21	2687	19
53r/zrc12	0·1214	18	0·00465	10	1·46716	1·88683	20	0·281410	17	0·281233	−9·8	0·6	3·09	2000[5]	1
53r/zrc12	0·1052	45	0·00401	15	1·46713	1·88680	21	0·281437	15	0·281285	−8·0	0·5	2·99	2000[5]	1
54co/zrc13	0·0541	39	0·00174	11	1·46710	1·88665	16	0·281140	21	0·281049	−0·1	0·7	3·12	2707	21
55co/zrc14	0·0602	15	0·00201	4	1·46709	1·88650	21	0·281111	13	0·281006	−1·5	0·5	3·20	2710	21
Sample Ma1h															
1/zrc1	0·0017	1	0·00005	0	1·46722	1·88671	32	0·281466	11	0·281464	−0·1	0·4	2·61	2064	20
2/zrc2	0·0077	1	0·00024	0	1·46720	1·88666	30	0·281446	9	0·281436	−1·2	0·4	2·67	2059	23
4/zrc4	0·0029	2	0·00009	1	1·46722	1·88667	27	0·281466	10	0·281462	−0·4	0·4	2·62	2056	20
6/zrc6	0·0026	0	0·00007	0	1·46722	1·88669	31	0·281467	9	0·281464	−0·5	0·4	2·62	2048	19
7/zrc7	0·0032	1	0·00009	0	1·46719	1·88669	28	0·281468	11	0·281465	−0·5	0·4	2·62	2046	19
8/zrc8	0·0091	3	0·00030	1	1·46724	1·88673	26	0·281458	12	0·281446	−1·1	0·5	2·65	2051	21
13/zrc12	0·0069	2	0·00022	1	1·46723	1·88672	27	0·281449	11	0·281441	−1·0	0·4	2·66	2060	21
14/zrc13	0·0060	1	0·00020	0	1·46720	1·88672	27	0·281461	9	0·281453	−0·6	0·4	2·63	2062	18
15/zrc14	0·0092	4	0·00028	1	1·46719	1·88660	25	0·281450	10	0·281439	−1·0	0·4	2·66	2066	19
16/zrc15	0·0114	5	0·00040	2	1·46719	1·88665	26	0·281457	10	0·281441	−0·7	0·4	2·65	2075	16
17/zrc16	0·0066	3	0·00021	1	1·46715	1·88657	25	0·281457	11	0·281449	−0·9	0·4	2·64	2053	19
18/zrc17	0·0016	0	0·00005	0	1·46722	1·88674	27	0·281452	8	0·281450	−0·6	0·3	2·64	2064	19
19/zrc18	0·0075	7	0·00023	2	1·46715	1·88660	25	0·281464	9	0·281455	−0·6	0·4	2·63	2057	19
20/zrc19	0·0052	8	0·00017	3	1·46727	1·88665	27	0·281463	9	0·281456	−0·5	0·4	2·63	2061	20
21/zrc20	0·0039	3	0·00012	1	1·46726	1·88674	28	0·281446	9	0·281441	−0·9	0·3	2·65	2067	24

(Continued)

Table 3: Continued

	$^{176}Yb/^{177}Hf$[1]	±2σ	$^{176}Lu/^{177}Hf$[1]	±2σ	$^{178}Hf/^{177}Hf$	$^{180}Hf/^{177}Hf$	VHf[2]	$^{176}Hf/^{177}Hf$	±2σ	$^{176}Hf/^{177}Hf(t)$[3]	εHf(t)[3]	±2σ	T_{DM}[4]	Age (Ma)	±2σ
Session 1 (March–April 2006)															
JMC 475, $n=10$	–	–	–	–	1·46714	1·88668	19	0·282156	9						
GJ-1, $n=16$	0·00735	15	0·000297	5	1·46719	1·88663	20	0·282007	15	0·282003	−13·7	0·5	2·18	611	6
Session 2 (July 2006)															
JMC 475, $n=10$	–	–	–	–	1·46717	1·88665	16	0·282153	11						
GJ-1, $n=10$	0·00696	15	0·000296	5	1·46723	1·88669	16	0·282006	15	0·282003	−13·8	0·5	2·18	611	6

[1] $^{176}Yb/^{177}Hf = (^{176}Yb/^{177}Hf)_{true} \times (^{173}Yb/^{177}Hf)_{meas} \times (M_{176(Yb)}/M_{173})^{\beta(Yb)}/(M_{176(Yb)}/M_{177})^{\beta(Hf)}$. $^{176}Lu/^{177}Hf$ values were calculated using $^{175}Lu/^{177}Hf$ and β_{Yb}. The effect of the inter-element fractionation on Lu/Hf was estimated to be less than 6%.
[2] Mean Hf signal in volts.
[3] Initial $^{176}Hf/^{177}Hf$ and εHf(t) calculated using the apparent LA-ICP-MS $^{207}Pb/^{206}Pb$ age of each spot. It should be noted that in many cases, as a result of non-zero Pb loss, this is not the age of zircon crystallization (see text for further explanation).
[4] Apparent depleted mantle two-stage model age in billion years using $^{76}Lu/^{177}Hf$ values of 0·0384 and 0·0113 for the depleted mantle and average continental crust, respectively. For calculation of the first stage the apparent $^{207}Pb/^{206}Pb$ age and $^{176}Lu/^{177}Hf$ of each zircon were used. Uncertainties (absolute) relate to the last quoted figure and are 2σ standard error for sample zircon grains and 2σ standard deviation for JMC 475 and GJ-1 zircon.
[5] Age presumed (for explanation see text).

of most zircon grains show cores with oscillatory zoning patterns, which are in some grains overgrown by structureless rims (Fig. 2a). In addition, a few completely structureless zircon crystals are observed (Fig. 2a). During this study 27 U–Pb spot analyses were carried out on cores and rims of 21 zircon grains (Table 2). In addition, Lu–Hf isotope spot analyses of nine zircon cores were obtained (Table 3). As shown in Fig. 3a, four groups of concordant to near-concordant U–Pb ages can be distinguished. Zircon cores yield concordant ages of about 3·28 Ga and one of 3·14 Ga, whereas zircon overgrowths and structureless zircon grains yield concordant ages of about 2·02 Ga and one of *c.* 2·61 Ga (Figs 2a and 3a). All four concordant age groups are also reflected in the Pb–Pb intercept ages of discordant zircon analyses (Table 2, Fig. 3a).

We suggest that the oldest concordant zircon grains, which yield a mean age of 3283 ± 8 Ma, identical to an upper intercept age of 3280 ± 7 Ma (Fig. 3a), reflect the time of the Sand River gneiss protolith intrusion, whereas the younger concordant age of 3143 ± 13 Ma dates the time of zircon growth during a Palaeoarchaean anatectic event. Our estimated intrusion age is identical to or slightly younger than that obtained by SHRIMP U–Pb analyses from the Sand River granitoid suite at the Causeway locality (3314 ± 5 Ma, 3240 ± 5 Ma), the Macloutse farm (3290 ± 17 Ma), Bellvue farm (3297 ± 7 Ma), Verbaard farm (3296 ± 4 Ma) and Vrouenroom farm (3292 ± 4 Ma), but older than zircon SHRIMP ages obtained from the Esmefour farm (3205 + 69/−62 Ma) and the Sand River bed (3240 ± 5 Ma; 3197 ± 30 Ma) (Kröner *et al.*, 1998, 1999). The suggested Palaeoarchaean anatectic event at 3143 ± 13 Ma conforms with field relationships and geochronological data; the highly deformed and migmatitized Sand River gneiss is locally cut by basalt dykes, which yielded Rb–Sr and Pb–Pb ages of 3060 Ma and 2922 Ma, respectively (Barton *et al.*, 1977; Barton *et al.*, 1990).

The upper intercept age of 2614 ± 11 Ma is interpreted to reflect zircon formation in the Sand River gneiss during a Neoarchaean metamorphic–magmatic event, whereas the upper intercept age of 2014 ± 10 Ma (five spots, MSWD = 1·0) dates zircon growth during the Palaeoproterozic granulite-facies metamorphic overprint. The latter age is slightly younger than U–Pb isotope dilution thermal ionization mass spectrometry (ID-TIMS) and Pb–Pb zircon evaporation ages of 2031 ± 6 and 2026 ± 1 Ma, respectively, which were obtained on metamorphic zircon grains from pelitic gneisses of the Causeway locality (Jaeckel *et al.*, 1997), but identical within error to the upper intercept ages of strongly discordant U–Pb ID-TIMS zircon analyses of 2006 ± 8 Ma and 2003 ± 11 Ma, which were obtained from zircon grains from melt patches in the Sand River gneisses and from a pegmatitic granite (Jaeckel *et al.*, 1997). The 2614 Ma age is identical within error to the intrusion age of several orthogneisses found throughout the Central Zone (Jaeckel *et al.*, 1997; Kröner *et al.*, 1999; this study). However, it is significantly younger than the two concordant U–Pb SHRIMP analyses of about 2734 ± 4 Ma in a *c.* 3·29 Ga quartz monzonitic augen gneiss, which were interpreted to represent a local melting event during the Neoarchaean (Kröner *et al.*, 1999).

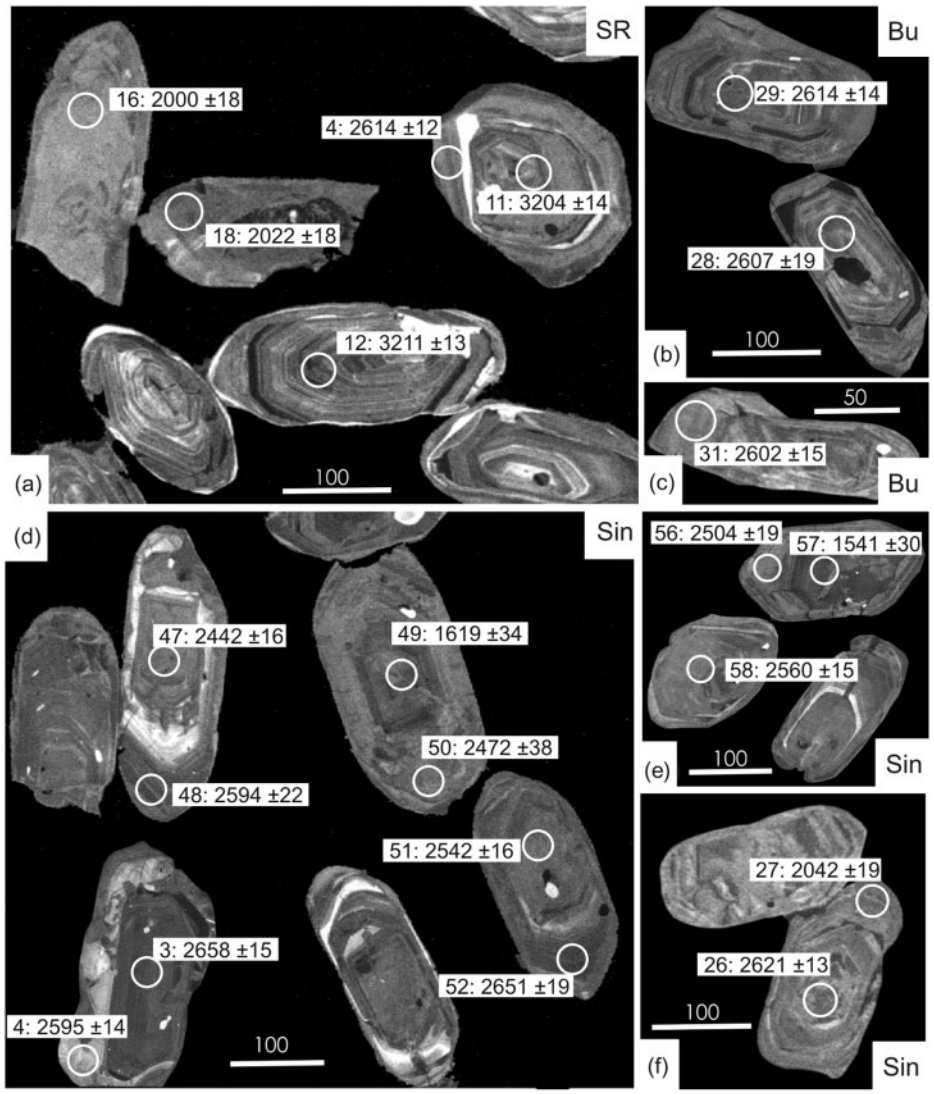

Fig. 2. CL images of zircon grain from the Beit Bridge Complex: (a) sample SR, Sand River gneiss; (b, c) sample Bu, Bulai granite; (d–f) sample Sin, Singelele gneiss. White circles indicate position of laser spots and the estimated Pb–Pb ages with 2σ error (in Ma).

The Lu–Hf analyses of eight zircon cores yielded relative homogeneous initial $^{176}Hf/^{177}Hf$ values between 0·28063 and 0·28066, which correspond to $\varepsilon Hf(t)_{initial}$ between −0·1 and −1·6, and provide evidence that the zircon cores crystallized in a magma, which was derived from a source with an average crustal residence age of $T_{DM}{}^{Hf}{}_{initial}$ 3·64 ± 0·04 Ga. A slightly higher initial $^{176}Hf/^{177}Hf$ value (0·28071) was obtained from the 3·14 Ga zircon domain (spot 32c/zrc19) interpreted to be formed during Palaeoarchaean anatexis about 140 Myr after the intrusion of the Sand River gneiss protolith (Figs 2a and 3a). The increased initial $^{176}Hf/^{177}Hf$ is consistent with the incorporation of additional radiogenic hafnium during anatectic zircon crystallization. This additional ^{176}Hf was formed by ^{176}Lu decay in the Sand River gneiss matrix between 3·28 and 3·14 Ga.

The presented hafnium model ages for the 3·28 Ga zircon cores are in line with the U–Pb age data, but older than the T_{DM} values of 3·1–3·4 Ga, which were derived by Sm–Nd whole-rock isotope analysis of the Sand River gneisses (Kröner *et al.*, 1999). The younger neodymium model ages may result from Palaeoarchaean open-system behaviour, which led to a resetting of the Sm–Nd system (see Moorbath *et al.*, 1997). In combination with the U–Pb ages, our $T_{DM}{}^{Hf}{}_{initial}$ values indicate that the crustal source was extracted from a depleted mantle reservoir about 300 Myr prior to the formation of the Sand River granitoid suite.

Bulai granite (sample Bu)

Sample Bu is a porphyric, weakly deformed granite containing K-feldspar, plagioclase, biotite and quartz,

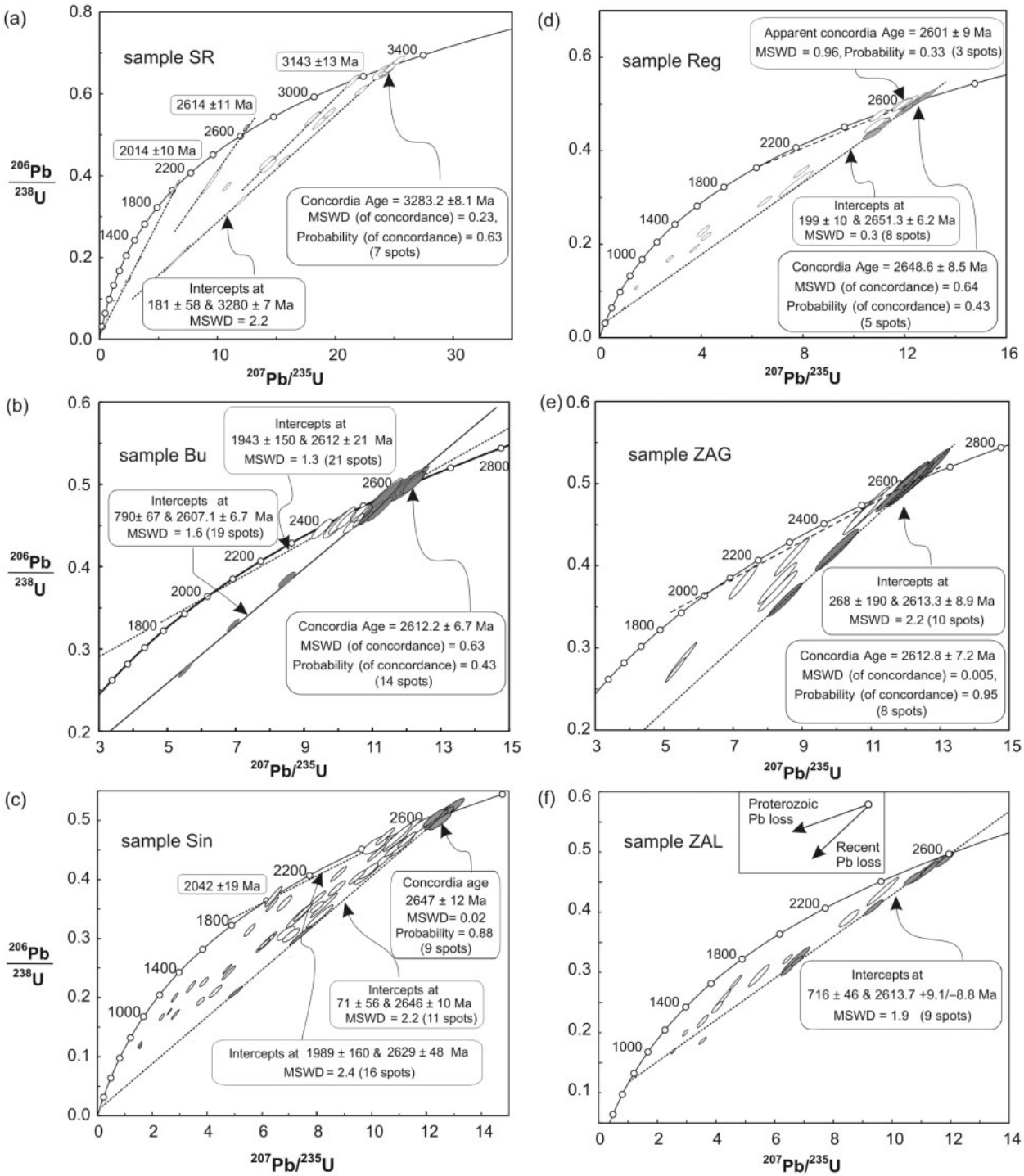

Fig. 3. Concordia diagrams for samples from the Beit Bridge Complex: (a) sample SR; (b) sample Bu; (c) sample Sin; (d) sample Reg; (e) sample ZAG; (f) sample ZAL. (For further explanation see text.)

and was taken from the type locality of the Bulai pluton (Table 1). From this sample 27 U–Pb spot analyses on 24 zircon grains and 19 Lu–Hf analyses were carried out (Tables 2 and 3; Fig. 4d–f). CL images of most zircon crystals reveal an oscillatory magmatic zoning and two bright zones (cores and rims), which are separated by a dark band of weak luminescence (Fig. 2b). Some zircon grains show additional overgrowths with a diffuse

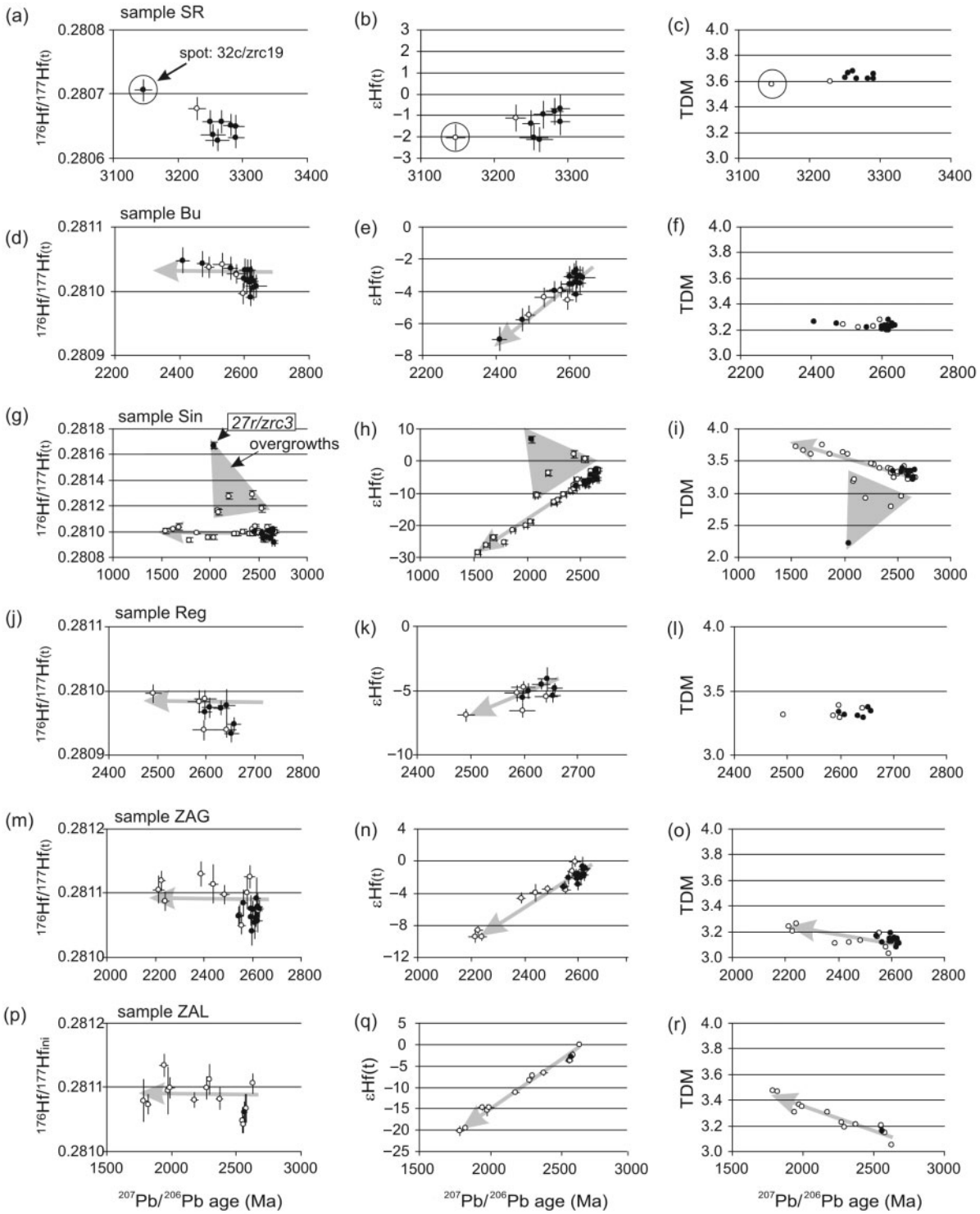

Fig. 4. Results of combined Lu–Hf and U–Pb zircon spot analyses of samples from the Beit Bridge Complex presented as $^{176}Hf/^{177}Hf(t)$ vs $^{207}Pb/^{206}Pb$ age, εHf(t) vs $^{207}Pb/^{206}Pb$ age and T_{DM} vs $^{207}Pb/^{206}Pb$ age. $^{176}Hf/^{177}Hf(t)$, initial $^{176}Hf/^{177}Hf$ calculated at the time t; t, apparent $^{207}Pb/^{206}Pb$ age obtained from the respective spot analysis; εHf(t) and T_{DM}, (hafnium model age) calculated for time t, using the constants and parameters as described in the text. •, Concordant analyses (98–102% concordance level); ○, discordant analyses.

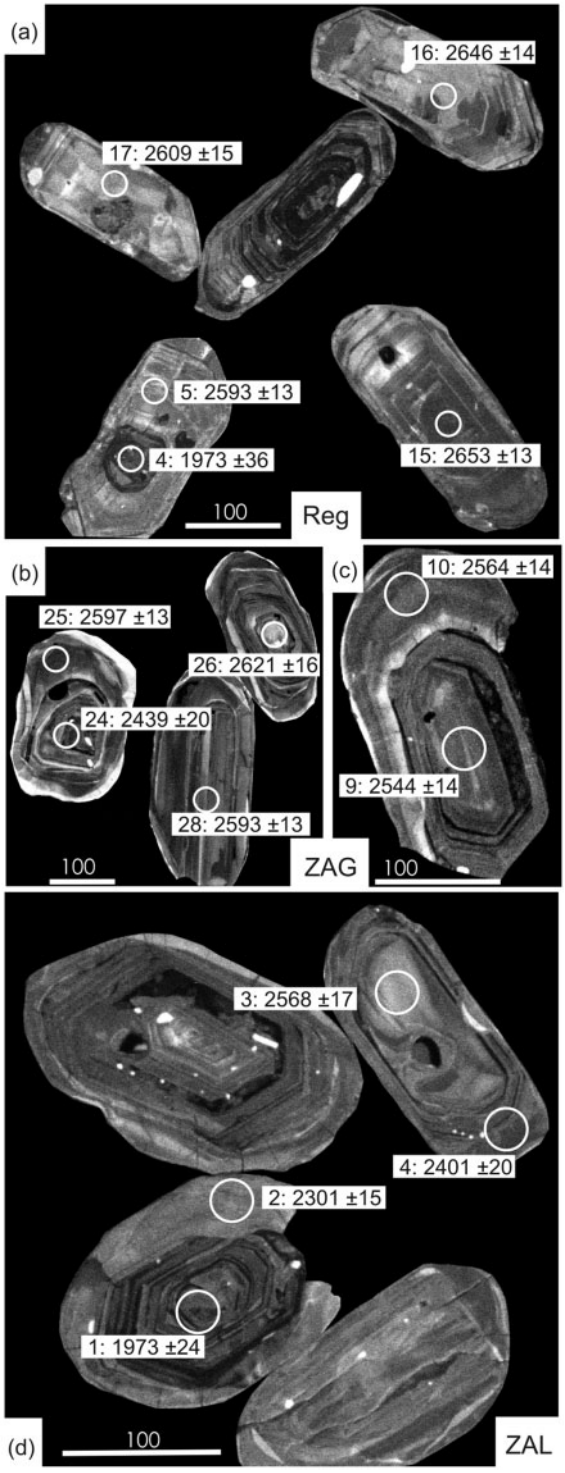

Fig. 5. Cathodoluminescence images of zircon grains from the Beit Bridge Complex: (a) sample Reg, Regina gneiss; (b, c) sample ZAG, Zanzibar granodiorite gneiss; (d) sample ZAL, Zanzibar granite gneiss. White circles indicate position of the laser spots and the estimated Pb–Pb ages with 2σ error (in Ma).

luminescence (Fig. 2c). U–Pb analyses obtained from all of these distinct zircon domains yielded within error identical ages (Fig. 2b and c), indicating that they were formed during the same magmatic event. Fourteen concordant U–Pb zircon analyses (99–101% concordance level) gave an age of 2612 ± 7 Ma, which is within error identical to an upper intercept age of 2607 ± 7 Ma obtained from five discordant analyses plus the 14 concordant zircon analyses (Fig. 3b). The lower intercept age of 790 ± 67 Ma is interpreted as geologically meaningless and may result from multiple Pb loss. Furthermore, there are seven U–Pb analyses that group together with the 14 concordant analyses on a discordia with a lower intercept at 1943 ± 150 Ma (Fig. 3b). This suggests that some zircon domains were affected by Pb loss during the Palaeoproterozoic, which is in agreement with previous age data of Barton & Sergeev (1997), Jaeckel *et al.* (1997) and Holzer *et al.* (1998).

The concordant 2612 ± 7 Ma U–Pb zircon age of the Bulai pluton is interpreted to reflect the time of emplacement. This age is identical within error to a U–Pb zircon SHRIMP upper intercept age of 2620 ± 8 Ma from a granitic phase (Kröner *et al.*, 1998) and an ID-TIMS U–Pb zircon upper intercept age of 2605 ± 2 Ma from a deformed enderbitic phase of the Bulai pluton (Barton *et al.*, 1994). However, it is significantly older than a U–Pb ID-TIMS zircon age of 2572 ± 4 Ma from a granitic phase (Barton *et al.*, 1994) and a Pb–Pb zircon evaporation age of 2587 ± 1 Ma from a deformed enderbitic phase (Kröner *et al.*, 1999). It should be noted that the younger zircon age reported by Barton *et al.* (1994) is an upper intercept U–Pb age, which results from the fitting of only two highly discordant zircon analyses. Thus, it cannot be excluded that these zircon grains were subjected to multiple Pb loss, an effect that is well documented by our *in situ* LA-ICP-MS analyses (Fig. 3b). Multiple Pb loss may also account for the young Pb–Pb evaporation age (2587 ± 1 Ma) obtained by Kröner *et al.* (1999).

Nineteen Lu–Hf analyses of concordant and discordant zircons were carried out. As shown in Fig. 4d, the zircons have initial $^{176}Hf/^{177}Hf$ ratios of about 0·28102 ± 0·00003 (2σ SD = standard deviation), which correspond to $\varepsilon Hf(t)_{initial}$ between −2·3 and −4·3 when the 2612 Ma Bulai granite crystallization age is applied to all Hf analyses. This procedure is justified, as the initial $^{176}Hf/^{177}Hf$ values of all analysed zircon domains show relatively minor variations. Nevertheless, there seems to be a small increase of the initial $^{176}Hf/^{177}Hf$ with decreasing Pb–Pb age (Fig. 4d), a feature that can be explained in different ways. Taking the errors into account, the initial $^{176}Hf/^{177}Hf$ of the apparently younger domains is identical to that obtained from most of the apparently older domains. Thus, the observed array can be interpreted (in the most simple way) to reflect multiple Pb loss in younger zircon domains, which preserved their initial

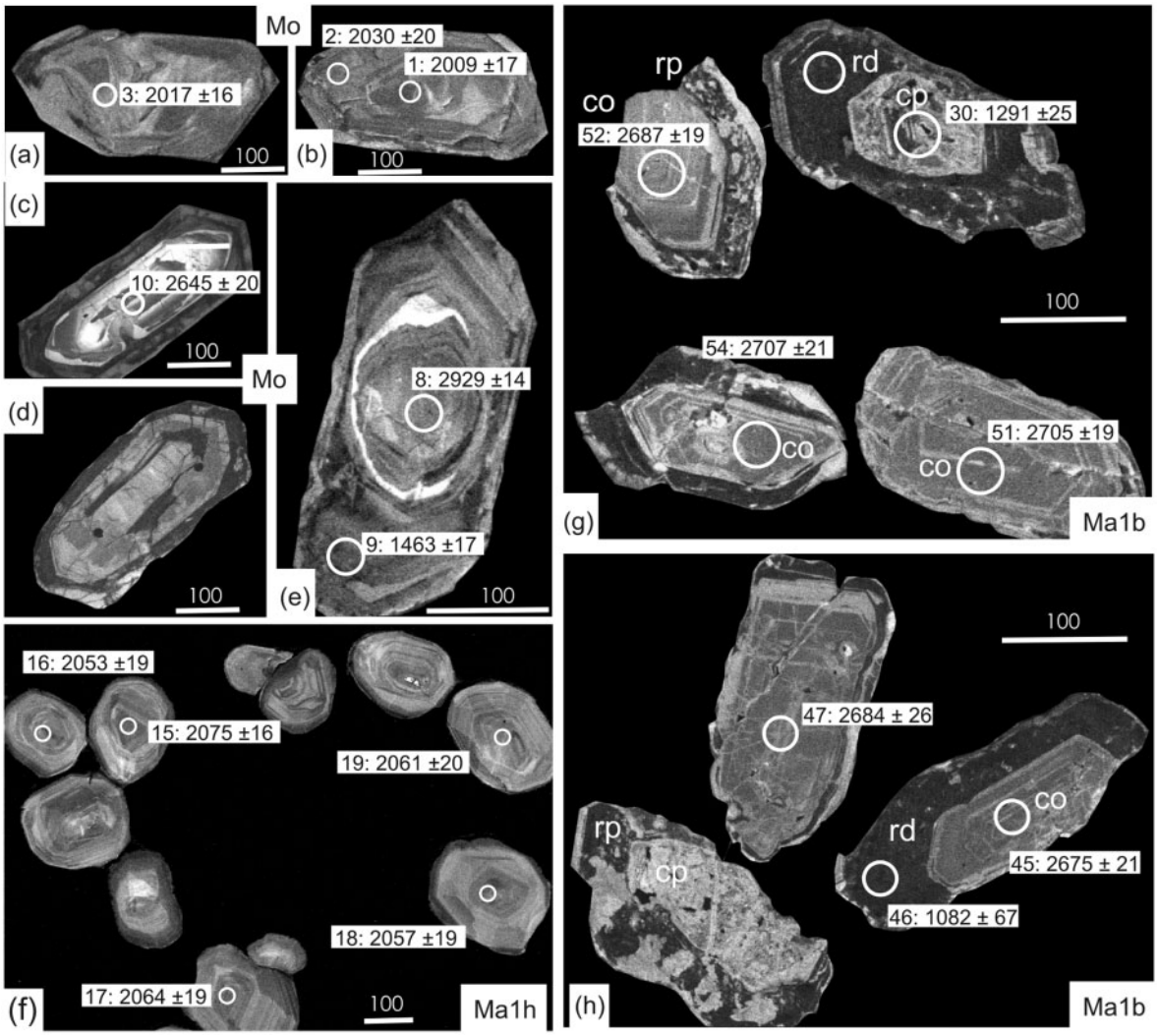

Fig. 6. Cathodoluminescence images of zircon grains from the Mahalapye Complex: (a–e) sample Mo, Mokgware granite; (f) sample Malh, garnet–biotite gneiss; (g, h) sample Malb, garnet-bearing leucosome. White circles indicate position of the laser spots and the estimated Pb–Pb ages with 2σ error (in Ma). co, core with oscillatory zoning; cp, core with a patchy zoning, rd, dark U-rich rim; rp, rim with a patchy zoning. (For further explanation see text.)

$^{176}Hf/^{177}Hf$ incorporated during magma crystallization. Alternatively, the small increase of the initial $^{176}Hf/^{177}Hf$ could reflect some minor incorporation of more radiogenic Hf in the younger zircon domains, perhaps during partial recrystallization of metamict zircon domains caused by fluid–zircon–matrix interactions. Initial hafnium model ages of 3·22 ± 0·06 Ga indicate that the Bulai granite was derived from a crustal source, which was extracted on average from a depleted mantle reservoir 600–700 Myr prior to the Bulai granite intrusion.

Singelele granodiorite gneiss (sample Sin)

Sample Sin is a high-grade granite gneiss, which was collected from the type locality at the Singelelekop near Messina (see Kröner *et al.*, 1999). It is characterized by the mineral assemblage plagioclase–K-feldspar–biotite–quartz–garnet. A total of 53 spots on 43 zircon grains from this sample were analysed for U–Pb and 45 spots for Lu–Hf (Tables 2 and 3; Figs 3c and 4g–i). The calculated $^{207}Pb/^{206}Pb$ ages show large variations from 1·54 to 2·66 Ga with 38 of 53 analyses yielding discordant results (below or above 95–105% concordance; Table 2, Fig. 3c). For many zircon grains core and rim domains were distinguished by their CL images (Fig. 2d–f). However, this textural relationship is not always reflected by the geochronological data. Based on the texture–(Pb–Pb)-age relationships three zircon groups can be distinguished: (1) zircon grains with significantly younger cores than rims (Fig. 2d); (2) zircon grains with nearly identical Pb–Pb ages of cores and rims (Fig. 2d); (3) zircon grains with older cores

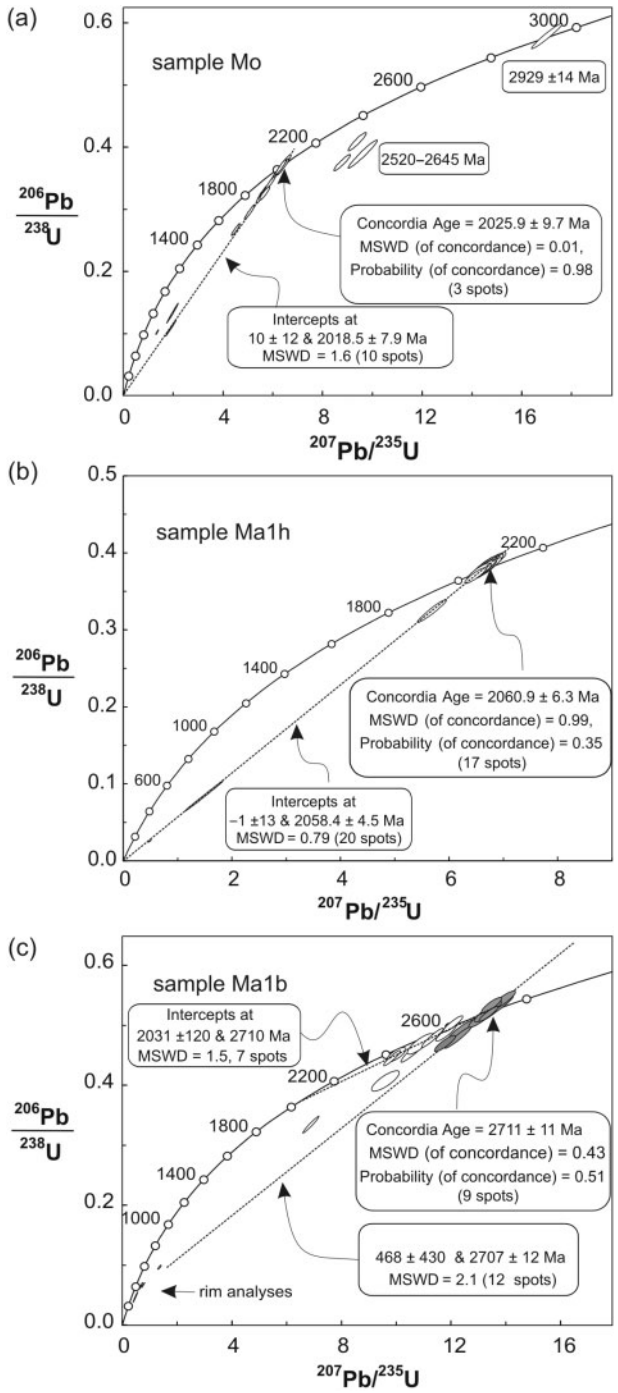

Fig. 7. Concordia diagrams for U–Pb analyses of samples from the Mahalapye Complex; (a) sample Mo; (b) sample Ma1h; (c) sample Ma1b. (For further explanation see text.)

and younger rims (Fig. 3f). These different texture–age relationships are interpreted to reflect that the zircon cores and rims grew either at the same time or at different times [textures (2) and (3)], and/or that the distinct zircon domains were affected by alteration processes causing non-zero or multiple Pb loss, effects that have been described in detail by several researchers (e.g. Vavra *et al.*, 1996; Geisler *et al.*, 2001).

Whereas the texture–age relationships are difficult to interpret, the additional Hf isotope data reveal a relatively simple story. In fact, they allow us to distinguish between zircon zones that either are affected by alteration or are the result of new zircon growth. Most zircon domains (Fig. 4g) have, despite their different apparent Pb–Pb ages, which range from 1539 to 2658 Ma, very similar initial $^{176}Hf/^{177}Hf$ values of about $0{\cdot}28099 \pm 0{\cdot}00005$ (2σ SD). Therefore, they display a simple trend in the εHf(t) vs age diagram, which is characterized by a positive correlation between apparent zircon Pb–Pb ages and εHf(t) (Fig. 4h). This trend is similar to that observed for the Bulai zircons (Fig. 4e), although more pronounced. It suggests that all of these zircon domains or grains (including most zircon cores and rims of sample Sin1; Tables 2 and 3) were formed during the same magmatic event, but were subjected to Pb loss with a different intensity. It should be noted that the calculated T_{DM}^{Hf} of these zircons become apparently older with decreasing apparent Pb–Pb age (Fig. 4i). This effect results from the two-stage model used. Thus, for the geological interpretation only initial hafnium model ages ($T_{DM}^{Hf}{}_{initial}$) can be used. These are between 3·2 and 3·5 Ga for the Singelele gneiss.

The Hf isotope analyses indicate that nearly all zircon grains or domains in sample Sin crystallized during a single magmatic event, and that the zircon grains are free of older inheritance. Thus, the oldest Pb–Pb and concordant ages obtained from these zircon domains are nearest to the crystallization age. Eleven spot analyses define a discordia with an upper intercept at 2646 ± 10 Ma, and nine of those define an identical concordia age of 2647 ± 12 Ma, which is interpreted as the intrusion age of the Singelele granite gneiss (Fig. 3c). In contrast, all younger concordant and discordant zircons, which have similar initial $^{176}Hf/^{177}Hf$ values ($0{\cdot}28099 \pm 0{\cdot}00005$, 2σ SD) are assumed to have undergone Pb loss. Among them are seven that fall on a discordia with a lower intercept age of 1989 ± 160 Ma (Fig. 3c), indicating a Palaeoproterozoic Pb loss similar to that obtained for sample Bu (Fig. 3b). However, the large scatter of the discordant analyses indicates that most zircon domains have undergone multiple Pb loss. In this context, it should be noted that the Pb–Pb evaporation ages and discordant U–Pb ID-TIMS ages of 2568–2582 Ga for the Singelele gneiss (Jaeckel *et al.*, 1997) could date the time of zircon alteration (Pb loss) rather than zircon formation.

In contrast to the zircon analyses discussed above, six zircon rim analyses, which show significantly higher initial $^{176}Hf/^{177}Hf$ values of up to 0·28166, do not follow the general εHf(t) trend and show significantly younger T_{DM}^{Hf} ages extending to 2·2 Ga (Fig. 4g–i). A concordant

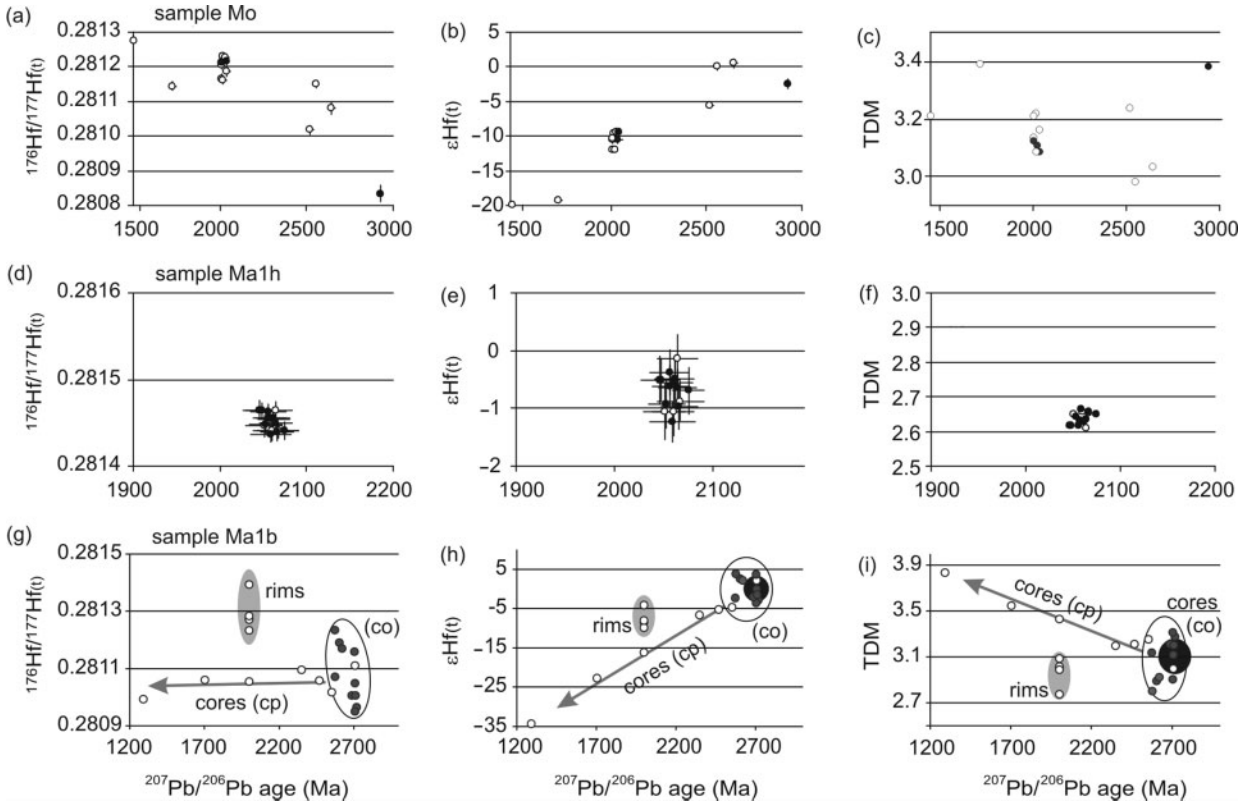

Fig. 8. Results of combined Lu–Hf and U–Pb zircon spot analyses of samples from the Mahalapye Complex presented as $^{176}Hf/^{177}Hf(t)$ vs $^{207}Pb/^{206}Pb$ age, εHf(t) vs $^{207}Pb/^{206}Pb$ age and T_{DM} vs $^{207}Pb/^{206}Pb$ age. •, Concordant analyses (98–102% concordance level); ○, discordant analyses. Black open ellipses in (g–i) mark analyses of zircon cores with oscillatory zoning (co); cp, core with a patchy zoning. Grey ellipses in (g–i) mark uranium-rich zircon overgrowths (rims). Large filled circles in (h) and (i) represent the range of initial εHf(t) and T_{DM} values, recalculated for cp zircons using the crystallization age of 2·71 Ga. (For further explanation see caption of Fig. 4 and text.)

U–Pb analysis of one of these rims (spot 27r/zrc3) indicates that it was formed at 2042 ± 19 Ma. This age is slightly younger than two Pb–Pb upper intercept ages of 2081 ± 20 Ma and 2091 ± 13 Ma, which were obtained for two other overgrowths (spots 15r/zrc19 and 20r/zrc23), but significantly older than three discordant Pb–Pb zircon ages of about 2196, 2444 and 2538 Ma (spots 54r/zrc38, 47r/zrc35 and 55r/zrc39). The three younger zircon ages suggest that these zircon overgrowths were formed during the Palaeoproterozoic, perhaps during the high-grade metamorphic event that was dated at 2·02–2·05 Ga (e.g. Barton & Sergeev, 1997; Jaeckel *et al.*, 1997; Holzer *et al.*, 1999). During this event the Singelele orthogneiss underwent partial anatexis, as evident from a few melt patches observed in the outcrops at the Singelelekop. The three older Pb–Pb ages could reflect mixing ages, which result from the analyses of older (2·65 Ga) and younger (2·04 Ga) zircon domains. These ages could not be resolved by the technique used. Consequently, their $^{176}Hf/^{177}Hf$ initial ratios should also represent mixtures.

The distinctly higher initial $^{176}Hf/^{177}Hf$ values of the six rims are thought to be due to partial melting of the Singelele orthogneiss at *c.* 2·04 Ga. During that melting event most of the *c.* 2·65 Ga zircon grains remained undissolved. Consequently, only minor amounts of Hf, incorporated by these zircon crystals (= zircon hafnium), were released into the melt from which the new zircon overgrowths were formed. Thus, the zircon overgrowths incorporated abundant radiogenic ^{176}Hf formed by ^{176}Lu decay in the granite gneiss matrix (= matrix hafnium) between 2·65 and 2·04 Ga. This assumption is best supported by spot 27r/zrc3, which shows nearly identical zircon crystallization and T_{DM}^{Hf} ages of 2·04 and 2·2 Ga, respectively (Table 2 and 3; Fig. 4i). In contrast, the other five spot analyses yield less radiogenic Hf, thereby indicating that these zircon domains incorporated a mixture of highly radiogenic 'matrix hafnium', and weakly radiogenic 'zircon hafnium', released by partial dissolution of 2·65 Ga zircons during anatexis.

In summary, the combined U–Pb and Lu–Hf analyses of the zircon grains indicate that the protolith of the Singelele orthogneiss intruded at about 2646 ± 10 Ma and that the magma contained considerable amounts of an older crust, as reflected by average crustal residence ages between 3·2 and 3·5 Ga. The Singelele gneiss underwent partial anatexis during the Palaeoproterozoic at

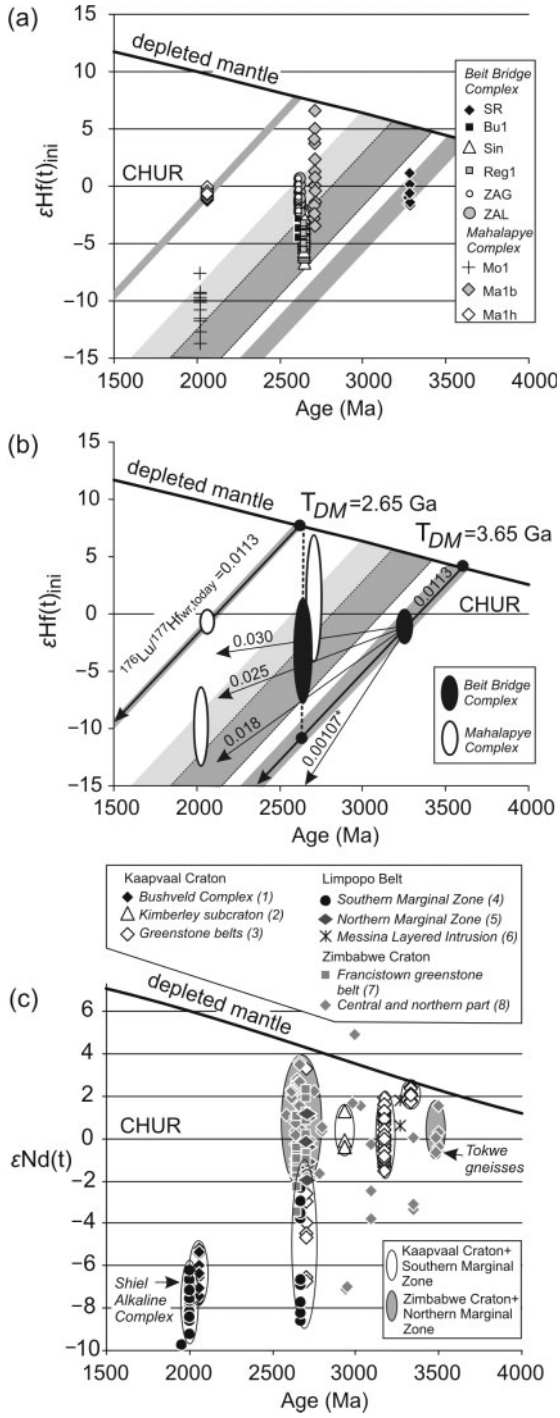

Fig. 9. (a, b) $\varepsilon Hf(t)_{initial}$ vs age diagram, showing a synopsis of all Lu–Hf results obtained from magmatic zircon domains of samples from the Central Zone of the Limpopo Belt. (a) Individual $\varepsilon Hf(t)_{initial}$ values recalculated using the intrusion age of the respective granitoids (see Figs 3 and 7). The chondritic uniform reservoir (CHUR) and the depleted mantle array were calculated with parameters defined in the text. The grey bands represent εHf(t) bulk-rock evolution trends, calculated using $^{176}Lu/^{177}Hf$ of 0·0113. (b) Summary of εHf(t) values obtained from granitoids from the Beit Bridge and Mahalapye complexes. The small black circles (T_{DM}) mark the time of juvenile crust formation in the Limpopo Belt. The arrows starting at $T_{DM} = 3{\cdot}65$ and 2·65 Ga illustrate the evolution trend of a bulk rock with a $^{176}Lu/^{177}Hf$ of 0·0113. The dotted vertical line defines the mixing line between evolved Palaeoarchaean crust and juvenile Neoarchaean crust at 2·65 Ga. The black arrows starting at 3·283 Ga (Sand River gneiss data) define the εHf(t) evolution trends of zircon (*) crystallized at 3·283 Ga in the Sand River gneiss, and of melts, which may have formed by partial anatexis (+ zircon fractionation) of the Sand River gneiss. (c) εNd(t) vs age diagram showing data for rocks from the Kaapvaal Craton, the Zimbabwe Craton and the Limpopo Belt. It should be noted that εNd(2·6–2·7 Ga) values of rocks from the Zimbabwe Craton and the Northern Marginal Zone are commonly higher than those for the Kaapvaal Craton and the Southern Marginal Zone. Data sources: (1) Maier *et al.* (2000); (2) Schmitz *et al.* (2004); (3) Wilson & Carlson (1989) and Kreissig *et al.* (2000); (4) Barton *et al.* (1995, 1996); (5) Berger *et al.* (1995); (6) Barton (1996); (7) Zhai *et al.* (2006); (8) Hamilton *et al.* (1977), Moorbath *et al.* (1986), Taylor *et al.* (1991) and Jelsma *et al.* (1996). (For further explanation see text.)

about 2·0 Ga, which caused Pb loss in many zircon domains and the formation of a few zircon overgrowths incorporating abundant highly radiogenic 'matrix hafnium'.

Regina granite gneiss (Reg)

This gneiss sample was collected from the Regina farm *c.* 30 km north of Alldays, and contains mainly plagioclase, K-feldspar, quartz, amphibole, garnet, and magnetite. The Regina gneiss is part of the Krone metamorphic terrane forming the basement below the Venetia klippen complex, which underwent an amphibolite-facies overprint at about 2·06–2·0 Ga (Barton *et al.*, 2003; Klemd *et al.*, 2003; Zeh *et al.*, 2005a, 2005b). So far, nothing is known about the timing of the orthogneiss protolith intrusions in this area. From sample Reg, 22 U–Pb spot analyses on 13 zircon grains and 11 Lu–Hf spots were analysed (Tables 2 and 3; Figs 3d and 4j–l).

The CL images indicate that most zircon grains have oscillatory zoning and some of them distinct cores and rims (Fig. 5a). Twelve U–Pb spot analyses yield similar $^{207}Pb/^{206}Pb$ ages of 2580–2660 Ma for the different domains, indicating that the grains formed during a Neoarchaean magmatic event. In detail, however, more than one age population seems to exist. Five grains yielded a concordia age of 2649 ± 9 Ma, which is identical to an upper intercept age of 2651 ± 6 Ma as defined by eight analyses (Fig. 3d). Three other zircon analyses, however, yielded a significantly younger concordia age of 2600 ± 11 Ma and one analysis a concordia age of 2530 ± 16 Ma. The remaining 10 spots gave 20–79% discordant results with $^{207}Pb/^{206}Pb$ ages that vary from 1684 to 2487 Ma. We interpret the older concordant age to represent the intrusion age of the Regina gneiss protolith, whereas the younger ages result from partial Pb loss either at about 2·0 Ga or during multiple events (inset in Fig. 3f).

All zircon grains have within error identical initial $^{176}Hf/^{177}Hf$ values of 0·28096 ± 0·00004 (2σ SD), which

correspond to $\varepsilon Hf(t)_{initial}$ of −3·4 to −5·5 and $T_{DM}^{Hf}{}_{initial}$ of 3·3–3·4 Ga. It is worth noting that these values are similar to that of the Bulai granite and to most values obtained from the Singelele gneiss.

Zanzibar granodiorite gneiss (sample ZAG)

The investigated grey gneiss sample was taken from the Seoka river bed near the Botswana–South Africa boundary (see Barton & Key, 1983). From this sample 23 U–Pb and Lu–Hf spot analyses were performed on 17 zircon grains (Tables 2 and 3; Figs 3e and 4m–o). CL images indicate complexly zoned zircon grains and most of them reveal a core and rim structure (Fig. 5b and c). In addition, there are abundant zircon grains that show parallel banding (Fig. 5b). U–Pb spot analyses provided a wide scatter of apparent Pb–Pb ages for all domains ranging between 2227 and 2629 Ma (Table 2). Some zircon grains yield within error identical ages for their core and rim (e.g. spots 9 and 10, Fig. 5c) whereas other zircon grains show apparently younger cores and older rims (e.g. spots 24 and 25, Fig. 5b). The latter indicates that the analysed core domains underwent a much stronger Pb loss than the rim domains of the same zircon.

Eight U–Pb analyses (99–101% concordance) yielded a concordia age of 2613 ± 7 Ma (Fig. 3e), which is interpreted as the time of granodiorite intrusion. Five apparently concordant zircon analyses (96–98% concordance) gave ages of around 2540 and 2596 Ma (Table 2). These ages are interpreted to result from partial Pb loss during a Palaeoproterozoic (*c.* 2·0 Ga) metamorphic event. The remaining eight spot analyses are 77–94% discordant, reflecting either partial Pb loss to zero or multiple Pb loss. It should be noted that the intrusion age of 2613 ± 7 Ma is significantly younger than the Rb–Sr whole-rock isochron age of 3227 ± 40 Ma from the same gneiss (Barton & Key, 1983). However, it is identical to or slightly younger than two SHRIMP U–Pb zircon ages of 2614 ± 13 Ma and 2659 ± 10 Ma of a granodiorite and monzonitic gneiss, respectively, which were collected from the nearby Tapalaphala river bed (Kröner *et al.*, 1999).

Lu–Hf analyses reveal that all 23 zircon spots have within error identical initial $^{176}Hf/^{177}Hf$ values of 0·28108 ± 0·00005 (2σ SD; Fig. 4m). This supports the conclusion that all investigated zircon domains were formed during the same magmatic event and that all of them underwent partial Pb loss during multiple events. This conclusion is also reflected by the array of the $\varepsilon Hf(t)$ values, which shows a straight line between −1·2 at 2·62 Ga and −9·4 at 2·2 Ga (Fig. 4n). Initial hafnium model ages between 3·01 and 3·18 Ga reveal that the Zanzibar gneiss results from remelting of substantial amounts of an older Archaean crust, which was formed on average *c.* 400–500 Myr prior to the intrusion.

Zanzibar granite gneiss (sample ZAL)

The Zanzibar granite gneiss sample was also collected in the Seoka river bed. Twenty U–Pb and 15 Lu–Hf spot analyses were obtained on 16 zircon grains from this sample (Tables 2 and 3; Figs 3f and 4p–r). Many zircon grains have cores, which are separated from their rims by dark, U-rich bands (Fig. 5d). Most of the cores show oscillatory zoning, whereas some of the rims are structureless.

U–Pb spot analyses of all zircon domains yield discordant results (97–48% discordance) with apparent Pb–Pb ages between 1785 and 2619 Ma (Table 2). However, the initial $^{176}Hf/^{177}Hf$ values of all spot analyses are identical within error (0·28108 ± 0·00005; 2σ SD). This indicates that all analysed zircon domains, comprising the different core and rim areas, must have been formed during the same magmatic event, which is also supported by the $\varepsilon Hf(t)$ and T_{DM}^{Hf} vs Pb–Pb age trends (Fig. 4q and r). The $T_{DM}^{Hf}{}_{initial}$ values indicate that the granite gneiss protolith stems from a crustal source with an average hafnium model age of 3·02–3·18 Ga, which is identical to that of the Zanzibar granodiorite.

Nine U–Pb spot analyses fall on a discordia (MSWD = 1·9) with intercepts at 2614 ± 9 Ma and 716 ± 46 Ma (Fig. 3f). The upper intercept age of 2614 ± 9 Ma is interpreted to date the time of the ZAL granite intrusion. In fact, this age is identical to that obtained from the nearby sample ZAG, which shows an identical Hf isotope composition (see above). The scatter of various data points in the concordia diagram of sample ZAL indicates than many zircon domains underwent post-crystallization multiple Pb loss, perhaps during Palaeoproterozoic and recent time (see inset in Fig. 3f).

Mahalapye Complex

Mokgware granite (sample Mo)

The investigated sample represents a medium-grained granite variety, which contains mainly K-feldspar, plagioclase, biotite and quartz. Seventeen U–Pb spot analyses on 14 zircon grains and an 14 Lu–Hf spot analyses were carried out (Tables 2 and 3). CL images indicate different zircon zoning patterns (Fig. 6a–e). Type-I zircons show U-poor cores with a bright luminescence and 'dark' U-rich overgrowths (Fig. 6c and d). Some of these cores display oscillatory zoning, whereas others are structureless–diffuse (Fig. 6d). The latter are similar to recrystallized metamict zircons as described by Vavra *et al.* (1996). Type-II zircons show a balanced luminescence throughout the entire crystal with a weak oscillatory zoning, although some of them have distinct cores and rims (Fig. 6a, b and e).

U–Pb spot analyses of most zircon domains from type-I zircon and from the oscillatory cores of type-II zircon define a discordia with intercepts at 10 ± 12 and 2019 ± 8 Ma (Fig. 7a). The upper intercept age is within

error identical to a concordia age of 2026 ± 10 Ma, which was calculated from three zircon analyses (Fig. 7a). It is interpreted to reflect the time of granite emplacement. In contrast, two younger, strongly discordant Pb–Pb analyses, which have apparent Pb–Pb ages of about 1463 and 1721 Ma, are interpreted to result from multiple Pb loss after 2·03 Ga. These two analyses show the highest U contents (1432 and 2832 ppm, respectively). In addition, a few zircon cores give significantly older ages. One zircon core yields a concordant age of 2929 ± 14 Ma (spot 8c/zrc6), and three others have discordant Pb–Pb ages between 2520 and 2645 Ma (Fig. 7a). The age data indicate that the Mokgware granite intruded at 2019 ± 8 Ma and contains some Archaean crustal components. This is in agreement with the results obtained from the Lu–Hf spot analyses (Fig. 8a–c), which reveal Archaean hafnium model ages between 3·0 and 3·4 Ga for the different zircon domains (Fig. 8c).

The 10 spots that define the 2·02 Ga Mokgware discordia age show slightly variable initial $^{176}Hf/^{177}Hf$ of 0·28120 ± 0·00005 (2σ SD). This suggests that magma homogenization during zircon crystallization was incomplete ($T_{DM}^{Hf}{}_{initial}$ = 3·1–3·2 Ga; $\varepsilon Hf(t)_{initial} = -10{\cdot}5 \pm 1{\cdot}9$). The inherited components with variable age (>2·02 Ga) and Hf isotope composition ($\varepsilon Hf_{(at\ 2019\ Ma)} = -11{\cdot}3$ to −20·1) clearly point to a heterogeneous crustal source.

It should be noted that the assimilation–melting of Archaean material during the Palaeoproterozoic granite formation in the Mahalapye Complex is not restricted to the Mokgware granite, but has also been reported from the nearby Mahalapye granite (Fig. 1). This granite intruded at 2023 ± 11 Ma and contains abundant zircon xenocrysts with Pb–Pb ages between 2·45 and 3·15 Ga (McCourt & Armstrong, 1998). The age of the oldest xenocryst is well within the range of the hafnium model ages, which are estimated in this study for the Mogkware granite.

Lose quarry samples

The Lose quarry is situated *c.* 50 km south of Palapye (Fig. 1) and exposes ortho- and paragneisses that are transected by garnet-bearing leucosomes. The leucosomes form veins of centimetre to several metres width, which occupy *c.* 25% of the outcrop volume. A detailed description of this outcroup, lithologies and metamorphic conditions has been given by Chavagnac *et al.* (2001) and Hisada *et al.* (2005). For this study two samples were collected, a dark garnet–biotite gneiss and a leucosome.

Garnet–biotite gneiss (sample Malh). This sample shows melanocratic and leucocratic domains on the centimetre scale, both of which contain garnet, biotite, plagioclase, quartz and gem quality zircon grains. CL images show typical magmatic zoning patterns such as oscillatory zoning, sector zoning and a similarly bright luminescence for all zircon grains (Fig. 6f). Twenty U–Pb spot analyses on 20 zircon grains and 15 Lu–Hf spot analyses were carried out (Table 2 and 3). All U–Pb analyses fall on a discordia with intercepts at zero and 2058 ± 5 Ma, which is identical to the concordia age of 2061 ± 6 Ma as defined by 17 analyses (Fig. 7b). The Lu–Hf analyses of all zircon grains yielded identical initial $^{176}Hf/^{177}Hf$ of 0·28145 ± 0·00002 (Fig. 8d), which corresponds to $\varepsilon Hf(t)_{initial}$ between 0·1 and −1·2 (Fig. 8e) and $T_{DM}^{Hf}{}_{initial}$ of 2·61–2·67 Ga (Fig. 8f).

Similar characteristic CL patterns, Hf isotope data and identical U–Pb ages of all zircon grains indicate that the protolith of the garnet–biotite gneiss was a magmatic rock, perhaps a diorite, which was emplaced at 2061 ± 6 Ma, and syn- or post-intrusively deformed and metamorphosed. Our LA-ICP-MS U–Pb age is identical to, but more precise than, the zircon SHRIMP U–Pb upper intercept age of 2053 ± 21 Ma, which was obtained by McCourt & Armstrong (1998) from a granodiorite dyke of the same outcrop. In contrast to McCourt & Armstrong (1998), we did not find zircon xenocrysts with ages between 2·6 and 3·19 Ga in our sample.

The proposed magmatic origin for the garnet–biotite gneiss contradicts the findings of Chavagnac *et al.* (2001), who designated texturally similar rocks as migmatitic paragneisses, which were interpreted to be due to *in situ* anatexis of metagreywackes. However, in such a scenario one would expect to find a more heterogeneous zircon population with different inherited cores (see Zeh *et al.*, 2003). Nevertheless, some sedimentary rocks must have been present in the Lose quarry, as documented by sillimanite- and andalusite-bearing metapelites (Hisada *et al.*, 2005).

Garnet-bearing leucosome (Malb). This sample was taken from a 5 m thick leucosome dyke, adjacent to sample Malh. It contains minor garnet in a leucocratic K-feldspar–plagioclase–quartz matrix. CL images of zircon grains reveal internal structures that are completely different from those from sample Malh (Fig. 6g and h). Most zircon grains have bright, U-poor cores with oscillatory zoning (co), which are surrounded by dark, U-rich rims (rd) (Fig. 6g and h). In some zircon grains the oscillatory zoning patterns of the cores are partly or completely replaced by patchy zoning patterns (cp), which can also be observed in some dark zircon overgrowths, where these patterns commonly start at the rims and grade inward (rp) (Fig. 6g and h). In other zircon grains such patterns are observed to form bands that penetrate both the cores and rims. Judging from these observations, we conclude that the patchy patterns result from recrystallization of metamict zircon domains, perhaps as a result of fluid–zircon interaction (see Rizvanova *et al.*, 2000; Geisler *et al.*, 2001). Most grains have euhedral cores (Fig. 6g and h), indicating that the dark U-rich rims represent zircon overgrowths and are not the result of

alteration processes. The latter commonly cause the formation of reaction fronts, which cross-cut older zircon zoning patterns (e.g. Vavra *et al.*, 1996).

Twenty-five U–Pb spot analyses on 20 zircon grains and 22 Lu–Hf spot analyses were performed (Tables 2 and 3). Most core U–Pb analyses, in particular those of oscillatory zoned domains (co), fall on a discordia with intercept ages at around 468 and 2707 ± 12 Ma (Fig. 7c). The latter age is within error identical to a concordia age of 2711 ± 11 Ma obtained from nine analyses. Seven spots, including two analyses of patchy zircon cores, yield somewhat younger Pb–Pb ages of about 2·47–2·62 Ga. They plot on a discordia with a lower intercept age of 2031 ± 120 Ma when forced through 2711 Ma, the age of the nine concordant spots. In contrast to the oscillatory zoned cores (co), no reliable U–Pb ages were obtained from the zircon rims (domains rd, rp), and from most of the patchy zircon cores (cp). These uranium-rich domains (1815–8477 ppm) yield strongly discordant U–Pb analyses, with Pb–Pb intercept ages between 2·35 and 1·1 Ga (Fig. 7c). This indicates that all of these domains underwent Pb loss, a feature commonly observed in uranium-rich zircons (e.g. Vavra *et al.*, 1996; Mezger & Krogstad, 1997). Judging from the textural relationship we believe that the U-rich zircon overgrowths grew during leucosome formation and crystallization. This assumption agrees with the fact that the zircon grains in leucosomes are commonly uranium-rich (e.g. Rubatto *et al.*, 2001; Zeh *et al.*, 2003). Because the leucosome veins observed in this study cross-cut the garnet–biotite (diorite) gneiss, the zircon rims must be younger than 2·06 Ga. This agrees with a U–Pb monazite age of 2002 ± 10 Ma, and Sm–Nd garnet ages between 2023 ± 7 and 1989 ± 38 Ma, which were reported for the leucosomes (Chavagnac *et al.*, 2001). Thus for $\varepsilon Hf(t)_{initial}$ and hafnium model age calculations we use an age of 2·0 Ga for the zircon rim analyses (Table 3).

Initial $^{176}Hf/^{177}Hf$ of the cores yield a wide scatter from 0·28095 to 0·28124 (Fig. 8g). This scatter is most pronounced for the >95% concordant analyses (mostly oscillatory zircon cores), where the εHf(t) values vary from −3·5 to 3·8 and the T_{DM}^{Hf} values are between 2·9 and 3·3 Ga (Fig. 8h and i). In contrast, the εHf(t) and T_{DM}^{Hf} data for the discordant, patchy zircon cores (cp) show well-defined positive or negative trends when correlated with the apparent $^{207}Pb/^{206}Pb$ age data (Fig. 8h and i). This indicates that the 'discordant' cores underwent multiple Pb loss, whereas their initial $^{176}Hf/^{177}Hf$ remained nearly unchanged. Thus, when these zircon analyses are recalculated with the 'true' zircon crystallization age of 2711 Ma their resulting $\varepsilon Hf(t)_{initial}$ (−0·6 to 2·6) and $T_{DM}^{Hf}{}_{initial}$ values (3·1 ± 0·3 Ga) are well within the range of the concordant analyses (Fig. 8h and i).

The Lu–Hf analyses of the uranium-rich overgrowths yield initial $^{176}Hf/^{177}Hf_{2\cdot0\,Ga}$ of 0·28123–0·28139, indicating that they contain more radiogenic hafnium than the zircon cores (Fig. 8g), and that the rims crystallized during a later (anatectic) event than the cores in the same precursor rock, similar to the scenario proposed for sample Sin (see above). It should be noted that most hafnium model ages obtained from the zircon cores and rims are higher ($T_{DM}^{Hf}{}_{initial} = 2\cdot8$–$3\cdot2$ Ga) than those previously estimated by Sm–Nd whole-rock analyses of leucosomes from the Lose quarry ($T_{DM}^{Nd} = 2\cdot7$–$2\cdot9$ Ga; Chavagnac *et al.*, 2001). This may have the same cause (open-system behaviour; see Moorbath *et al.*, 1997) as previously discussed for the Sand River gneiss.

The combined U–Pb and Lu–Hf data indicate that the zircon cores in sample Malb were formed at 2711 ± 11 Ma. The wide scatter of the $\varepsilon Hf(t)_{initial}$ values may indicate that the cores were formed in different magmatic rocks, which contained different amounts of recycled Palaeoarchaean crust [$\varepsilon Hf(t)_{initial} = -3\cdot5$; $T_{DM}^{Hf}{}_{initial} \geq 3\cdot3$ Ga] and juvenile Neoarchaean crust [$\varepsilon Hf_{initial} = +6\cdot3$; $T_{DM}^{Hf}{}_{initial} \leq 2\cdot8$ Ga]. During the Palaeoproterozoic (at *c.* 2·0 Ga) this heterogeneous crust was remelted and new zircon overgrowths formed.

The isotope dataset and the CL images indicate that the garnet–biotite (diorite) gneiss (sample Malh) is neither the palaeosome nor the restite of the abundant leucosomes exposed in the Lose quarry. It seems more likely that the leucosomes were formed by partial anatexis of a deeper crustal source, rather than from *in situ* anatexis as proposed by Chavagnac *et al.* (2001). In fact, the thick leucosome veins of the Lose quarry may represent magma conduits, which are genetically unrelated to the surrounding diorite gneiss. Our isotope data in combination with the field relationships from the Lose quarry support a model in which the diorite gneiss protolith results from Palaeoproterozoic (2·06 Ga) melting of a juvenile Neoarchaean lower crust formed at 2·6–2·7 Ga. In contrast, the younger garnet-bearing leucosomes resulted from Palaeoproterozoic melting of the upper crust, which was predominantly made up of pre-Neoarchaean material and affected by magmatism at *c.* 2·7 Ga.

DISCUSSION

Zircon formation vs alteration

From our combined CL, U–Pb and Lu–Hf dataset we are able to discriminate between zircon growth and alteration processes. Zircon domains affected by single or multiple Pb loss yield initial $^{176}Hf/^{177}Hf$ values that are identical within error to those of unaffected zircon domains formed at the same time. This is generally reflected by zircon spot analyses obtained from the samples Bu, Sin, ZAG, ZAL and Malb, as the analyses of co-genetically formed zircon domains form horizontal lines in the $^{176}Hf/^{177}Hf_{initial}$ vs apparent Pb–Pb age diagram and show a positively correlated array in the εHf(t) vs apparent Pb–Pb age

diagram (Figs 4 and 8). In contrast, newly formed zircon overgrowths, which may result from partial anatexis of the orthogneisses during later events, always show significantly higher radiogenic $^{176}Hf/^{177}Hf_{initial}$ and εHf(t) than the older zircon domains. This is well demonstrated by zircon analyses from samples Sin and Ma1b (Fig. 4g and i), and agrees with results obtained from migmatitic gneisses from the Antarctic Peninsula (Flowerdew *et al.*, 2006). Therefore, our results indicate that the hafnium isotopes once incorporated into a certain zircon domain will not (or only slightly) be fractionated during later metamictization and fluid-driven processes, which generally lead to partial or complete Pb loss in distinct zircon domains (e.g. Vavra *et al.*, 1996; Rizvanova *et al.*, 2000; Geisler *et al.*, 2001). Increased initial $^{176}Hf/^{177}Hf$ values of zircon overgrowths with respect to zircon cores indicate that the overgrowths were formed during partial anatexis, with most zircon cores not being dissolved.

Timing of magmatism and metamorphism

The combined information from CL images, U–Pb and Lu–Hf isotope spot analyses provides evidence that zircon grains in granites and orthogneisses of the Limpopo Central Zone were formed during distinct magmatic events at about 3·28, 2·71, 2·65, 2·61, 2·06 and 2·02 Ga. In addition, our data indicate that some zircon domains were formed during anatectic events at about 3·14, 2·61 and 2·02 Ga, whereas others were subject to single and/or multiple Pb loss. Our age data combined with those from previous studies (e.g. Jaeckel *et al.*, 1997; Holzer *et al.*, 1998, 1999; Kröner *et al.*, 1998, 1999; McCourt & Armstrong, 1998) indicate that granitoid rocks with ages of 3·28 Ga and 2·61–2·65 Ga are restricted to the Beit Bridge Complex, whereas granitoids with ages of 2·06 and 2·02 Ga occur only in the Mahalapye Complex (Fig. 1). However, zircon xenocrysts reveal that the Mahalapye Complex also comprises large quantities of Archaean magmatic rocks formed at 2·52–2·8 Ga and >2·9–3·15 Ga (McCourt & Armstrong, 1998, and references therein). In fact, most xenocryst ages of the Mahalapye granitoids are identical to orthogneiss protolith ages obtained from the Beit Bridge Complex. This also holds true for the zircon cores with an age of 2711 ± 11 Ma found in the Lose quarry leucosomes. Their ages are identical to U–Pb SHRIMP ages of 2718 ± 5 and 2717 ± 3 Ma obtained from granodiorite or dacite samples from the Beit Bridge Complex (Kröner *et al.*, 1999).

A concordant 3143 ± 13 Ma zircon age and rare 2614 ± 11 Ma zircon overgrowths around 3·28 Ga zircon cores indicate that the Sand River gneiss of the Beit Bridge terrane was subject to partial anatexis during the Palaeo- and Neoarchaean, respectively. So far, the reason for the Palaeoarchaean thermal overprint, which is also suggested by the age data of Barton *et al.* (1977, 1990) and our hafnium isotope results (see above), is not clear. The Neoarchaean event was obviously induced by the voluminous granite intrusions in the Central Zone, comprising the Singelele gneiss (2647 ± 12 Ma), the Regina gneiss (2649 ± 9 Ma), the Zanzibar gneiss (2613 ± 7 Ma), and the Bulai pluton (2612 ± 7 Ma). In fact, these granitic intrusions occurred contemporaneously with the Razi granite of the Northern Marginal Zone (2627 ± 7 Ma; Mkweli *et al.*, 1995; 2·52–2·67 Ga: mostly discordant ages of Frei *et al.*, 1999), and the Matok granite of the Southern Marginal Zone (2620 ± 75: Barton *et al.*, 1983; 2667–2664 Ma: Barton *et al.*, 1992; 2643 ± 1 Ma: Kreissig *et al.*, 2001).

Numerous U–Pb analyses provide evidence that new zircon overgrowths were formed during partial anatexis of the Sand River and Singelele orthogneisses at 2·02–2·04 Ga. In addition, the U–Pb analyses indicate that many zircon grains and/or domains in orthogneisses from the Beit Bridge Complex underwent Pb loss at the same time. This is well supported by data from the Bulai granite, the Singelele gneiss, the Regina gneiss and the Zanzibar gneiss (Fig. 3b–e). We assume that new zircon growth as well as partial or complete Pb loss at about 2·02 Ga is related to structural–metamorphic processes, which affected the Central Zone during the Palaeoproterozoic, in agreement with data and conclusions suggested by several other workers (e.g. Jaeckel *et al.*, 1997; Holzer *et al.*, 1998, 1999; Kröner *et al.*, 1999; Zeh *et al.*, 2004; Buick *et al.*, 2006). During the Palaeoproterozoic parts of the Central Zone were affected by a high-grade metamorphic event, as confirmed by petrological data from the Messina, Alldays and Mahalapye areas (Van Reenen *et al.*, 2004; Zeh *et al.*, 2004; Hisada *et al.*, 2005; Buick *et al.*, 2006), whereas the area around the Venetia kimberlite pipes underwent amphibolite-facies metamorphism (Barton *et al.*, 2003; Klemd *et al.*, 2003; Zeh *et al.*, 2005a, 2005b).

Crustal evolution of the Central Zone

Palaeoarchaean granitoids

The Lu–Hf isotope data indicate that the 3·28 Ga Sand River TTG suite results from melting of a crust with an average crustal residence age of $T_{DM}^{Hf}{}_{initial} = 3{\cdot}64 \pm 0{\cdot}04$ Ga. This indicates that the oldest crust of the Limpopo Central Zone was formed *c.* 300–400 Myr prior to the formation of the Sand River TTG suite. It is interesting to note that the *c.* 3·6–3·7 Ga hafnium model age is identical to a Pb–Pb SHRIMP age of a single detrital zircon grain from a pelitic schist of the Beit Bridge formation (Kröner *et al.*, 1998). This suggests that the oldest crust constituting the Central Zone was recycled immediately after its formation. Nevertheless, a detrital zircon U–Pb SHRIMP age of 3·8 Ga, as reported by Armstrong *et al.* (1988), indicates that the Limpopo Belt may contain even older crust, which, however, is not confirmed by our data.

The $T_{DM}^{Hf}{}_{initial}$ values obtained from the Limpopo Belt are similar to those calculated for felsic rocks of the Barberton greenstone belt (Amelin *et al.*, 2000; $T_{DM}^{Hf} = 3{\cdot}61–3{\cdot}75$ Ga), and to Sm–Nd isotope data for basic and ultrabasic rocks from the Kaapvaal Craton (Wilson & Carlson, 1989) and for felsic rocks of the Tokwe segment of the Zimbabwe Craton ($T_{DM}^{Nd} = 3{\cdot}55–3{\cdot}67$ Ga, data from Moorbath *et al.*, 1986; Taylor *et al.*, 1991). Similarly to the Sand River gneiss area, the Tokwe segment also contains a minor 3·75–3·8 Ga zircon population (Dodson *et al.*, 1988). This suggests that the Sand River TTG suite and some of the associated metasedimentary rocks could be part of the same Palaeoarchaean 'granite–greenstone belt crust', which now constitutes the cratons south and north of the Limpopo Belt. However, these similarities do not necessarily mean that these 'granite–greenstone belt crusts' were formed in a close geographical proximity to each other.

Neoarchaean and Palaeoproterozoic granitoids

The protoliths of all investigated Neoarchaean orthogneisses of the Beit Bridge Complex (Bulai granite, Singelele gneiss, Regina gneiss, Zanzibar gneiss) intruded between 2·65 and 2·61 Ga. Zircon grains from these granitoids show $\varepsilon Hf(t)_{initial}$ values between +0·5 and −7·1 (Fig. 9a and b), and $T_{DM}^{Hf}{}_{initial}$ of 3·01–3·46 Ga. Similar $T_{DM}^{Hf}{}_{initial}$ values are also obtained from the 2·5–2·9 Ga zircon xenocrysts of the Mokgware granite from the Mahalapye Complex. In contrast, the 2·71 Ga zircon cores from the Lose quarry leucosome of the Mahalapye Complex (sample Ma1b) show a wide range of $\varepsilon Hf(t)_{initial}$ from −3·7 to +6·3, and T_{DM}^{Hf} between 2·76 and 3·32 Ga. The highest $\varepsilon Hf(t)_{initial}$ of these zircon grains is close to that of the depleted mantle (Fig. 9a).

The oldest $T_{DM}^{Hf}{}_{initial}$ age of 3·46 Ga is based on a zircon grain from the 2·65 Ga Singelele orthogneiss. This model age is only slightly younger than those obtained from the nearby Sand River orthogneiss (3·60–3·68 Ga), indicating that the Singelele gneiss may have formed by partial melting of Sand River gneiss equivalents at about 2·65 Ga. In fact, anatexis of the Sand River gneiss during the Neoarchaean is reflected by zircon overgrowths, which yielded U–Pb ages of about 2·61 Ga (Fig. 3a). The minor age differences between the Singelele granite gneiss intrusion (2·65 Ga) and the Sand River gneiss anatexis (2·61 Ga) may be explained by partial Pb loss of the analysed zircon overgrowths. Apart from the 3·46 Ga hafnium model age, most zircon grains of the Singelele gneiss yield somewhat younger $T_{DM}^{Hf}{}_{initial}$ values of 3·17–3·40 Ga (Fig. 9a), which correspond to higher initial $^{176}Hf/^{177}Hf$ and $\varepsilon Hf(t)_{initial}$ (Figs 4g, h, and 9a). It should be noted that the younger hafnium model ages of the Singelele gneiss are identical to those obtained from the Bulai pluton ($T_{DM}^{Hf}{}_{initial} = 3{\cdot}17–3{\cdot}28$ Ga) and the Regina gneiss ($T_{DM}^{Hf}{}_{initial} = 3{\cdot}25–3{\cdot}37$ Ga), but are predominantly older than those obtained from the Zanzibar granodiorite ($T_{DM}^{Hf}{}_{initial} = 3{\cdot}01–3{\cdot}18$ Ga) and Zanzibar granite gneiss ($T_{DM}^{Hf}{}_{initial} = 3{\cdot}04–3{\cdot}18$ Ga) (Fig. 9a and b).

In general, two models can explain the younger hafnium model ages of the Neoarchaean gneisses with respect to those of the Palaeoarchaean Sand River gneisses. According to the first model, abundant zircon was fractionated during partial melting of the *c.* 3·65 Ga 'Sand River gneiss' crust at 2·65 Ga and thereby causing the ascending magmas to have higher radiogenic hafnium (matrix hafnium) than the re-molten precursor rocks. It should be noted that this model does not require the addition of any juvenile magma at *c.* 2·65 Ga. If true, however, the Neoarchaean gneisses should have higher $^{176}Lu/^{177}Hf$ ratios than their Palaeoarchaean precursor rocks. As illustrated in Fig. 9b, the Neoarchaean gneisses should have whole-rock $^{176}Lu/^{177}Hf$ ratios between 0·018 and 0·030 if they are formed by partial anatexis of Sand River gneiss. These values are higher than the mean Archaean–Palaeoproterozoic crustal composition ($^{176}Lu/^{177}Hf = 0{\cdot}0113$) as suggested by Taylor & McLennan (1985) and Wedepohl (1995). Unfortunately, there are no $^{176}Lu/^{177}Hf$ whole-rock isotope data available, which could prove or disprove this model.

The second model is based on the assumption that all of the Neoarchaean gneisses represent mixtures of remelted *c.* 3·65 Ga crust (Sand River gneiss equivalents) and a juvenile component derived from the depleted mantle at *c.* 2·65 Ga. So far, there is only one Rb–Sr isotope dataset, that of Watkeys & Armstrong (1985), which provides evidence for the existence of Neoarchaean juvenile magmas in the Limpopo Belt, whereas all the Lu–Hf and Sm–Nd data are ambiguous (Fig. 9a). The Rb–Sr dataset was derived from alkaline lamprophyre dykes, which transect the 2·61 Ga Bulai granite. These dykes yield an initial $^{86}Sr/^{87}Sr$ of 0·70228 and Rb–Sr and Pb–Pb ages of 2671 ± 163 Ma and 2641 +125/−131 Ma, respectively (Watkeys & Armstrong, 1985). These data are interpreted to reflect the formation of the lamprophyres from a Neoarchaean primitive mantle source beneath the Central Zone of the Limpopo Belt, which was 'fertilized' by an incompatible trace element-enriched fluid derived from the dehydration of a slab, which subducted beneath the region at about 2·7 Ga.

Further evidence for the existence of Neoarchaean juvenile magmas underneath the Limpopo Belt is provided by our zircon Hf isotope data from the Mahalapye Complex. The first set of evidence comes from zircon grains of the 2·061 Ga garnet–biotite (diorite) gneiss of the Lose quarry, which shows hafnium model ages between 2·61 and 2·67 Ga (Fig. 9a). They indicate that the protolith of the diorite gneiss perhaps results from melting of a lower mafic crust, which was derived from the

depleted mantle during the Neoarchaean. Identical initial $^{176}Hf/^{177}Hf$ ratios obtained from all zircon grains of sample Malh (Fig. 8d–f) may reflect that the source region of the diorite melt was homogeneous at 2·06 Ga. Alternatively, the homogeneity of the initial $^{176}Hf/^{177}Hf$ could also result from intense mixing between a Palaeoproterozoic (2·06 Ga) juvenile magma and a 'heterogeneous' Neo- to Palaeoarchaean crust (<2·6 Ga). This possibility, however, is considered to be less likely. In fact, there is no evidence for the formation (existence) of any juvenile Palaeoproterzoic magma throughout the Limpopo Belt and the adjacent Kaapvaal and Zimbabwe Cratons (see Fig. 9c). Even the rocks of the nearby mantle-derived Bushveld layered intrusion (Fig. 1), which has the same intrusion age as the Lose quarry diorite (2·06 Ga, Walraven & Hattingh, 1993; Buick *et al.*, 2001), show Archaean neodymium model ages between 3·0 and 3·7 Ga (Maier *et al.*, 2000), which are much older and more variable than the hafnium model ages obtained from the Lose quarry diorite.

The second set of evidence is provided by $\varepsilon Hf(t)_{initial}$ values of +6·3 to −3·7, as obtained from the 2·7 Ga zircon cores of the Lose quarry leucosome, which itself was formed during the Palaeoproterozoic at *c.* 2·0 Ga (Fig. 9a). The most positive $\varepsilon Hf(t)_{initial}$ is close to that of the depleted mantle (Fig. 9a) and, thus, suggests that zircon was formed in a juvenile magma at *c.* 2·7 Ga. The large scatter of the $\varepsilon Hf(2{\cdot}71\ Ga)_{initial}$ values of the zircon cores conforms with an interpretation that the leucosome of the Lose quarry was formed by anatexis of a mixed crust, which contained Palaeoarchaean (T_{DM}^{Hf} >3·3 Ga) and juvenile Neoarchaean components (T_{DM}^{Hf} = 2·7–2·8 Ga). Recycling of Palaeoarchaean crust during the Palaeoproterozoic is reflected by negative $\varepsilon Hf(t)_{initial}$ values of −7·1 to −12·6 obtained from zircon grains of the Mokgware granite (Fig. 9a).

Geotectonic model for the Neoarchaean–Palaeoproterozoic evolution

The formation of juvenile magmas at 2·6–2·7 Ga, as suggested from the Lose quarry data and the Bulai lamprophyes, is probably linked with the formation of the abundant Neoarchaean TTGs and greenstone belts, which constitute wide parts of the Zimbabwe Craton to the north of the Limpopo Belt (e.g. Hamilton *et al.*, 1977; Moorbath *et al.*, 1986; Taylor *et al.*, 1991; Jelsma *et al.*, 1996; Zhai *et al.*, 2006). As shown in Fig. 9c, most magmatic rocks of these greenstone belts show positive to slightly negative $\varepsilon Nd(2{\cdot}6–2{\cdot}7\ Ga)$ values between +3·8 to −2·2, indicating the formation of new juvenile crust as well as the recycling of some older material during the Neoarchaean. Figure 9c also shows that the $\varepsilon Nd(2{\cdot}6–2{\cdot}7\ Ga)$ data from the Zimbabwe Craton overlap with those of the Northern Marginal Zone, which is interpreted to represent an active continental, Andean-type, margin at 2·7 Ga (Berger & Rollinson, 1997). In contrast, rocks from the Neoarchaean greenstone belts of the Kaapvaal Craton and the Southern Marginal Zone generally show lower $\varepsilon Nd(2{\cdot}6–2{\cdot}7\ Ga)$ values, indicating their different crustal evolution, which is also documented by their different Pb isotope data [see compilation by Barton *et al.* (2006)].

The occurrence of juvenile and mixed 2·6–2·7 Ga magmatic rocks in the Limpopo Central Zone is explained by a model that starts with the Neoarchaean subduction of juvenile oceanic crust underneath evolved pre-Neoarchaean crust (T_{DM}^{Hf} of 3·65 Ga) of the Limpopo Belt. The absence of any juvenile Neoarchaean granitoids (TTGs) throughout the Limpopo Belt, including the marginal zones, may indicate that the exposed granite bodies are not the result of Neoarchaean juvenile slab-melting. Instead, it is more likely that the subducted slab underwent dehydration, which caused melting (and incompatible trace element enrichment by the released fluid) of the overlying subcontinental mantle wedge and led to the formation of juvenile Neoarchaean mafic magmas. Such a scenario conforms with the interpretation of Watkeys & Armstrong (1985) for the formation of the Bulai lamprophyres (see above). The juvenile mafic magmas, because of their high density, ponded at the crust–mantle boundary, where they caused magmatic underplating, which in turn triggered the melting of the overlying Palaeoarchaean crust. In consequence, the juvenile, mantle-derived mafic magma and evolved crustal materials were mixed to different degrees, leading to the formation of different types of magmatic rocks with distinct hafnium isotope composition at 2·6–2·7 Ga. Rocks with the oldest T_{DM}^{Hf} values, such as the Singelele granite gneiss (3·3–3·5 Ga), perhaps represent nearly pure crustal melts, whereas rocks with younger T_{DM}^{Hf} values, such as the Bulai granite and the Zanzibar gneisses (3·1–3·2 Ga), may contain a higher amount of juvenile components. The crust constituting the Mahalapye Complex was intruded by granitoids with the largest compositional variations, as reflected by the Hf isotope data of sample Malb (T_{DM}^{Hf} = 2·8–3·3 Ga). In addition to the granitoid formation, some portions of the underplated mantle-derived mafic magma solidified without any significant isotopic modification, and formed a Neoarchaean lower crust. During Palaeoproterozoic heating at 2·06 Ga, this Neoarchaean mafic crust was remelted, leading to the formation of diorite magmas with T_{DM}^{Hf} of about 2·65 Ga. Solidified relics of such a magma are now exposed in the Lose quarry in the Mahalapye Complex. The same heating event caused the melting of the isotopically more variable upper crust (T_{DM}^{Hf} = 2·8–3·3 Ga), which led to the formation of the garnet-bearing leucosomes exposed in the Lose quarry and the final intrusions of the Mokgware and Mahalapye granites at about 2·02 Ga. So far, the reason for the Palaeoproterozoic heating event,

which caused the high-grade metamorphic overprint throughout wide areas of the Limpopo Belt, is not understood. *P–T* paths, structural investigations and the geochronological data of Holzer *et al.* (1998, 1999), Kröner *et al.* (1999) and Zeh *et al.* (2004, 2005a, 2005b) indicate that the 2·02 Ga event is related to crustal convergence that was caused by the oblique collision between the Zimbabwe and Kaapvaal Cratons.

CONCLUSIONS

The results indicate that by combining the U–Pb with the Lu–Hf isotope system primary magmatic zircon domains can be distinguished from those formed during later metamorphic events, even if the distinct zircon domains underwent multiple Pb loss and the texture–age relationships, as obtained by CL images and U–Pb analyses, are ambiguous. Furthermore, the applied technique allows us to distinguish zircon grains formed in juvenile magmas from those generated by melting of older continental crust or affected by substantial crustal contamination.

Taking all data into account we conclude that most Palaeoarchaean to Palaeoproterozoic granitoids of the Central Zone of the Limpopo Belt result from major recycling of an old Archaean crust, which was derived from the depleted mantle at *c.* 3·65 Ga, and is equivalent to some of the oldest rocks constituting the Kaapvaal and Zimbabwe Cratons. At 3·283 Ga this old crust was at least partially remelted, leading to the formation of the Sand River TTG suite, which underwent a first anatectic overprint at 3·14 Ga. Subsequently, during the Neoproterozoic at 2·7–2·6 Ga, large quantities of the Palaeoarchaean crust were recycled again and mixed with new juvenile magma to different degrees, causing variable hafnium model ages between 3·0 and 3·45 Ga. The influence and amount of juvenile magmas seems to increase from east to west, as supported by increasing $\varepsilon Hf(2{\cdot}6–2{\cdot}7\ Ga)_{initial}$ from the Sand River area of the Beit Bridge Complex (−7·1 to −1·8), to the Zanzibar area (−2·3 to +0·6) and to the Mahalapye Complex (−3·7 to +6·3) (Fig. 9a and b).

The coexistence of juvenile and mixed 2·6–2·7 Ga magmatic rocks in the Limpopo Belt is considered to result from the subduction of juvenile Neoarchaean oceanic crust beneath pre-Neoarchaean continental crust constituting the Limpopo Belt. This subducted crust underwent dehydration, triggering mantle wedge melting, and caused the underplating of mantle-derived mafic magma below the pre-Neoarchaean continental crust. This underplated juvenile magma triggered the formation of crustal melts and of mixed crust–mantle-derived melts, and parts of it formed a Neoarchaean mafic lower crust. Finally, the juvenile Neoarchaean lower crust and the mixed upper crust were remelted during the Palaeoproterozoic at 2·02–2·06 Ga.

ACKNOWLEDGEMENTS

A.Z. thanks Hartwig Frimmel for stimulating discussions, Wolfgang Dörr for help with the sample preparation, and the German Science Foundation (DFG) for financial support (grants KL 692/15-2 and GE 1152/2-2). Furthermore, we thank Kent C. Condie, Jan Kramers and Hugh Rollinson for their constructive critical reviews of an earlier version of the manuscript.

REFERENCES

Albarède, F. & Brouxel, M. (1987). The Sm/Nd secular evolution of the continental crust and the depleted mantle. *Earth and Planetary Sciences Letters* **82**, 25–35.

Albarède, F., Scherer, E. E., Blichert-Toft, J., Rosing, M. T., Simionovici, A. & Bizzarro, M. (2006). Gamma-ray irradiation in the early Solar System and the conundrum of the ^{176}Lu decay constant. *Geochimica et Cosmochimica Acta* **70**, 1261–1270.

Aldiss, D. T. (1991). The Motloutse Complex and the Zimbabwe Craton/Limpopo Belt transition in Botswana. *Precambrian Research* **50**, 89–109.

Allègre, C. J. (1987). Isotope geodynamics. *Earth and Planetary Science Letters* **86**, 175–203.

Allègre, C. J. & Lewin, E. (1989). Chemical structure and history of the Earth: evidences from global non-linear inversion of isotopic data in a three box model. *Earth and Planetary Science Letters* **96**, 61–88.

Amelin, Y., Lee, D., Halliday, A. N. & Pidgeon, R. T. (1999). Nature of the Earth's earliest crust from hafnium isotopes in single detrital zircons. *Nature* **399**, 252–255.

Amelin, Y., Lee, D.-C. & Halliday, A. N. (2000). Early–middle Archean crustal evolution deduced from Lu–Hf and U–Pb isotopic studies of single zircon grains. *Geochimica et Cosmochimica Acta* **64**, 4205–4225.

Armstrong, R., Compston, W., Dodson, M. H., Kröner, A. & Williams, I. S. (1988). Archean crustal history in southern Africa. In: *Research School of Earth Sciences. Australian National University, Annual Report 1987*, pp. 62–64.

Armstrong, R. L. (1968). A model for Sr and Pb isotope evolution in a dynamic Earth. *Reviews of Geophysics* **6**, 175–199.

Armstrong, R. L. (1991). The persistent myth of crustal growth. *Australian Journal of Earth Sciences* **38**, 613–630.

Barton, J. M., Jr (1983). Pb-isotopic evidence for the age of the Messina Layered Intrusion, Central Zone, Limpopo Mobile Belt. *Special Publication, Geological Society of South Africa* **8**, 43–44.

Barton, J. M., Jr (1996). The Messina layered intrusion, Limpopo belt, South Africa, an example on the in-situ contamination of an Archean anorthosite complex by continental crust. *Precambrian Research* **78**, 139–150.

Barton, J. M., Jr & Key, R. M. (1983). Rb–Sr ages and geological setting of certain rock units from the Central Zone of the Limpopo Mobile Belt, near Zanzibar, southern Africa. *Special Publication, Geological Society of South Africa* **8**, 19–26.

Barton, J. M., Jr & Sergeev, S. (1997). High precision, U–Pb analyses of single grains of zircon from quartzite in the Beit Bridge Group yield a discordia. *South African Journal of Geology* **100**, 37–41.

Barton, J. M., Jr, Fripp, R. E. P. & Ryan, B. (1977). Rb/Sr ages and geological setting of ancient dykes in the Sand River area, Limpopo mobile belt, South Africa. *Nature* **267**, 487–490.

Barton, J. M., Jr, Du-Toit, M. C., Van Reenen, D. D. & Ryan, B. (1983). Geochronologic studies in the Southern Marginal Zone of the

Limpopo Mobile Belt, southern Africa. *Special Publication, Geological Society of South Africa* **8**, 55–64.

Barton, J. M., Jr, Van Reenen, D. D. & Roering, C. (1990). The significance of 3000 Ma granulite-facies mafic dikes in the central zone of the Limpopo belt, southern Africa. *Precambrian Research* **48**, 299–308.

Barton, J. M., Jr, Doig, R., Smith, C. B., Bohlender, F. & Van Reenen, D. D. (1992). Isotopic and REE characteristics of the intrusive charnoenderbite and enderbite geographically associated with the Matok Pluton, Limpopo Belt, southern Africa. *Precambrian Research* **55**, 451–467.

Barton, J. M., Jr, Holzer, L., Kamber, B., Doig, R., Kramers, J. D. & Nyfeler, D. (1994). Discrete metamorphic events in the Limpopo belt, southern Africa: implications for the application of *P–T* paths in complex metamorphic terranes. *Geology* **22**, 1035–1038.

Barton, J. M., Jr, Doig, R. & Smith, C. B. (1995). Age, origin, and tectonic significance of the Entabeni granite, northern Transvaal, South Africa. *South African Journal of Geology* **98**, 326–330.

Barton, J. M., Barton, E. S. & Smith, C. B. (1996). Petrography, age and origin of the Shiel alkaline complex, northern Transvaal, South Africa. *Journal of African Earth Sciences* **22**, 133–145.

Barton, J. M., Jr, Barnett, W. P., Barton, E. S., Barnett, M., Doorgapershad, A., Twiggs, C., Klemd, R., Martin, J., Millonig, L. & Zenglein, R. (2003). The geology of the area surrounding the Venetia kimberlite pipes, Limpopo Belt, South Africa, a complex interplay of nappe tectonics and granitoid magmatism. *South African Journal of Geology* **106**, 109–128.

Barton, J.M., Jr, Klemd, R. & Zeh, A. (2006). The Limpopo Belt: a result of Archean to Proterozoic, Turkic-type orogenesis? In: Reimold, W. U. & Gibbson, R. (eds) *Processes on the Early Earth. Geological Society of America, Special Papers* **405**, 315–332.

Berger, M. & Rollinson, H. (1997). Isotopic and geochemical evidence for crust–mantle interaction during late Archean crustal growth. *Geochimica et Cosmochimica Acta* **61**, 4809–4829.

Berger, M., Kramers, J. D. & Nägler, T. F. (1995). An Archaean high grade province adjacent to a granite greenstone terrain: geochemistry and geochronology of charnoenderbites in the Northern Marginal Zone of the Limpopo Belt, Southern Africa and genetic models. *Schweizerische Mineralogische und Petrographische Mitteilungen* **75**, 17–42.

Blichert-Toft, J. & Albarède, F. (1997). The Lu–Hf isotope geochemistry of chondrites and the evolution of the mantle–crust system. *Earth and Planetary Science Letters* **148**, 243–258.

Brandl, G. (1992). Geological map of the Limpopo Belt and its environs 1:500 000. *Contribution to a Field Workshop on Granulites and Deep Crustal Tectonics, 1990.* Pretoria: Geological Survey of South Africa.

Buick, I. S., Maas, R. & Gibson, R. (2001). Precise U–Pb titanite age constraints on the emplacement of the Bushveld Complex, South Africa. *Journal of the Geological Society, London* **158**, 3–6.

Buick, I. S., Williams, I. S., Gibbson, R. L., Cartwright, I. & Miller, J. A. (2003). Carbon and U–Pb evidence for a Palaeoproterozoic crustal component in the Central Zone of the Limpopo Belt, South Africa. *Journal of the Geological Society, London* **160**, 601–612.

Buick, I. S., Hermann, J., Williams, I. S., Gibson, R. L. & Rubatto, D. (2006). A SHRIMP U–Pb and LA-ICP-MS trace element study of the petrogenesis of garnet–cordierite–orthoamphibole gneisses from the Central Zone of the Limpopo Belt, South Africa. *Lithos* **88**, 150–172.

Chauvel, C. & Blichert-Toft, J. (2001). A hafnium isotope and trace element perspective on melting of the depleted mantle. *Earth and Planetary Science Letters* **190**, 137–151.

Chavagnac, V., Kramers, J. D., Nägler, T. F. & Holzer, L. (2001). The behaviour of Nd and Pb isotopes during 2·0 Ga migmatiztion in paragneisses of the Central Zone of the Limpopo Belt (South Africa and Botswana). *Precambrian Research* **112**, 51–86.

Chu, N. C., Taylor, R. N., Chavagnac, V., Nesbitt, R. W., Boella, R. M., Milton, J. A., German, C. R., Bayon, G. & Burton, K. (2002). Hf isotope ratio analysis using multi-collector inductively coupled plasma mass spectrometry: an evaluation of isobaric interference corrections. *Journal of Analytical Atomic Spectrometry* **17**, 1567–1574.

Compston, W., Williams, I. S. & Meyer, C. (1984). U–Pb geochronology of zircons from Lunar Breccia 73217 using sensitive high mass resolution ion microprobe. *Journal of Geophysical Research, Supplement* **89**, B525–B534.

Condie, K. C., Beyer, E., Belousova, E., Griffin, W. L. & O'Reilly, S. Y. (2005). U–Pb isotopic ages and Hf isotopic composition of single zircons: the search for juvenile Precambrian continental crust. *Precambrian Research* **139**, 42–100.

Coward, M. P., James, P. R. & Wright, L. (1976). Northern margin of the Limpopo mobile belt, southern Africa. *Geological Society of America Bulletin* **87**, 601–611.

Davis, D. W., Amelin, Y., Nowell, G. M. & Parrish, R. R. (2005). Hf isotopes in zircon from the western Superior province, Canada: implications for Archean crustal development and evolution of the depleted mantle reservoir. *Precambrian Research* **114**, 295–325.

Dodson, M. H., Compston, W., Williams, I. S. & Wilson, J. F. (1988). A search for ancient detrital zircons in Zimbabwean sediments. *Journal of the Geological Society, London* **145**, 977–983.

Erikson, K. A., Kidd, W. S. & Krapez, B. (1988). Basin analyses in regionally metamorphosed and deformed early Archean terrains: examples from southern Africa and Western Australia. In: Kleinspehn, K. L. & Poala, C. (eds) *Frontiers in Sedimentary Geology, New Perspectives in Basin Analysis*. New York: Springer, pp. 329–335.

Flowerdew, M. J., Millar, I. L., Vaughan, A. P. M., Horstwood, M. S. A. & Fanning, C. M. (2006). The source of granitic gneisses and migmatites in the Antarctic Peninsula: a combined U–Pb SHRIMP and laser ablation Hf isotope study of complex zircons. *Contributions to Mineralogy and Petrology* **151**, 751–768.

Frei, R., Schönberg, R. & Blenkinsop, T. G. (1999). Geochronology of the late Archaean Razi and Chilimanzi suites of granites in Zimbabwe; implications for the late Archaean tectonics of the Limpopo Belt and Zimbabwe Craton. *South African Journal of Geology* **102**, 55–63.

Geisler, T., Ulonska, M., Schleicher, H., Pidgeon, R. T. & van Bronswijk, W. (2001). Leaching and differential recrystallization of metamict zircon under experimental conditions. *Contributions to Mineralogy and Petrology* **141**, 53–65.

Gerdes, A. & Zeh, A. (2006). Combined U–Pb and Hf isotope LA-(MC) ICP-MS analyses of detrital zircons: comparison with SHRIMP and new constraints for the provenance and age of an Armorican metasediment in Central Germany. *Earth and Planetary Science Letters* **249**, 47–61.

Griffin, W. L., Belousova, E. A., Shee, S. R., Pearson, N. J. & O'Reilly, S. Y. (2004). Archean crustal evolution in the northern Yilgarn Craton: U–Pb and Hf-isotope evidence from detrital zircons. *Precambrian Research* **131**, 231–282.

Hamilton, P. J., O'Nions, R. K. & Evensen, N. M. (1977). Sm–Nd dating of Archean basic and ultrabasic volcanics. *Earth and Planetary Science Letters* **36**, 263–268.

Harris, N. B. W., Hawkesworth, C. J., Van Calsteren, P. & McDermott, F. (1987). Evolution of continental crust in southern Africa. *Earth and Planetary Science Letters* **83**, 85–93.

Harrison, T. M., Blichert-Toft, J., Müller, W., Albarède, F., Holden, P. & Mojzsis, S. J. (2005). Heterogeneous Hadean hafnium: evidence of continental crust by 4·4–4·5 Ga. *Science* **310**, 1947–1950.

Hawkesworth, C. J. & Kemp, A. I. S. (2006). Using hafnium and oxygen isotopes in zircons to unravel the record of crustal evolution. *Chemical Geology* **226**, 144–162.

Hisada, K. & Miyano, T. (1996). Petrology and microthermometry of aluminous rocks in the Botswanan Limpopo Central Zone: evidence for isothermal decompression and isobaric cooling. *Journal of Metamorphic Geology* **14**, 183–197.

Hisada, K., Perchuk, L. L., Gerya, T. V., Van Reenen, D. D. & Paya, B. K. (2005). *P–T*–fluid evolution in the Mahalapye Complex, Limpopo high-grade terrane, eastern Botswana. *Journal of Metamorphic Geology* **23**, 313–334.

Holzer, L., Frei, R., Barton, J. M., Jr & Kramers, J. D. (1998). Unraveling the record of successive high grade events in the Central Zone of the Limpopo Belt using Pb single phase dating of metamorphic minerals. *Precambrian Research* **87**, 87–115.

Holzer, L., Barton, J. M., Jr, Paya, B. K. & Kramers, J. D. (1999). Tectonothermal history in the western part of the Limpopo Belt: test of tectonic models and new perspectives. *Journal of African Earth Sciences* **28**, 383–402.

Iizuka, T., Hirata, T., Komiya, T., Rino, S., Katayama, I. & Motoki, A. (2005). U–Pb and Lu–Hf isotope systematics of zircons from the Mississippi River sand: implications for reworking and growth of continental crust. *Geology* **33**, 485–488.

Iizuka, T., Komiya, T., Maruyama, S., Hirata, T., Hidaka, H. & Windley, B. (2006). 4·2 Ga zircon xenocryst in an Acasta gneiss from northwestern Canada: evidence for early continental crust. *Geology* **34**, 245–248.

Jaeckel, P., Kröner, A., Kamo, S. L, Brandl, G. & Wendt, J. I. (1997). Late Archaean to early Proterozoic granitoid magmatism and high-grade metamorphism in the central Limpopo belt, South Africa. *Journal of the Geological Society, London* **154**, 25–44.

Janousek, V., Gerdes, A., Vrana, S., Friedl, G., Finger, F. & Vojtech, E. (2006). Mafic granulites of the Lisov Massif, southern Bohemia: middle-crustal relics of a Late Devonian magmatic arc? *Journal of Petrology* **47**, 705–744.

Jelsma, H. A. & Dirks, P. H. G. M. (2002). Neoarchean tectonic evolution of the Zimbabwe Craton. In: Fowler, C. M. R., Ebinger, C. B. & Hawkesworth, C. J. (eds) *The Early Earth: Physical, Chemical and Biological Development. Geological Society, London, Special Publications*, pp. 183–211.

Jelsma, H. A., Vinyu, M. L., Valbracht, P. J., Davies, G. R., Wijbrans, J. R. & Verdurmen, E. A. T. (1996). Constraints on Archean crustal evolution of the Zimbabwe craton: a U–Pb zircon, Sm–Nd and Pb–Pb whole rock isotope study. *Contributions to Mineralogy and Petrology* **124**, 55–70.

Kamber, B. & Biino, G. G. (1995). The evolution of high *T*–low *P* granulites in the Northern Marginal Zone *sensu stricto*, Limpopo Belt, Zimbabwe—the case for petrography. *Schweizerische Mineralogische und Petrographische Mitteilungen* **75**, 427–454.

Kamber, B., Blenkinsop, T. G., Villa, I. M. & Dahl, P. S. (1995a). Proterozoic transpressive deformation in the Northern Marginal Zone, Limpopo Belt, Zimbabwe. *Journal of Geology* **103**, 493–508.

Kamber, B., Kramers, J. D., Napier, R., Cliff, R. A. & Rollinson, H. R. (1995b). The Triangle Shear zone, Zimbabwe, revisited: new data document an important event at 2·0 Ga in the Limpopo Belt. *Precambrian Research* **70**, 191–213.

Klemd, R., Schmidt, A., Martin, J. & Barton, J. M., Jr (2003). *P–T* path constraints from metapelitic rocks east of the Venetia kimberlite pipes, Central Zone, Limpopo Belt, South Africa: have these rocks seen granulite-facies conditions? *South African Journal of Geology* **106**, 129–148.

Kreissig, K., Nägler, T. F., Kramers, J. D., Van Reenen, D. D. & Smit, C. A. (2000). An isotopic and geochemical study of the northern Kaapvaal Craton and the Southern Marginal Zone of the Limpopo Belt: are they juxtaposed terranes? *Lithos* **50**, 1–25.

Kreissig, K., Holzer, L., Frei, R., Villa, I. M., Kramers, J. D., Kröner, A., Smit, C. A. & Van Reenen, D. D. (2001). Chronology of the Hout River Shear Zone and the metamorphism in the Southern Marginal Zone of the Limpopo Belt, South Africa. *Precambrian Research* **109**, 145–173.

Krogh, T. E. (1973). A low contamination method for the hydrothermal decomposition of zircon and extraction of U and Pb for isotopic age determinations. *Geochimica et Cosmochimica Acta* **37**, 485–495.

Kröner, A., Jaeckel, P., Hofmann, A., Nemchin, A. A. & Brandl, G. (1998). Field relationships and age of supracrustal Beit Bridge Complex and associated granitoid gneisses in the Central Zone of the Limpopo Belt, South Africa. *South African Journal of Geology* **101**, 201–213.

Kröner, A., Jaeckel, P., Brandl, G., Nemchin, A. A. & Pidgeon, R. T. (1999). Single zircon ages for granitoid gneisses in the Central Zone of the Limpopo Belt, Southern Africa and geodynamic significance. *Precambrian Research* **93**, 299–337.

Ludwig, K. (2001). *Isoplot/Ex, rev. 2.49. A Geochronological Toolkit for Microsoft Excel. Berkeley Geochronology Center, Special Publications* **1a**.

Maier, W. D., Arndt, N. T. & Curl, E. A. (2000). Progressive crustal contamination of the Bushveld Complex: evidence from Nd isotopic analyses of the cumulate rocks. *Contributions to Mineralogy and Petrology* **140**, 316–327.

Mason, R. (1973). The Limpopo mobile belt—Southern Africa. *Philosophical Transactions of the Royal Society of London, Series A* **273**, 463–485.

McCourt, S. & Armstrong, R. A. (1998). SHRIMP U–Pb geochronology of granites from the Central Zone, Limpopo Belt, southern Africa: implications for the age of the Limpopo Orogeny. *South African Journal of Geology* **101**, 329–338.

McCourt, S. & Vearncombe, J. R. (1987). Shear zones bounding the central zone of the Limpopo mobile belt, southern Africa. *Journal of Structural Geology* **9**, 127–137.

McCourt, S. & Vearncombe, J. R. (1992). Shear Zones of the Limpopo Belt and adjacent granitoid– greenstone terranes, implications for late Archaean collision tectonics in Southern Africa. *Precambrian Research* **55**, 553–570.

Mezger, K. & Krogstad, E. J. (1997). Interpretation of discordant U–Pb zircon ages—an evaluation. *Journal of Metamorphic Geology* **15**, 127–140.

Mkweli, S., Kamber, B. & Berger, M. (1995). Westward continuation of the craton–Limpopo Belt tectonic break in Zimbabwe and new age constraints on the timing of the thrusting. *Journal of the Geological Society, London* **152**, 77–83.

Moorbath, S., Taylor, P. N. & Jones, N.W. (1986). Dating the oldest terrestrical rocks—fact and fiction. *Chemical Geology* **57**, 63–86.

Moorbath, S., Whitehouse, H. J. & Kamber, B. S. (1997). Extreme Nd-isotope heterogeneity in the early Archean—fact or fiction? Case histories from northern Canada and West Greenland. *Chemical Geology* **135**, 213–231.

O'Nions, R. K. & Hamilton, P. J. (1981). Isotope and trace element models of crustal evolution. *Philosophical Transactions of the Royal Society of London, Series A* **301**, 473–487.

O'Nions, R. K., Evensen, N. M. & Hamilton, P. J. (1979). Geochemical modelling of mantle differentiation and crustal growth. *Journal of Geophysical Research* **84**, 6091–6101.

Patchett, P. J., Kouvo, O., Hedge, C. E. & Tatsumoto, M. (1981). Evolution of continental crust and mantle heterogeneity: evidence from Hf isotopes. *Contributions to Mineralogy and Petrology* **78**, 279–297.

Rino, S., Komiya, T., Windley, B. F., Katayama, I., Motoki, A. & Hirata, T. (2004). Major episodic increase of continental crustal growth determined from zircon ages of river sands; implications for mantle overturns in the Early Precambrian. *Physics of the Earth and Planetary Interiors* **146**, 369–394.

Rizvanova, N. G., Levchenkov, O. A., Belous, A. E., Bezman, N. I., Maslenikov, A. N., Komarov, A. N., Makeev, A. F. & Levskii, L. K. (2000). Zircon reaction and stability of the U–Pb isotope system during interaction with carbonate fluid: experimental hydrothermal study. *Contributions to Mineralogy and Petrology* **139**, 101–114.

Roering, C., Van Reenen, D. D., Smit, C. A., Barton, Jr. M., J., De Beer, J. H., De Wit, M. J., Stettler, E. H., Van Schalkwyk, J. F., Stevens, G. & Pretorius, S. (1992). Tectonic model for the evolution of the Limpopo Belt. *Precambrian Research* **55**, 539–552.

Rollinson, H. R. & Blenkinsop, T. (1995). The magmatic, metamorphic and tectonic evolution of the Northern Marginal Zone of the Limpopo Belt in Zimbabwe. *Journal of the Geological Society, London* **152**, 66–75.

Rubatto, D., Williams, I. S. & Buick, I. L. (2001). Zircon and monazite response to prograde metamorphism in the Reynolds Range, Central Australia. *Contributions to Mineralogy and Petrology* **140**, 458–468.

Rudnick, R. L. & Gao, S. (2003). Composition of the continental crust. In: Rudnick, R.L. (ed.) *The Crust, Treatise on Geochemistry, Vol. 3*, Amsterdam: Elsevier, pp. 1–64.

Schaller, M., Steiner, O., Studer, I., Holzer, L., Herwegh, M. & Kramers, J. D. (1999). Exhumation of the Limpopo Central Zone granulites and dextral continent-scale transcurrent movement at 2·0 Ga along the Palala Shear Zone, Northern Province, South Africa. *Precambrian Research* **96**, 263–288.

Scherer, E., Münker, C. & Mezger, K. (2001). Calibration of the lutetium–hafnium clock. *Science* **293**, 683–687.

Scherer, E. E., Whitehouse, M. J. & Münker, C. (2007). Zircon as a monitor of crustal growth. *Elements* **3**, 19–24.

Schmitz, M. D., Bowring, S. A., de Wit, M. J. & Gartz, V. (2004). Subduction and terrane collision stabilize the west Kaapvaal craton tectosphere 2·9 billion years ago. *Earth and Planetary Science Letters* **222**, 363–376.

Söderlund, U., Patchett, J. P., Vervoort, J. D. & Isachsen, C. E. (2004). The ^{176}Lu decay constant determined by Lu–Hf and U–Pb isotope systematics of Precambrian mafic intrusions. *Earth and Planetary Science Letters* **219**, 311–324.

Stacey, J. S. & Kramers, J. D. (1975). Approximation of terrestrial lead isotope evolution by a two-stage model. *Earth and Planetary Science Letters* **26**, 207–221.

Stevenson, R. K. & Patchett, P. J. (1990). Implications for the evolution of continental crust from Hf isotope systematics of Archean detrital zircons. *Geochimica et Cosmochimica Acta* **54**, 1683–1697.

Taylor, P. N., Kramers, J. D., Moorbath, S., Wilson, J. F., Orpen, J. L. & Martin, A. (1991). Pb/Pb, Sm–Nd and Rb–Sr geochronology in the Archean Craton of Zimbabwe. *Chemical Geology* **87**, 175–196.

Taylor, S. R. & McLennan, S. M. (1985). *The Continental Crust: its Composition and Evolution*. Oxford: Blackwell, 312 pp.

Van Reenen, D. D., Barton, J. M., Jr, Roering, C., Smit, C. A. & Van Schalkwyk, J. F. (1987). Deep crustal response to continental collision: the Limpopo belt of southern Africa. *Geology* **15**, 11–14.

Van Reenen, D. D., Roering, C., Ashwal, L. D. & de Wit, M. L. (1992). Regional geological setting of the Limpopo Belt. *Precambrian Research* **55**, 1–5.

Van Reenen, D. D., Perchuk, L. L., Smit, C. A., Varlamov, D. A., Boshoff, R., Huizenga, J. M. & Gerya, T. V. (2004). Structural and *P–T* evolution of a major cross fold in the Central Zone of the Limpopo high-grade terrain, South Africa. *Journal of Petrology* **45**, 1413–1439.

Vavra, G., Gebauer, D., Schmid, R. & Compston, W. (1996). Multiple zircon growth and recrystallisation during polyphase Late Carboniferous to Triassic metamorphism in granulites of the Ivrea Zone (Southern Alps): an ion microprobe (SHRIMP) study. *Contributions to Mineralogy and Petrology* **122**, 337–358.

Vervoort, J. D. & Blichert-Toft, J. (1999). Evolution of the depleted mantle: Hf isotope evidence from juvenile rocks through time. *Geochimica et Cosmochimica Acta* **63**, 533–556.

Walraven, F. & Hattingh, E. (1993). Geochronology of the Nebo Granite, Bushveld Complex, South Africa. *South African Journal of Geology* **96**, 31–41.

Watkeys, M. K. & Armstrong, R. A. (1985). The importance of being alkaline—deformed late Archean lamprophyric dykes, Central Zone, Limpopo Belt. *Transactions of the Geological Society of South Africa* **88**, 195–206.

Wedepohl, K. H. (1995). The compositions of the continental crust. *Geochimica et Cosmochimica Acta* **59**, 1217–1232.

Wilson, A. H. & Carlson, R. W. (1989). A Sm–Nd and Pb isotope study of Archean greenstone belts in the southern Kaapvaal Craton, South Africa. *Earth and Planetary Science Letters* **96**, 89–105.

Zeh, A., Williams, I. S., Brätz, H. & Millar, I. L. (2003). Different age response of zircon and monazite during the tectono-metamorphic evolution of a high grade paragneiss from the Ruhla Crystalline Complex, Central Germany. *Contributions to Mineralogy and Petrology* **145**, 691–706.

Zeh, A., Klemd, R., Buhlmann, S. & Barton, J. M. (2004). Pro- and retrograde *P–T* evolution of granulites of the Beit Bridge Complex (Limpopo Belt, South Africa): constraints from quantitative phase diagrams and geotectonic implications. *Journal of Metamorphic Geology* **22**, 79–95.

Zeh, A., Klemd, R. & Barton, J. M., Jr (2005a). Petrological evolution in the roof of the high-grade metamorphic Central Zone of the Limpopo Belt, South Africa. *Geological Magazine* **142**, 229–240.

Zeh, A., Holland, T. J. B. & Klemd, R. (2005b). Phase relationships in grunerite–garnet-bearing amphibolites in the system CFMASH, with applications to metamorphic rocks from the Central Zone of the Limpopo Belt, South Africa. *Journal of Metamorphic Geology* **23**, 1–17.

Zhai, M., Kampunzu, A. B., Modisi, M. P. & Bagai, Z. (2006). Sr and Nd isotope systematics of the Francistown plutonic rocks, Botswana: implications for Neoarchean crustal evolution of the Zimbabwe craton. *Geologische Rundschau* **95**, 355–369.